Department of Food and Nutrition,
University of Helsinki,
Finland

EKT-series 1828

NOVEL FUNCTIONAL MATERIALS FROM UPGRADED BIOPOLYMERS: POLYSACCHARIDE AEROGELS

ABDUL GHAFAR

ACADEMIC DISSERTATION

To be presented, with the permission of the Faculty of Agriculture and Forestry, University of Helsinki, for public examination in lecture room 235 (sali 2), Infokeskus Korona (Viikinkaari 11) Viikki, on March 2nd, 2018, at 12 O'clock noon.

Helsinki 2018

Custos: Associate Professor Kati Katina
Department of Food and Nutrition
University of Helsinki
Helsinki, Finland

Supervisors: Assistant Professor Kirsi S. Mikkonen
Department of Food and Nutrition
University of Helsinki
Helsinki, Finland

Professor Maija Tenkanen
Department of Food and Nutrition
University of Helsinki
Helsinki, Finland

Docent Kirsti Parikka
Department of Food and Nutrition
University of Helsinki
Helsinki, Finland

Reviewers: Director of Research Françoise Quignard
Institute of Charles Gerhardt Montpellier
Montpellier, France

Associate Professor Eero Kontturi
Department of Bioproducts and Biosystems
Aalto University
Espoo, Finland

Opponent: Professor Kristiina Oksman
Department of Engineering Sciences and Mathematics
Division: Material Science
Luleå University of Technology, Sweden

ISBN 978-951-51-4061-6 (paperback)
ISBN 978-951-51-4062-3 (PDF; http://ethesis.helsinki.fi)

Unigrafia
Helsinki 2018

Ghafar, A. 2018. Novel functional materials from upgraded biopolymers: polysaccharide aerogels (dissertation). EKT-series 1828. University of Helsinki, Department of Food and Nutrition. 91 + 48 pp.

ABSTRACT

Aerogel is a highly porous and lightweight solid material that is prepared by replacing the liquid phase of a gel with air in such a way that the three-dimensional polymeric network remains intact in a dry state. Polysaccharides as aerogel-forming materials have attracted attention over the past few years due to their excellent innate properties, such as their non-toxicity, eco-friendliness, and derivation from renewable resources. Therefore, aerogels from polysaccharides have enormous potential for biomedical, pharmaceutical, and food industrial applications. Formation of the gel is the first step towards the aerogel preparation, though not all polysaccharides tend to form a gel in their native form. It is therefore required to make some modifications to their structures. The choice of modification technique is of the greatest importance in developing polysaccharide-based aerogels for food and food-related applications because the modification technique should be safe.

In this thesis, galactose oxidase (GaO) was used as a safe and environmentally friendly modification technique to oxidize and cross-link the polysaccharides guar galactomannan (GM) and tamarind seed xyloglucan (XG). Furthermore, the oxidation ability of GaO and the formation of GM and XG hydrogels were studied in the presence of varying quantities (5–25%) of nanofibrillated cellulose (NFC) as a reinforcing agent to obtain composite hydrogels. The liquid phase of the hydrogels was removed using two different drying techniques: lyophilization and supercritical CO_2 (sc-CO_2) drying, and the relationship of these techniques to the aerogels' properties, such as volumetric shrinkage, morphology, specific surface area, and mechanical behavior, were also studied. In this thesis, the synchrotron X-ray microtomography (XMT) technique was used as a modern and non-invasive imaging technique to characterize the aerogels for qualitative and quantitative morphological features in relation to their processing conditions.

The enzymatic oxidation of GM and XG with and without NFC-reinforcement allowed for the formation of elastic hydrogels. This study showed that the addition of NFC up to 25% did not hinder the enzymatic activity, and in this way, composite hydrogels were obtained. NFC-reinforcement significantly increased the elastic modulus (G′) as compared to the corresponding plain GM and XG hydrogels, but this effect depended on the type of polysaccharide (GM or XG). Replacing the liquid phase of the hydrogels with solvent also showed the strengthening effect of NFC in relation to the GM hydrogel matrix. NFC reduces the volumetric shrinkage, which is dependent on the type of solvent.

The lyophilization drying technique is more efficient in terms of preserving the hydrogel's original volume when converting to the aerogel, especially as compared to supercritical CO_2 drying, which showed significant volumetric shrinkage during the drying process. However, supercritical CO_2-

dried aerogels displayed mesoporous structures with pores sizes in the range of few nanometers to a few hundred nanometers that resulted in high surface areas up to 330 m^2/g of such aerogels. In contrast, lyophilized aerogels displayed different morphologies; for example, the size of the pores ranged from 125 to 250 μm, and they exhibited a low surface area (< 10 m^2/g). The three-dimensional structures of the studied polysaccharide-based aerogels were successfully visualized. Quantitative data provided a complete range of pore sizes and pore wall thickness distributions that were dependent on the ice-templating methods and NFC reinforcement.

In conclusion, this study revealed that the properties of the studied polysaccharide-based composite aerogels depend on processing parameters, the choice of drying techniques, and the addition of a reinforcing agent. The properties of GM- or XG-based aerogels can be tailored to a desired application through the selection of a drying method with carefully controlled processing conditions. XMT proved to be a promising characterization technique for bio-based porous materials for understanding their structural properties in relation to their functional properties.

PREFACE

All praises and thanks to the ***Almighty Allah***, the Merciful, the only creator of the universe and source of all knowledge and wisdom Who blessed me with health, thoughts, kind teachers, helping friends and with afforded opportunity to complete this study. I offer my humble gratitude to the ***Holy Prophet Hazrat Muhammad (Peace be Upon Him)*** whose moral and spiritual teachings enlightened my heart, mind and flourished thoughts towards achieving high ideas of life.

This study was carried out at the Department of Food and Environmental Sciences (now Department of Food and Nutrition), University of Helsinki Finland. Parts of the study were carried out during research visits to the Hamburg University of Technology (TUHH), Germany and Paul Scherrer Institut (PSI), Switzerland. The research was funded by the Magnus Ehrnrooth Foundation Finland, University of Helsinki Research Foundation Finland, AEROWOOD project funded by the WoodWisdon-Net Research Program and Academy of Finland (project no. 281628), Finnish Cultural Foundation Finland, COST FP1105 network under Short-Term- Scientific-Mission (STSM), BIOREGS Graduate School and Doctoral Programme in Food Chain and Health-University of Helsinki. The financial support from all sources is greatly appreciated. The Center for Scientific Computing (CSC), Espoo, Finland, is acknowledge for the provision of the supercomputer facility for data analyses.

I am greatly indebted to my supervisors; Assistant Prof. Kirsi Mikkonen, Prof. Maija Tenkanen and Docent Kirsti Parikka. I thank Kirsi Mikkonen for introducing me to the world of aerogel and Kirsti Parikka for introducing me the chemistry behind the aerogel, and their excellent advice, support and encouragement throughout the study. I am deeply grateful to Maija Tenkanen for giving me a chance to work in her research group, guidance and for your moral support during the study. It has been a privilege to work with all of you.

I am grateful to my co-authors: Prof. Irina Smirnova, Prof. Pavel Gurikov, Associate Prof. Monika Österberg, Docent Tuula Sontag-Strohm, Post-Doc David Haberthür, Dr. Jussi-Petteri Suuronen, and Dr. Raman P. Subrahmanyam. Thank you for making your invaluable expertise available and your contribution to the success of this research. I greatly appreciate Prof. Françoise Quignard and Associate Prof. Eero Kontturi for pre-examination of this dissertation and thank you for critically evaluating my thesis and for constructive comments and suggestions. I also want to thank the AEROWOOD-project partners; Prof. Falk Liebner, Prof. Bodo Saake, Dr. Tatiana Budtova, Dr. Uroš Maver and their team members for sharing the knowledge and expertise in the field of aerogel, and wonderful time spent during the project. I would like to thank Dr. Sybe Hartmans, Prof. Harry Brumer and Prof. Lisbeth Olson for providing the galactose oxidase, Marko Vehkamäki for the FIB-SEM analyses, Dr. Inkeri Kontro and Aki Kallonen for their help with the XMT experiments and Dainippon Sumitomo Pharma for providing tamarind galactoxyloglucan.

I would like to express my warm thanks to my present and former colleagues in the hemicellulose research group (now Food Materials Science Research Group), especially to Suvi Alakalhunmaa, Jose Martin Ramos-Diaz, Mamata Bhattarai, Ida Nikkilä and Minna Juvonen for friendly work atmosphere and for good memories of group activities. My sincere gratitude to all lab assistants, lab technicians and people in the administration for their help and smile.

I cannot thank my friends outside the academia for their loving support especially to Ayesha Irtiza, Yasir Ali, Zubair Rafique, Muhammad Kashif and Empire Cricket Club Finland members.

Most important of all, I express my deep sense of gratitude to my most affectionate and beloved parents (Mom, I miss you a lot), brothers and sisters for their love, their undying encouragement, their wisdom, their advice and for being there in every aspect of my life has meant everything to me and will be always remembered. I honestly could not have completed this without your support.

Helsinki, March 2018

Abdul Ghafar

LIST OF ORIGINAL PUBLICATIONS

This thesis is based on the following original publications, which are referred to in the text by Roman numerals (i.e., study I):

I Abdul Ghafar, Kirsti Parikka, Tuula Sontag-Strohm, Monika Österberg, Maija Tenkanen, Kirsi S. Mikkonen. 2015. Strengthening effect of nanofibrillated cellulose is dependent on enzymatically oxidized polysaccharide gel matrices. European Polymer Journal, 71:171–184.

II Abdul Ghafar, Kirsti Parikka, David Haberthür, Maija Tenkanen, Kirsi S. Mikkonen, Jussi-Petteri Suuronen. 2017. Synchrotron microtomography reveals the fine three-dimensional porosity of composite polysaccharide aerogels. Materials, 10(8):871.

III Abdul Ghafar, Pavel Gurikov, Raman Subrahmanyam, Kirsti Parikka, Maija Tenkanen, Irina Smirnova, Kirsi S. Mikkonen. 2017. Mesoporous guar galactomannan based biocomposite aerogels through enzymatic cross-linking. Composites: Part A: Applied Science and Manufacturing, 94:93–103.

Contribution of the author to papers I through III:

I Abdul Ghafar planned the study together with the other authors, and he was responsible for the experimental work. He had the main responsibility for interpreting the results, manuscript writing, and acted as the corresponding author of the paper.

II Abdul Ghafar designed the experiment with the other authors. He prepared the samples and performed the mechanical characterization. He participated in synchrotron analysis and carried out the major part of data handling and manuscript writing. He was the corresponding author of the paper.

III Abdul Ghafar planned the study together with the other authors. He performed the experimental work, carried out the main responsibility for data interpretation, and wrote the manuscript. He was the corresponding author of the paper.

ABBREVIATIONS

BET	Brunauer-Emmett-Teller
CF	Conventional freezing
DMF	N′N-Dimethyl formamide
DMSO	Dimethyl sulfoxide
DO	Degree of oxidation
3D	Three-dimensional
EtOH	Ethanol
FIB-SEM	Focused ion beam scanning electron microscopy
G′	Elastic/storage modulus
G″	Viscous/loss modulus
GaO	Galactose oxidase
GM	Guar galactomannan
IUPAC	International Union of Pure and Applied Chemistry
IPA	Isopropyl alcohol
LVER	Linear viscoelastic region
MEK	Methyl ethyl ketone
MeOH	Methanol
NFC	Nanofibrillated cellulose
Ox	Oxidized
PCA	Principal component analysis
PEEK	Polyether-ether-ketone
RT	Room temperature
sc-CO_2	Supercritical CO_2
UF	Unidirectional freezing
VS	Volumetric shrinkage
XG	Tamarind seed xyloglucan
XMT	Synchrotron X-ray microtomography

TABLE OF CONTENTS

1 INTRODUCTION

Polysaccharides are polymeric carbohydrate molecules composed of long chains of monosaccharide units bound together by glycosidic linkages. The sources of polysaccharides include numerous plants and the by-products of industrial processes, such as from the side-streams of the agriculture and forestry industries (Perez et al. 2002; Soderqvist Lindblad et al. 2005). Polysaccharides are diverse in their structures, which can range from linear to highly branched, and are composed of repeating units of the same monosaccharide or contain various monosaccharides in different compositions with different molar masses. These characteristics make them multipurpose biopolymers for modern industrial applications (Scheller and Ulvskov 2010; Van Vlierberghe et al. 2011). Furthermore, the non-toxicity and biodegradability of polysaccharides make them attractive candidates for bio-based materials, with the potential to replace petroleum-based materials in the future (Wahab and Razak 2016). An example of this would be the highly porous and lightweight material known as an aerogel, which is currently in development.

Aerogel is a man-made, ultralight, solid material that is characterized by a highly porous structure and a low density with a very high surface area. Aerogels can be formed by replacing the liquid phase of a gel with air/gas using techniques that maintain the three-dimensional (3D) structure of the gel in a dry state (Kistler 1931; Quignard et al. 2008). The history of the aerogel started in 1931 when Kistler reported a silica aerogel prepared by supercritical CO_2 drying (Kistler 1931). This invention opened a new era for the development of lightweight materials with unique properties. Due to their excellent properties, silica and their precursors from the inorganic family have been widely studied for aerogel formation (Hüsing and Schubert 1998; Soleimani Dorcheh and Abbasi 2008; Gurav et al. 2010; Olalekan et al. 2014). Silica aerogels display porosities of up to 99.8%, densities of approximately 0.003 g/cm^3, and surface areas up to 1200 m^2/g. In addition, these aerogels have a low thermal conductivity (< 3 mW/mK), and a low sound velocity (~100 m/s) (Gurav et al. 2010; Cuce et al. 2014; Stergar and Maver 2016). Such properties are well adapted for adsorption, sensing, catalysis, and thermal and acoustic insulation applications.

The research has been extended to organic polymers for aerogel formation. Resorcinol-formaldehyde and melamine-formaldehyde have been extensively study as aerogel-forming matrices from organic polymers (Hair et al. 1988; Pierre and Pajonk 2002; Mulik and Sotiriou-Leventis 2011). These organic aerogels also possess characteristic properties of the traditional, silica aerogels, like a low density of around 0.24 g/cm^3, high surface areas up to 1000 m^2/g, and excellent mechanical and thermal properties (Hrubesh and Pekala 1994; Hüsing and Schubert 1998; Pierre and Pajonk 2002). Aerogels considered for life-science applications should be non-toxic, biocompatible, and biodegradable, but silica aerogels are brittle and non-biodegradable, while resorcinol-formaldehyde and melamine-formaldehyde aerogels involve toxic elements in their processing (Pierre and Pajonk 2002; Mehling et al. 2009).

Most of the polysaccharides in their native form do not possess the optimal functionality, for

example, strong gel forming ability at low concentrations which is required for certain applications like aerogel formation. Therefore, polysaccharides require some modifications to achieve such functionality. Chemical cross-linking is an easy and quick way to introduce a new functionality to polysaccharides. When using modified polysaccharides for material in contact with humans or for human consumption, then chemical cross-linking is considered a safety risk due to the toxicity of the chemical used as a cross-linker (Cumpstey 2013; Reddy et al. 2015). Another drawback of chemical cross-linking is the non-selective catalytic activity of the chemicals, which results in side product formation (Cumpstey 2013). Enzymes were exploited as an alternative way for polysaccharide functionalization in order to avoid the limitations faced by chemical modification (Gu and Cheng 2005; Karaki et al. 2016). Enzymatic modification has many advantages, including a regio-selective reaction, mild reaction treatments, and the ability to introduce desired functionality to polysaccharide products (Cheng and Gu 2002; Gu and Cheng 2005; Cheng and Gu 2012; Karaki et al. 2016). Galactose-containing polysaccharides were also successfully modified using galactose oxidase to create a cross-linking network that resulted in the formation of a gel (Parikka et al. 2010). Using an enzyme as a cross-linker is advantageous for making the final product safe.

Polysaccharides have attracted attention over the past few years (García-González et al. 2011; Mikkonen et al. 2013; Stergar and Maver 2016). Aerogels from a single biopolymer sometimes exhibit poor properties or lack some properties, such as displaying a poor mechanical performance or having a brittle structure, like in the case of calcium-alginate aerogels (Cheng et al. 2012). Therefore, efforts have been made to incorporate fiber or inorganic clay as a reinforcing agent into the gel matrix of the inorganic aerogels (Pojanavaraphan and Magaraphan 2008; Yang et al. 2011; Cai et al. 2012; Sedighi Gilani et al. 2016). Biocomposite aerogels with optimal mechanical properties are advantageous for various applications (Köhnke et al. 2012; de Souza et al. 2013; Quraishi et al. 2015; Raman et al. 2015a; Gonçalves et al. 2016; Barros et al. 2016). To accelerate the use of bio-based composite aerogels in the future, it is important to know the relationship between the processing conditions and the role of a reinforcing agent in regards to the porous structure of the aerogels and their related properties.

In this thesis, a literature review provides an overview of plant polysaccharides, particularly relating to galactose-containing plant polysaccharides, their structure, galactose oxidase as a modification tool, and the properties of aerogels in relation to drying technique and reinforcement agent. The experimental part summarizes the data presented in three publications (I-III). In this thesis, the potential for enzymatic oxidation of galactose-containing polysaccharides (guar galactomannan and tamarind seed xyloglucan) on the formation of hydrogels and their properties were thoroughly studied in the presence of nanofibrillated cellulose (NFC). The effect of processing conditions, drying techniques, and NFC reinforcement on the 3D porous structures of the aerogels were investigated with synchrotron X-ray microtomography (XMT), a high-resolution characterization and non-invasive imaging technique.

2 LITERATURE REVIEW

2.1 Polysaccharides

The depletion of fossil oil reserves and their ever-increasing prices drive the search for alternative cheap and sustainable resources to produce fuels and chemicals that have a minimal impact on the environment, which can produce long-term economic benefits. This shifts the society from fossil fuel-dependence to a more sustainable-based resource economy (Deutschmann and Dekker 2012). In the future, to make economic growth more sustainable and secure, actions are needed to convert biomass into biofuels, chemicals, and raw material inputs for modern biorefineries. Plant polysaccharides are abundant, and their full utilization potential is vital for a future sustainable bioeconomy because plant polysaccharides are labeled as non-toxic, biodegradable, and biocompatible. Most importantly, they come from renewable resources. These inherit properties of plant polysaccharides make them a highly valuable raw material for modern industry.

Plant polysaccharides are widely available on this planet. They are long-chain biopolymers of carbohydrate molecules, and their backbone is comprised of monosaccharide units bound together by glycosidic linkages. Cellulose is the predominant polysaccharide of the plant cell wall, where it makes up 45–55% of the cell wall. Because of its high prevalence in plant cells, cellulose is naturally part of the human diet as dietary fiber. It is also utilized for food-contact material in the form of food packaging due to its safety. Cellulose is a distinct and well-defined polysaccharide, as it is composed entirely of β-(1→4)-linked chains of glucose (O'Sullivan 1997). NFC is nano-sized cellulose fiber that is produced by high-shear disintegration and homogenization from wood pulp (Turbak et al. 1983). Due to the peculiar properties of NFC, plant cellulose regained interest in research for bio-based materials and novel food applications (Gómez H. et al. 2016).

Other non-cellulosic, cell-wall polysaccharides are grouped into pectins and hemicelluloses. Pectins are cell-wall polysaccharides that are rich in galacturonic acid and can be extracted with chelating agents, such as oxalate, in combination with heating. They are widely used in the food industry, such as in the making of jam, for their gelling and thickening properties (Voragen et al. 2009). Hemicelluloses comprise the second-most abundant group of plant polysaccharides after cellulose (Limayem and Ricke 2012; Zabed et al. 2016). They can be extracted from the cell wall with base. They are heterogeneous, short-chain, branched biopolymers, and their side branches are comprised of different sugar units. These polysaccharides are composed of different monosaccharide units such as pentoses (D-xylose and L-arabinose), hexoses (D-galactose, D-mannose, and D-glucose), and sugar acids (Moreira and Filho 2008). They are grouped into xylans, xyloglucans, mannans, and β-(1→3,1→4)-glucans based on the main types of sugar residues present in the backbone chain (Scheller and Ulvskov 2010). They are present in both softwood and hardwood, but their distributions among these wood types are different. For example, xylans are mostly present in hardwood, whereas in softwood, mainly glucomannans are present. These groups of polysaccharides can be extracted in large quantities from numerous resources, like plants and

the by-products of industrial processes, such as from side-streams of the agriculture and forestry industries (Perez et al. 2002).

Hemicelluloses play a structural role in the plant cell wall where they provide strength by tethering the adjacent cellulose fibers and sometimes also interact with lignin (Perez et al. 2002). Additionally, mannans and xyloglucans are present in the endosperms of various plants where they function as seed-storage polysaccharides (nonstarch). These seed-storage polysaccharides have a similar structure to hemicelluloses, but due to their properties, they are considered to be a part of the group of plant-originated gums (Mikkonen and Tenkanen 2012; Prajapati et al. 2013; Thombare et al. 2016). For example, mannans (e.g., galactomannas, a sub-family of mannans) are obtained from the seeds of guars and xyloglucans are obtained from the seeds of tamarinds (Wielinga 2009; Mishra and Malhotra 2009). Galactomannans and xyloglucans are mostly present in the seeds of cotyledons and endosperms. They act as energy reserves for germination and water retention to avoid complete drying of the seeds (Moreira and Filho 2008). Galactomannans and xyloglucans have a long history in the food industry, serving as thickeners, viscosity modifiers, and stabilizers (Mishra and Malhotra 2009; Mudgil et al. 2014; Thombare et al. 2016).

Galactomannans and xyloglucans, due to their water solubility, thickening, emulsifying, gel-forming ability, stability in a wide range of pH, and more importantly, biodegradability, have been extensively explored by various researchers (Nishinari et al. 2007; Prajapati et al. 2013) in their native form or with structural modifications (Thombare et al. 2016). From the last decade, they received more attention for bio-based material development due to their safety, availability, and low-cost as a raw material (Simi and Abraham 2010; Mikkonen and Tenkanen 2012; Prajapati et al. 2013). These polysaccharides exhibited different solution properties due to differences in molar mass, side-chain substitution, and sugar units in the backbone chain that are more likely to also affect their gel properties and, consequently, the properties of bio-based materials made from them. Therefore, this literature review is focused on the structure, modification techniques, and properties of bio-based materials of these polysaccharides.

2.1.1 Guar galactomannan

Guar galactomannan (GM) is derived from the seeds of an annual agricultural crop of guar (*Cyamopsis tetragonoloba*), a member of the Leguminosae family (Figure 1). It is mostly grown in India, Pakistan, Sudan, and some parts of the USA, though India and Pakistan account for 90% of world's guar production, in which India has the higher share (Mudgil et al. 2011; Thombare et al. 2016). GM is readily available and a cheaper source of galactomannans than other sources, such as locust bean and tara gums. GM consists of linear backbone chains of (1→4)-β-D-mannosyl (Man*p*) units with branch points of α-D-galactosyl (Gal*p*) units attached by (1→6) linkages (Figure 1D). Many studies have shown that the mannose to galactose ratios are varied, however, within the range of 1.6:1 to 1.8:1. GM contains 40% galactosyl units as a side branch and 60% mannosyl units as the backbone (Daas et al. 2000) (Table 1).

GM is a high molar mass (M = 2.6 x 10^6 g/mol) and water soluble polysaccharide. Some mannans and xylans are water insoluble, and partial acetylation is required to make them water soluble (Pawar et al., 2013; Chokboribal et al., 2015). In aqueous solutions, the side-chain galactosyl residues of GM interact with water molecules. This causes inter-molecular chain entanglement (hydrogen bonding), which results in a viscous solution, even at low concentrations (Iqbal and Hussain 2010). This entanglement increases further to induce gelling or thickening with the increase in the concentration of GM in the solution. An aqueous solution of GM (1%) displayed a viscosity up to 10 Pa. s (Parija et al. 2001) and exhibited shear-thinning properties with a pseudoplastic flow (Tripathy and Das 2013).

Table 1: Approximate carbohydrate composition (The ratio of sugar units is presented as a molar percentage) and molar mass of guar galactomannan (GM) and tamarind seed xyloglucan (XG). Gal = galactose, Man = mannose, Glc = glucose, Xyl = xylose.

	Gal (%)	Man (%)	Glc (%)	Xyl (%)	Molar mass (M) (g/mol)	References
GM	40	60	-	-	2.6 x 10^6	(Dea and Morrison 1975; York et al. 1993; Parikka et al. 2010)
XG	16	-	48	36	4.7 x 10^5	

GM is widely used as a viscosity modifier and stabilizer in food, textiles, paper, cosmetics, bioremediation, drug delivery, medical use, and pharmaceuticals (Prajapati et al. 2013; Thombare et al. 2016). Additionally, GM-based films (Mikkonen et al. 2007) have the potential to serve as sustainable food-packaging materials (Mikkonen and Tenkanen 2012). Various modifications in the structure of GM have been adopted to add new properties (Zhang et al. 2005), such as etherification (Pal et al. 2007), esterification (Fujioka et al. 2009; Shenoy and D'Melo 2010), chemical oxidation (Gong et al. 2011), enzymatic oxidation (Parikka et al. 2015), cross-linking (Gliko-Kabir et al. 1998), enzymatic hydrolysis (Cheng et al. 2002), and grafting (Tiwari and Prabaharan 2010). The physiochemical properties of modified GM (Wientjes et al. 2000; Sandolo et al. 2007) are utilized in various technological fields, such as for colon-specific drug delivery (Gliko-Kabir et al. 2000) and in controlled drug delivery systems (Prabaharan 2011; Aminabhavi et al. 2014).

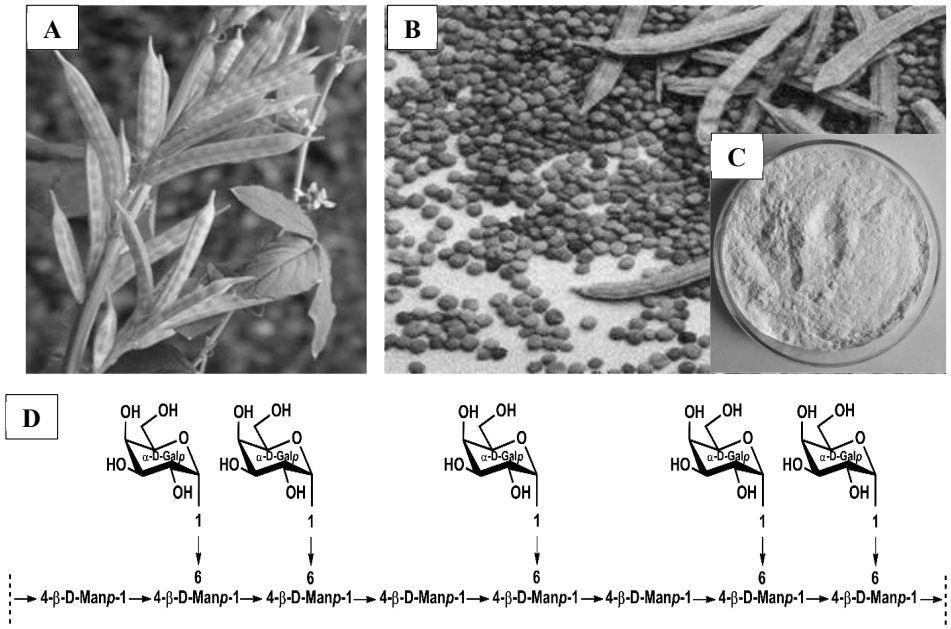

Figure 1: A) Guar (*Cyamopsis tetragonoloba*) plant, B) guar seed, and C) guar gum powder. D) The partial structure of guar galactomannan (GM). The terminal galactosyl unit is highlighted by the ring structure. Photos A, B, and C are licensed for non-commercial use.

2.1.2 Tamarind seed xyloglucan

The tamarind tree (*Tamarindus indica*) is widely present in the tropics and in subtropical regions. The fruit of the tamarind tree is pod-like (Figure 2A) and contains a fleshy part and seeds with a very hard covering (Figure 2B). Tamarind seeds are the by-product of the tamarind industry, and they contain almost 60% xyloglucan, making them a commercial and abundant source of xyloglucan (Figure 2). Other sources of xyloglucans are *Detarium senegalense*, *Afzelia africana*, and *Jatoba* (Kochumalayil et al. 2010).

Tamarind seed xyloglucan (XG) is composed of a β-(1→4)-D-glucosyl (Glc*p*) backbone chain (48%) that is partially substituted by α-(1→6)-D-xylopyranosyl (Xyl*p*) (36%). Some of the xylose residues are further substituted by β-(1→2)-D-galactosyl (Gal*p*) units (16%) (Table 1, Figure 2D) (Mishra and Malhotra 2009). XG is a water-soluble, seed-storage polysaccharide (non-starch). Picout et al. reported that the individual macromolecules do not tend to fully hydrate, and therefore, supramolecular chain aggregations were found in very dilute aqueous solutions of XG (Picout et al. 2003). XG can form different chain conformations in aqueous solutions, such as a cross-like

conformation when aggregated, parallel-like assemblies, and rope-like structures, as well (Kozioł et al. 2015).

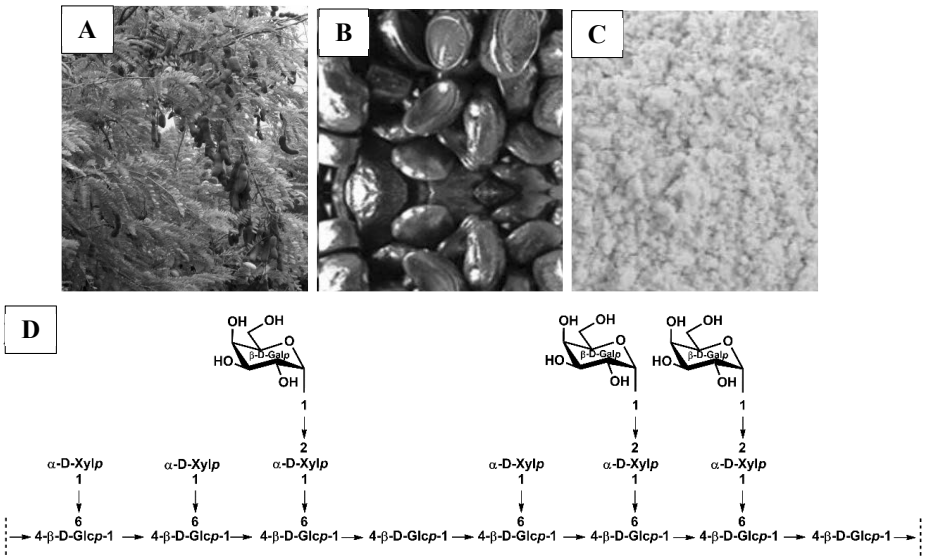

Figure 2: A) Tamarind seed (*Tamarindus indica*) plant, B) tamarind seeds, and C) xyloglucan powder from the tamarind seed. D) The partial structure of tamarind seed xyloglucan (XG). The terminal galactosyl unit is highlighted by the ring structure. Photos A, B, and C are licensed for non-commercial use.

XG in solution can form a gel through enzymatic degradation by β-galactosidase (Shirakawa et al. 1998) or through the addition of alcohol, polyphenols, or an iodine solution (Yuguchi et al. 2004). XG formed a thermally responsive gel when more than 35% of the galactose from the side chain was cleaved using fungal enzyme β-galactosidase (Shirakawa et al. 1998; Brun-Graeppi et al. 2010), and this can be thermo-reversible upon cooling. A higher percentage of galactose removal increased the temperature range of gelation for XG (Shirakawa et al. 1998). XG is commonly used in food and cosmetics as a gelling agent, an emulsion stabilizer, or as thickener (Mishra and Malhotra 2009) due to its excellent stability to heat and acids. It is also used as a wet-end additive in the paper industry (Mishra and Malhotra 2009). Ocular film from XG can be used for the delivery of ocular drugs, such as ciprofloxacin (Mahajan and Deshmukh 2015). Recently, XG became an attractive biopolymer for the preparation of biodegradable films for the controlled release of drugs (Simi and Abraham 2010; Kochumalayil et al. 2010; Cerclier et al. 2013).

2.1.3 Nanofibrillated cellulose

Cellulose is the most abundant, renewable, and biodegradable natural biopolymer present on earth. It is the main structural component of plants, with an annual production of 7.5 x 10^{10} tons (Habibi et al. 2010). Cellulose is also present in tunicate animals, and some bacteria are also capable to produce extracellular cellulose (de Souza Lima and Borsali 2004). It is a linear-chain polysaccharide, and the degree of polymerization (number of monomeric units in a polymer) in wood cellulose is approximately 10,000 glucose units (John and Thomas 2008). In plant cell walls, cellulose plays a structural role and provides strength and flexibility to the plants. Plant cellulose regained scientific interest recently due to its hierarchically ordered material. Cellulose is present as aggregates of microfibrils (elementary supramolecular units of cellulose), with each microfibril having diameter of 3–4 nm in wood and about 20 nm in some algae, and stretching to several tens of micrometers in length. Each microfibril consists of alternating crystalline and disordered parts (Nishiyama et al., 2013). Turbak et al. reported the isolation of cellulose microfibrils from wood pulp for the first time (Turbak et al. 1983). Recent developments in the technology and methodology have been used to obtain high-quality, nano-sized cellulose fibers from cellulose fibrils aggregates (Nakagaito and Yano 2004; Pääkkö et al. 2007; Pääkkö et al. 2008). A high-shear homogenization or refining process, often in combination with enzymatic or chemical pre-treatment of the pulp, is used (Zimmermann et al. 2010; Abdul Khalil et al. 2014; Lee et al. 2014). Pre-treatment using enzymes (cellobiohydrolases and endoglucanases) and chemicals (alkaline-acid) helps to lower the energy consumption and degrades or modifies the lignin and hemicelluloses that improve the fibrillation during mechanical processing (Henriksson et al. 2007; Alemdar and Sain 2008). Currently, the more commonly used chemical pre-treatment is TEMPO (2,2,6,6-tetramethylpiperidine-1-oxly radical)-mediated oxidation (Isogai et al., 2011; Missoum et al., 2013). NFC, after mechanical disintegration, forms an entangled network in aqueous suspensions that behaves like a gel due to physical gelation (Figure 3) and creates highly intertwined structures upon freeze drying.

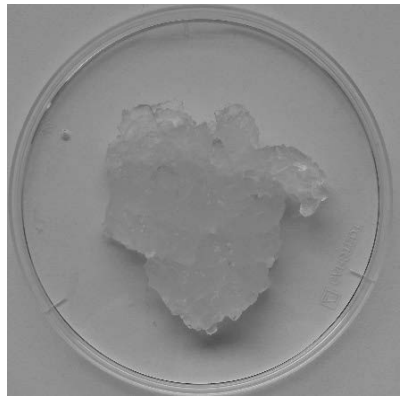

Figure 3: Anionic nanofibrillated cellulose gel (2.65 wt.% dry content).

NFC is also called microfibrillated cellulose, cellulose nanofibrils, or cellulose nanofibers (Zimmermann et al. 2010; Abdul Khalil et al. 2014). The term nanofibrillated cellulose, or NFC for short, is used in this study. NFC is a nano-sized cellulose fiber whose diameter is nanometer in scale (≤100 nm) and can be several micrometers long (Nechyporchuk et al. 2014). NFC shows excellent mechanical properties; the Young's modulus of a single NFC crystal was measured to be 134 GPa, and the strength was in the range of GPa (Nishino et al. 1995). NFC is widely studied for the preparation of novel functional materials (Eichhorn et al. 2010; Gómez H. et al. 2016) for various applications, such as materials for controlled release, scaffolds, and matrices for cell growth

in bio-medical fields (García-González et al. 2011); materials for thermal insulation (Kobayashi et al. 2014); and as a support for catalysis (Xiong et al. 2013). Increasing interest in the development of high-performance biocomposites makes NFC a next-generation renewable reinforcement in the polymer matrix (Zimmermann et al. 2010; Peng et al. 2011; Cai et al. 2012; Lee et al. 2014; De France et al. 2017).

2.2 Hydrogels

A gel is defined as a 3D network of polymers that absorbs and holds a large amount of solvent. The term "network" infers the physical or chemical cross-links needed to maintain the polymeric structure of hydrophilic groups or domains to avoid dissolution in the aqueous phase. Gels are called hydrogels when the solvent is water (Ahmed 2015). Chemical cross-linking methods involve the introduction of permanent linkages (covalent bonding) via a cross-linking agent. Physical cross-linking can result in noncovalent interactions or combinations of hydrogen bonding, van der Waals, electrostatic, hydrophobic, and stereo-complexation interactions (Ikada et al. 1987; Hirschberg et al. 2000; de Jong et al. 2001; Reches and Gazit 2003). Hydrogels are characterized by an ability to retain a significant amount of water or biological fluids under physiological conditions and behavior similar to soft, living tissues, which make them interesting materials.

Hydrogels can be prepared from natural, synthetic polymers and their blends. Natural polymers, mainly plant polysaccharides, have received much attention from researchers because they are economical and readily available (Nisbet et al. 2006; Coviello et al. 2007; Sandolo et al. 2007; Leone and Barbucci 2009; Borges et al. 2011; Yang et al. 2013; Li et al. 2015). Many polysaccharides in aqueous solutions form intra- and inter-molecular associations, and their functional groups, such as hemiacetal oxygens, hydroxyls, or methyl groups, undergo hydrogen bonding or van der Waals forces of attraction formation. These interactions lead to viscous solutions or gel formation. For example, NFC forms a gel at different concentrations due to hydrogen bonding (Pääkkö et al. 2007). The chain mobility of β-glucan in aqueous solutions and inter- and intra-chain hydrogen bonding results in gel formation (Lazaridou and Biliaderis 2007). Although, all native polysaccharides do not naturally form a gel, they can be cross-linked using various cross-linking techniques to induce gel formation. The gel-forming ability of polysaccharides is used in different applications, such as foods, cosmetics, pharmaceuticals, tissue engineering, and bio-based material development – like for aerogels (Mikkonen et al. 2013; Tako 2015).

Polysaccharides are diverse in nature and carry various functional groups (acetamido, amino, carboxyl, and/or hydroxyl groups) and have various backbone chain-length repeating units. The structural diversity allows them to be used for the creation of hydrogels with various functionalization techniques, such as chemical modification, enzymatic oxidation, and reinforcement with other biopolymers (Salam et al. 2011; Cumpstey 2013; Köhnke et al. 2014; Mikkonen et al. 2014; Alakalhunmaa et al. 2016; Qi et al. 2016; Karaki et al. 2016). Hydrogels

from polysaccharides have many advantages over synthetic polymers due to their peculiar physicochemical properties that are suitable for many applications, particularly in drug delivery systems (Coviello et al. 2007); biomedical applications, such as soft-tissue regeneration and the delivery of biologically active substances (Coviello et al. 2007; Leone and Barbucci 2009; Van Vlierberghe et al. 2011; Yuan et al. 2013); and in food materials (Liu et al. 2012).

Polysaccharide-based hydrogels have recently attracted attention for the development of biomaterials (Das et al. 2011; Coma 2013; de Souza et al. 2013). The mechanical properties and brittleness of traditional, physically cross-linked hydrogels limit their applications in biomaterials (Gong 2010). To overcome these limitations, polysaccharides were chemically cross-linked with glutaraldehyde, phosphate, and borate to form elastic and mechanically strong hydrogels (Gliko-Kabir et al. 1998; Gliko-Kabir et al. 2000; Burruano et al. 2002). Hydrogels with enhanced mechanical properties were also prepared from quaternized polysaccharides and acrylic acid by free radical copolymerization in the presence of *N,N′*-methylenebisacrylamide as a cross-linker (Qi et al. 2016).

Chemical modifications of polysaccharides seem easy, quick, and introduces the required properties to the polysaccharides. However, the main drawback of this technique is the toxicity of the chemical reagents used and the lack of selectivity in their reaction which may results in side product formation (Cumpstey 2013). Therefore, chemically modified polysaccharides possess a risk when these products are considered for food and human contact-related applications. For example, there is a paradox associated with the cytotoxicity of glutaraldehyde-cross-linked materials in that the cytotoxicity depends on the concentration of the glutaraldehyde (Reddy et al. 2015). Periodate oxidation of polysaccharides resulted in depolymerization, like in the case of alginate and chitosan reviewed by Cumpstey (Cumpstey 2013). Also, periodate is unstable and decomposes in the presence of light to form free radicals. Polysaccharides possess diverse functional groups, so the regioselectivity of the reaction is very important for polysaccharide modifications (Cumpstey 2013) to prevent the formation of side products, such as regioisomers, di-substituted, or tri-substituted products, etc. The product is also required to be purified from the mixture by crystallization or chromatographic techniques. The purification of the modified polysaccharide is always difficult and often impossible because the selectively- and non-selectively-modified monosaccharide residues are covalently linked to each other. Therefore, regioselective modification reactions are preferred for polysaccharide modifications. To avoid the limitations caused by the chemical modification of polysaccharides, efforts were diverted towards more environmentally friendly modification techniques.

Enzymatic modifications have been explored intensively in the last decade as alternatives to chemical reagents for the structural modification of polysaccharides, and hence, the properties of these materials (Cheng and Gu 2012; Karaki et al. 2016). Most enzymes are chemo-specific, regio-specific, and/or enantio-specific in their reaction, which allows the formation of a distinct product with desired properties and a fixed structure (Cheng and Gu 2002; Gu and Cheng 2005; Cheng and

Gu 2012; Karaki et al. 2016). Furthermore, the enzymatic reaction requires mild reaction conditions as compared to a chemical reaction (Cheng and Gu 2012; Karaki et al. 2016). Enzymatic modification has been successfully applied to the modification of polysaccharides such as chitosan, cellulose, pectin, and starch (Karaki et al. 2016). Enzymatic cross-linking has also been extended to other polysaccharides, such as galactose-containing polysaccharides (Parikka et al. 2010), and has even been used in combination with chemical modification to introduce additional functionality (Parikka et al. 2012b; Parikka et al. 2015).

2.2.1 Galactose oxidase

Galactose oxidase (GaO, EC 1.1.3.9) is a single copper-containing enzyme that has a molecular weight of 65–68 kDa (Whittaker 2003). GaO catalyzes the stereospecific oxidation of the hydroxyl group present on the C-6 galactosyl unit and the formation of the corresponding aldehyde (Figure 4). During the GaO-catalyzing oxidation, there is a formation of different side products (Figure 5), which were reviewed by Parikka et al. (2015). The C-6 oxidized galactose derivatives are important starting materials for further chemical conversions. GaO-catalyzed product has been utilized for further applications such as oxidation to carboxylic acid (Frollini et al., 1995) or reductive amination (Yalpani and Hall 1982). For example, uronic acid, deoxy sugars, allylated galactose, and N-acetyl lactosamines can be derived from mono- and oligosaccharides (Schoevaart and Kieboom 2004; Parikka et la., 2015). GaO has also been studied as a cross-linker for proteins with D-galactose dialdehyde (Schoevaart and Kieboom 2002). GaO has been widely studied for the catalyzed oxidation of mono- and oligosaccharides, and these studies have resulted in several patents and patent applications, as reviewed by Parikka et al. (2015). During the catalytic reaction, GaO uses molecular oxygen from the environment as an oxidant. The catalytic reaction includes oxidative and reductive half reactions. In the oxidative reaction, primary alcohols are oxidized, and in the reductive reaction, dioxygen is reduced to hydrogen peroxide (Whittaker 2003). The substrates for GaO are e.g. mono- and oligosaccharides containing primary hydroxyl group, such as D-galactose, and polysaccharides containing D-galactosyl units with free C-6 hydroxyl groups at their branches.

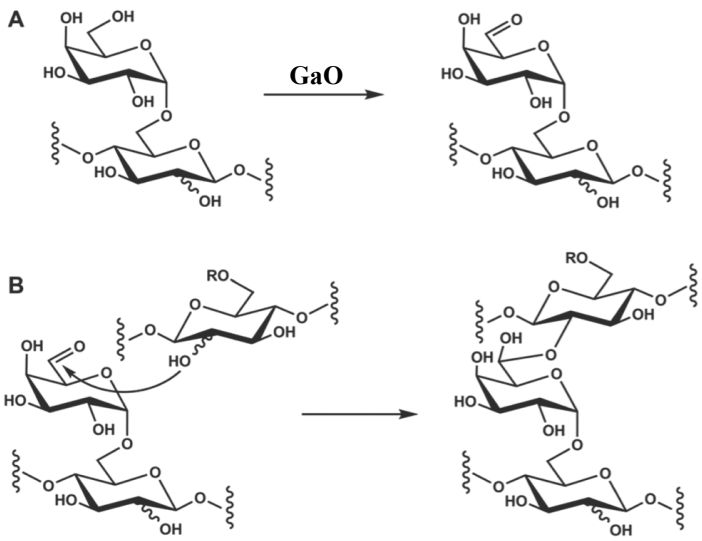

Figure 4: A) GaO-catalyzed oxidation of the galactose units of polysaccharides. B) An example of the proposed mechanism for the cross-linking of the products, hemiacetal bond formation. R = H or galactosyl unit. Adopted from Parikka et al. 2012.

GaO has been studied on several substrates, like D-galactose, methyl α- and β-D-galactopyranoside, lactose, lacitol, lactulose, lactobionic acid, melibiose, and raffinose (Siebum et al. 2006). Studies were carried out using two enzymes, GaO and catalase, under oxygen atmospheres, and the conversion rate was 100% for galactose monosaccharides and galactose-containing oligosaccharides with the exception of lactose and lactobionic acid, where the conversion rates were 10% and 20%, respectively. Many polysaccharides contain oxidizable galactosyl units, such as GM (40% oxidizable galactosyl units), locust bean gum (20% oxidizable galactosyl units), and XG (16% oxidizable galactosyl units), etc., that have been oxidized using GaO (Frollini et al. 1995). The optimized reaction conditions for GaO were first reported by Parikka et al. using methyl α-D-galactopyranoside as the monosaccharide model system in water instead of using buffer solution (Parikka and Tenkanen 2009). This study also showed that formation of side product is minimized with the optimized reaction conditions and higher yield of aldehyde is obtained. The optimized reaction conditions using GaO were studied on the oxidation of galactose-containing polysaccharides, such as GM, spruce galactoglucomannan, XG, arabinoxylan from corn, and arabinogalactan from larch, in detail (Parikka et al. 2010). In this study, GC-MS analysis showed that there was no side product formation such as galacturonic acid, which was the major side product in earlier study (Parikka and Tenkanen 2009).

GaO catalyzes the oxidation of primary hydroxyl groups at C-6 of terminal galactosyl units in higher molar mass polysaccharides (GM, locust bean gum, and XG) into aldehyde groups. The aldehyde groups enable cross-linking through hemiacetal bonds (Figure 4), and thus, the formation of hydrogels (Parikka et al. 2012a). As the enzymatic oxidation proceeds, the aldehyde group produced is simultaneously cross-linked via hemiacetal bonds to the neighboring suitable hydroxyl group of the polysaccharide chain (Parikka et al., 2010) and the viscosity of the polysaccharide solution increases. The enzymatic oxidation reactions started soon after the addition of GaO to the polysaccharide solution. Therefore, hydrogels with varying consistency (weak to strong gel) can be obtained by controlling the oxidation time and inactivation of enzyme by heating the hydrogel. Thee catalytic activity of GaO for galactose-containing polysaccharides in the presence of reinforcement agents has not been exploited to form a composite hydrogel.

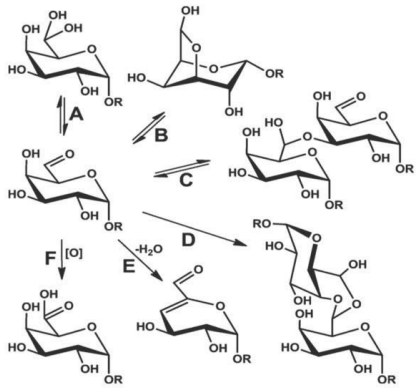

Figure 5: Formation of side products in the GaO-catalyzed oxidation. A) hydrate; B) intramolecular hemiacetal; C) intermolecular hemiacetal; D) dimer; E) α,β- unsaturated aldehyde; F) galacturonic acid. R = H/Me/oligo- or polysaccharide backbone. Adopted from Parikka et al., 2015.

2.3 Aerogels

Aerogel is an advanced, highly porous, and lightweight solid material. The history of the aerogel started in 1931 when Kistler prepared a solid foam from silica using a supercritical CO_2 drying technique, which allowed the retention of the gel network in a dry state (Kistler 1931). The inventor named it “aerogel” (air + gel).

Although this material exhibited some excellent properties, nevertheless, it did not get broad attention from researchers until 1970. After that, research on aerogels become a subject of debate that resulted in several polymers being studied as aerogel-forming materials, which lead to the

development of new formation methods and drying techniques (Du et al. 2013). However, aerogel formation involves three common steps, as shown in Figure 6 (Zha and Roggendorf 1991). All of the steps in the aerogel formation are very important, as each will affect the properties and applications of the aerogels. In the literature, there are many drying methods reported for aerogel formation, such as ambient drying, surface-modified ambient drying, solvent-replaced ambient drying, lyophilization, high-temperature supercritical drying, and low-temperature supercritical drying. (Du et al. 2013).

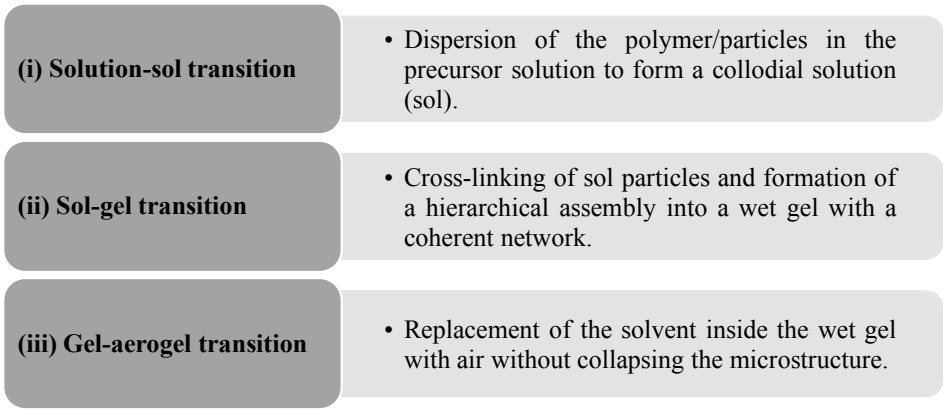

Figure 6: The three basic steps in aerogel formation.

The unique porous structure of aerogels depends on the type of aerogel-forming material, the preparation method, and the drying technique. The use of term "aerogel" for porous materials is still in debate. After its original development, Quignard et al. described the aerogel as "a gel that has been dried and retains the dispersion of the wet state" (Quignard et al. 2008). However, the highly porous and low-density solid materials are called either aerogels from supercritically dried gels (Kistler 1931), cryogels from freeze-dried/lyophilized gels (Lozinsky et al. 2003), or foams (Han et al. 2013). Regardless, the term "aerogel" is becoming accepted for low-density and highly porous solid structures, no matter if they are lyophilized or supercritically dried (Figure 7) (Du et al. 2013; Borisova et al. 2015). Therefore, in this thesis, the term "aerogel" is used for both lyophilized and supercritically dried material. Lyophilization and supercritical CO_2 drying are widely used drying techniques for aerogel formation.

2.3.1 Lyophilization

Lyophilization (freeze-drying) is a straightforward and versatile method to produce aerogels. In lyophilization, the liquid phase (water) of the hydrogel/gel is pre-frozen, and ice crystals of varying sizes and shapes are formed. The lyophilization process involves the removal of the ice crystals from the materials through sublimation at a low atmospheric pressure. Sublimation involves the

conversion of solids (ice crystals) directly into a vapor/gaseous state without first going through the liquid (water) phase. The resulting morphologies of the obtained aerogels are the direct replica of the size and shape of the ice crystals formed during the freezing process, which mostly depend on the freezing temperature (Barros et al. 2016).

The simplicity of the lyophilization process permits more control for tailoring and designing the porosity of the aerogels for specific applications (Borisova et al. 2015). For example, controlling the freezing temperature and freezing direction (unidirectional freezing) can produce either small pore sizes, honeycombs, or lamellar morphologies (Mukai et al. 2004; Nishihara et al. 2005; Deville et al. 2006; Deville et al. 2007; Gutiérrez et al. 2008). In unidirectional freezing, the gel or suspension is in contact with the freezing medium from one side, and the growth of ice crystals is allowed perpendicular to the freezing medium, which results in the alignment of the gel or suspension structure in the freezing direction. Supercritical CO_2 drying does not provide such control over the porous structure modification. Lyophilization is extended to various types of polymers (Deville et al. 2007; Gutiérrez et al. 2008; Pawelec et al. 2014; Deville et al. 2015) for the development of aerogels. The unidirectional ice-templating process can be used to align the structure to optimize the mechanical properties (Lee and Deng 2011; Pourhaghgouy and Zamanian 2015; Martoïa et al. 2016). Lyophilization is simple and allows for the tailoring of the porous structure, but due to large pore sizes, lyophilized aerogels are limited in their use for applications that require small porous structures and high surface areas.

2.3.2 Supercritical CO_2 drying

The supercritical CO_2 (sc-CO_2) technique is well known for preserving the micro- and mesoporous structure of the gel. The characteristic morphology of the sc-CO_2-dried aerogels consists of small pores in the range of tens of microns to a nanometer (García-González et al. 2012; Błaszczyński et al. 2013). In sc-CO_2 drying, the liquid phase (water) of the hydrogels is first replaced with a solvent that is compatible with the hydrogel's structure as well as with the supercritical CO_2. The solvent is extracted at the supercritical conditions of the CO_2, which leaves behind a dried gel with a high porosity. The compatibility of the solvent with the hydrogel structure and the miscibility of that solvent with the sc-CO_2 are considered very critical in sc-CO_2 drying to avoid collapsing the 3D structure of the dried gel (Raman et al. 2015b).

sc-CO_2 drying is mostly used for the preparation of inorganic and organic aerogels in the laboratory (Kistler 1931, Tewari, Hunt et al. 1985, Tsioptsias, Stefopoulos et al. 2008, García-González, Camino-Rey et al. 2012b, Błaszczyński, Ślosarczyk et al. 2013), and it is also used for the large-scale production of silica aerogels (Perrut 2000). Industrial sc-CO_2 drying can be optimized economically so that the CO_2 is recycled and reused. sc-CO_2 drying has also been applied to the preparation of aerogels from polysaccharides, such as agar (Brown, Fryer et al. 2010), alginate (Mallepally, Bernard et al. 2013, Gurikov, Raman et al. 2015), starch (García-González, Camino-Rey et al. 2012b), and cellulose (Fischer, Rigacci et al. 2006, Liebner, Potthast et al. 2008, Buchtová, Budtova 2016).

The sc-CO_2 drying of polysaccharide gels, such as those from calcium-alginate, chitosan, and potato starch, caused considerable volumetric shrinkage ranging from 60 to 85% (Quignard et al. 2008; Mehling et al. 2009; Raman et al. 2015b). The volumetric shrinkage depended on the pre-history of the gels, such as the concentration of the polymers, cross-linking technique, and solvent-exchange procedure. Using sc-CO_2 drying technology widens the potential applications of polysaccharide-based aerogels. However, the selection of a solvent with a good compatibility with the hydrogel's structure is very important to keep the high volume to mass ratio for low-density aerogels. Some solvents exhibit a good compatibility with the hydrogel's structure, but these solvents can be difficult to extract with sc-CO_2 due to their low miscibility with supercritical fluid (Raman et al. 2015b). Polysaccharide-based hydrogels cross-linked via enzymatic oxidation have not been reported for sc-CO_2 drying to prepare aerogels.

2.3.3 Polysaccharides as an aerogel-forming matrix

Polysaccharides are abundant in nature, though the physicochemical properties of native polysaccharides are not always optimal for different applications. By applying various modification techniques, such as enzymatic oxidation and chemical modifications, their properties can be enhanced or altered to suit the application purposes (Cumpstey 2013; Parikka et al. 2015). For example, the gel-forming ability of modified polysaccharides can be utilized for the development of aerogels (Soderqvist Lindblad et al. 2005; Liebner et al. 2008; Quignard et al. 2008; Mikkonen et al. 2013; Buchtová and Budtova 2016). The sustainability, biodegradability, and biocompatibility of the polysaccharides in combination with the required technical properties of aerogels make them advantageous materials over inorganic polymers (Mehling et al. 2009; Mikkonen et al. 2013; Stergar and Maver 2016). Many polysaccharides have been studied for aerogel formation, particularly marine-based ones, such as alginate and chitosan (Quignard et al. 2008). From plant polysaccharides, cellulose and its derivatives are widely studied as aerogel-forming materials (Fischer et al. 2006; Liebner et al. 2008; Buchtová and Budtova 2016). Examples of other plant polysaccharides that are used include starch (Lotfinia et al. 2013; Ago et al. 2016), GM, and XG (Mikkonen et al. 2014).

The performance of aerogels is enhanced/altered with the addition of a reinforcing agent. For example, their performance can be enhanced by producing composite aerogels with biopolymer reinforcement, such as through the use of NFC (Cai et al. 2012; Sedighi Gilani et al. 2016) and chitosan (Wang et al. 2015). Sehaqui et al. reported that composite aerogels made from NFC as the main matrix material with xyloglucan resulted in improved mechanical properties (Sehaqui et al. 2009).

2.3.4 Properties of polysaccharide-based aerogels

Morphology, including porosity, pore size, pore size distribution, and surface area, as well as mechanical properties are the key characteristics of the aerogels that determine their applications

in different fields. These characteristic properties depend on the types of starting materials, cross-linking methods, reinforcement, and drying methods.

Aerogels prepared by lyophilization mostly do not show volumetric shrinkage and preserve the intact volume that leads to low-density aerogels. Calcium-alginate aerogels produced by the internal gelation method and barley β-glucan prepared by lyophilization showed densities of 0.023 g/cm^3 and 0.17 g/cm^3, respectively (Cheng et al. 2012; Comin et al. 2012). GM and XG aerogels prepared via enzymatic oxidation followed by lyophilization showed densities in the range of 0.012 to 0.016 g/cm^3 (Mikkonen et al. 2014). The sc-CO_2 drying of polysaccharide aerogels involves volumetric shrinkage during both the solvent exchange step and the drying process. Raman et al. reported the volumetric shrinkage values for calcium-alginate (1 wt.%) hydrogels were 71% and 53% after solvent exchange in ethanol and DMSO, respectively (Raman et al. 2015b). The gels from calcium-alginate (2 wt.%) and potato starch (12.5 wt.%) showed volumetric shrinkages of 64% and 77%, respectively, after solvent exchange in ethanol (Mehling et al. 2009). Literature has shown that sc-CO_2 drying can cause considerable volumetric shrinkage for polysaccharide aerogels, such as those from calcium-alginate, chitosan, and potato starch, which were in the range of 60 to 85% (Quignard et al. 2008; Mehling et al. 2009; Raman et al. 2015b). However, the volumetric shrinkage is based on the type of gel, such as the polymer type, the concentration, cross-linking technique, and the solvent-exchange procedure. Due to the volumetric shrinkage of sc-CO_2-dried aerogels, their density values are slightly higher compared to lyophilized aerogels. sc-CO_2-dried aerogels from cellulose in ionic liquid, cellulose and lignin in ionic liquid, barley β-glucan, starch from potato starch, and starch from corn starch, etc., showed density values in the range of 0.048 to 0.46 g/cm^3 (García-González et al. 2011; Mikkonen et al. 2013).

In lyophilization, the pore size is dependent on the size of the ice crystals formed during the freezing process, so the pores of lyophilized aerogels were in the range of a few hundred to several hundred micrometers. For example, starch-based composite aerogels with lignin-containing NFC (3 wt.% amylopectin and 3 wt.% NFC) had pore sizes in the range of 100 to 250 μm (Ago et al. 2016). Chemically cross-linked spruce galactoglucomannan-composite aerogels reinforced with NFC showed pore sizes between 50 and 100 μm in size, prepared by unidirectional ice-templating followed by lyophilization (Alakalhunmaa et al. 2016). However, sc-CO_2-dried aerogels exhibited much smaller pore sizes, in the range of a few micrometers to a few hundred nanometers, as compared to lyophilized aerogels (Figure 7). Lyophilized aerogels, due to the larger pore size, had low specific surface areas as compared to sc-CO_2-dried aerogels. Because of this, the specific surface area of polysaccharide aerogels can have a very wide range, starting from 10 m^2/g for lyophilized aerogels and increasing to 845 m^2/g for sc-CO_2-dried aerogels (García-González et al. 2011; Mikkonen et al. 2013; Sehaqui et al. 2010).

Polysaccharide-based aerogels are mostly ductile and flexible (Pääkkö et al. 2008; Mikkonen et al. 2014) and exhibit high adsorption capacity. Starch-based aerogels prepared with lignin-containing NFC showed a water absorption capacity of 12 g/g (Ago et al. 2016). Spruce galactoglucomannan

aerogels reinforced with NFC can absorb water up to 34 g/g while the GM and XG aerogels showed water absorption capacities up to 40 g/g (Mikkonen et al. 2014; Alakalhunmaa et al. 2016). Polysaccharide-based aerogels displayed repeatable shape recovery after squeezing out the water and re-immersing them again in water (Li et al. 2016; Alakalhunmaa et al. 2016). Polysaccharide-based aerogels also showed shape repeatability in dry state. Composite aerogel (2 wt.% dry content) prepared from NFC and modified carbon nanotubes showed the reversible recyclability properties up to 100 cycles when it was compressed to the strain of 8 %. Only small change was reported between first compression cycle hysteresis and last compression cycle hysteresis (Wang et al., 2016).

Although polysaccharide-based aerogels are not very strong materials compared inorganic aerogels, they still possess very good mechanical properties that can be tailored by adjusting the processing conditions (Mikkonen et al. 2014) and through the addition of reinforcing agents to make composite aerogels (Köhnke et al. 2012). Spruce galactoglucomannan (GGM) and NFC (2 wt.%; GGM:NFC=70:30 ratio) composite aerogels prepared by lyophilization exhibited compressive modulus of 177 kPa (Alakalhunmaa et al., 2016). Lyophilized Xylan (5 wt. %) – cellulose (1.25 wt.%) composite aerogels showed the compressive modulus of 285 kPa. Thermal conductivity of the solid material is largely based on solid fraction of the material because large amount of heat transported via solid conduction. Therefore, the materials for insulation is preferred to have small amount of solid fraction. This can only be achieved by creating porous structure in the solid material. Polysaccharide-based aerogels exhibit low thermal conductivity due to their high porosity (> 90 %). For example, the thermal conductivity of high-methoxyl pectin (porosity 96.6 %), low-methoxyl pectin (porosity 97 %), xanthan (porosity 94.9 %) , alginate (porosity 95 %), and guar gum (porosity 86.9 %) aerogels were in the range of 18 to 89 mW $m^{-1}K^{-1}$ (Rudaz et al. 2014; Horvat et al. 2017). The properties of different plant polysaccharide-based aerogels are presented in Table 2.

The morphology of aerogels is characterized using microscopic techniques and N_2-physisorption methods (Robitzer et al. 2011a; Robitzer et al. 2011b). Both techniques are widely used for the characterization of morphology, though both techniques have limitations. The macroporous structure of the lyophilized aerogels limits the determination of the porosity (pores ca. > 50 nm in diameter) of the aerogels using N_2-physisorption due to the large pore size of several hundred micrometers (Sing et al. 2008; Robitzer et al. 2011a). Most of the aerogels prepared by lyophilization have a macroporous structure (Podlipec et al. 2014; Borisova et al. 2015). According to the IUPAC system, porous material is categorized into microporous material, which has a pore diameter < 2 nm, and macroporous material with a pore diameter > 50 nm, while mesoporous material has a pore diameter > 2 nm but < 50 nm (Rouquerol et al. 1994). In addition, the N_2-physisorption method does not provide information about the shape of the pores. However, coupling physisorption data with scanning electron microscopy provides a better understanding about the shape of the surface and pores (Robitzer et al. 2011a).

Currently deployed probing techniques for the structural characterization of aerogels, such as scanning electron microscopy (SEM) and focused ion beam SEM (FIB-SEM), are limited to surface-level characterizations. It is still difficult to characterize the actual representation of the 3D structure of the aerogels, the connectivity of the pores, the pore-size distribution, and the interface of the polymer reinforcement within the aerogel matrix. Recent advancements in experimental techniques, such as synchrotron X-ray microtomography (XMT) enable the visualization and quantification of the 3D morphology of the materials at the micron and sub-micron levels. The XMT technique has been used across several disciplines, including physics, materials science,

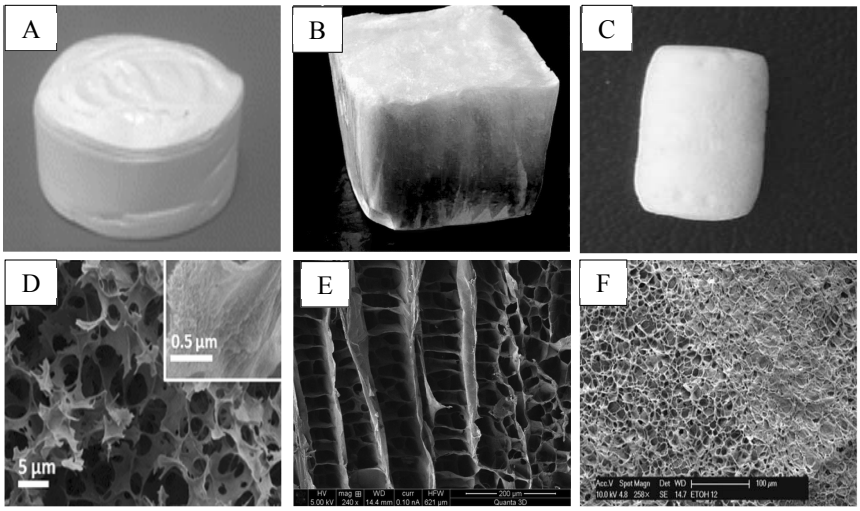

Figure 7: Images and cross-sections of polysaccharide aerogels produced using various methods. (A) Lyophilized aerogel from regenerated cellulose (D) and the cross-sectional view of its porous structure. (B) Lyophilized aerogel from oxidized guar galactomannan (GM) prepared by unidirectional ice-templating (E) and the cross-sectional view of its porous structure. (C) Supercritical CO_2-dried aerogel from regenerated cellulose (F) and the cross-sectional view of its porous structure. The figures are adopted from: Buchtová and Budtova, 2016 (A & D); Mikkonen et al. 2014 (B & E); and Liebner et al. 2008 (C & F).

medicine, and powder technology, to illustrate the detailed internal structure of a material (Moreno-Atanasio et al. 2010). The XMT technique is also extended to aerogels (Köhnke et al. 2012; Mikkonen et al. 2014; Sedighi Gilani et al. 2016) but has not yet been used to its full potential for the quantitative measurement of morphological parameters, such as pore size and pore wall thickness distributions. A detailed study of the qualitative and quantitative morphology of aerogels is desirable, as the pore size and its distribution in the aerogel's structure are critical parameters in biomedical applications as a scaffold for soft-tissue regeneration (Ikada 2006) because the minimum pore size of the scaffold must exceed the cell size; otherwise, the penetration of the cells into the scaffold is compromised. The interconnectivity of the pores is an asset of the aerogel that facilitates the movement of nutrients and oxygen to the growing cells, as well as the transportation of metabolic products from the cells.

2.3.5 Applications of polysaccharide-based aerogels in life sciences

The unique properties of aerogels make them fascinating materials for modern industrial applications. Polysaccharides are abundant in nature, and their sustainability and biodegradability in combination with aerogel's technical properties make them advantageous materials over other polymers (Mehling et al. 2009). Thus, polysaccharides as aerogel-forming materials show great potential, with very vast usability and applicability in life sciences. García-González et al. reviewed the potential of polysaccharide-based aerogels in the pharmaceutical industry and discussed their production technologies and the processing conditions that govern the material's end properties (García-González et al. 2011). Stergar and Maver (Stergar and Maver 2016) discussed the perspective of aerogels in biomedical applications in relation to their properties. The potential of polysaccharide-based aerogels in the food industry and food-related applications with respect to their properties and preparation were reviewed by Mikkonen et al. (Mikkonen et al. 2013).

The utilization of polysaccharide-based aerogels as food materials requires the safety assessment of aerogels. Although polysaccharides themselves are safe for human consumption as food, one needs to make sure there is no side-product formation during the cross-linking step (enzymatic or chemical). Initially, polysaccharide-based aerogels can be used as food-packaging materials (secondary packaging) due to their ductile and elastic structure with good mechanical stiffness. Polysaccharide-based aerogels can absorb large amount of water while maintaining their structural integrity and can be used in fresh meat packaging applications, to absorb the water (drip loss) which came out from meat. Starch foams prepared from high-amylose starch with encapsulated plant essential oils used as active packaging to extend the shelf life of packed bread presented a practical application of polysaccharide-based aerogels (Lotfinia et al. 2013). More recently, a patent application on the loading of flavor into aerogels and flavor-impregnated, food-grade aerogels was reported by Yan et al. (Yan et al. 2016). Véronique Coma reviewed polysaccharide-based biomaterials in the context of antimicrobials and their antioxidant properties for food-packaging applications (Coma 2013). Other possible applications include serving as a carrier for active ingredients and a supporting material for catalysts. Aerogels from barley β-glucan were suggested as carriers for nutraceuticals, and these aerogels were studied as carriers of flax oil (Comin et al. 2012). Silica aerogels were studied for the encapsulation of microbes, such as *Saccharomyces cerevisiae* (Pope 1995), or for the immobilization of enzymes, such as lactate dehydrogenase, in the silica porous structure (Ramanathan et al. 1997). Polysaccharide-based aerogels have the potential to replace silica-based aerogels for such applications.

Due to the highly porous structure and low thermal conductivity of polysaccharide-based aerogels (Rudaz et al. 2014; Horvat et al. 2017), some studies have pointed out their application as thermal insulators (Duong and Nguyen 2016; Horvat et al. 2017), and flame retardants can be incorporated into the aerogel matrix (Fan et al. 2017). In the food industry, the thermal-insulating properties of polysaccharide-based aerogels can be utilized to replace polystyrene-based materials for

controlling the temperature of hot or chilled food. Other advantages of polysaccharide-based aerogels over polystyrene is the biodegradability. In addition, polysaccharide-based aerogels are elastic in nature, and their shape-recovery properties can be utilized for environmental applications, for example, sodium alginate-NFC composite aerogels with hydrophobic surfaces were obtained by manipulating processing techniques that can efficiently absorb the oil from water surface (Li et al. 2016). Surface modification is another way to introduce hydrophobic surface, like hydrophobic NFC aerogels obtained by oleophilic coating with titanium dioxide for recyclable oil absorbents (Korhonen et al., 2011). Shape recovery and elastic properties can also be used to make the aerogel mechanoreponsive conducting and pressure sensing applications (Wang et al, 2013).

Poysaccharide-based aerogels possess various physical properties, like a high porosity, a good mechanical stiffness, a highly-interconnected structure, and an ease of tailoring the porous structure, that make them perfect candidates for tissue engineering as scaffolds (Martins et al. 2015; Stergar and Maver 2016). Quraishi et al. reported the hybrid aerogels prepared from alginate-lignin as promising materials for tissue engineering applications (Quraishi et al. 2015). Composite aerogels from cross-linked dialdehyde derivatives of nanocellulose and collagen exhibited good compatibility and no cytotoxicity, which makes them ideal candidates for tissue engineering as scaffolds (Lu et al. 2014). Polysaccharide-based aerogels feature high water uptake in addition to other properties that can be utilized in wound care. Chitin and chitosan possess antifungal and bactericidal effects, which make them new biomaterials for wounds and burn treatments (Jayakumar et al. 2011). Other example of polysaccharide-based aerogels for wound dressing for burn and wounds repair are aerogels from gum acacia (Singh et al. 2013), bacterial cellulose (Lin et al. 2013), and cross-linked nanocellulose and collagen (Lu et al. 2014).

Table 2: Properties of polysaccharide-based aerogels.

Aerogel	Concentration	Cross-linking method	Drying method	Density (g/cm^3)	Compressive/ Young's modulus	Surface area (m^2/g)	Pore size	Absorption (g/g)	Compression recovery (%)	VS* (%)	TC* (W/m.K)	References
Sodium alginate (beads)	2%	Chemical	sc-CO_2	2.15	-	419	50–200 nm	-	-	-	-	(Deze et al. 2012)
Sodium alginate (SA) + CMC*	1.5% SA and 0.76 wt.% CMC	Chemical	Lyophilization (CF)*	0.041	20 kPa (compressive strength)	-	-	Peanut oil = 36.5	-	30	-	(Cheng et al. 2012)
Alginate aerogel	4 wt.%	Immersing in EtOH*	sc-CO_2	-	-	147	15 nm	-	-	-	0.0814	(Horvat et al. 2017)
NFC*-xyloglucan	2% (70:30 NFC-xyloglucan)	Physical	Lyophilization (UF)*	0.02	1,470 kPa	11.9	< 100 µm	-	-	-	-	(Sehaqui et al. 2010)
Spruce galacto-glucomannan (GGM) + NFC	2 wt.% (GGM: NFC = 70:30)	Chemical	Lyophilization (UF)	0.023	177 kPa	-	50 and 100 µm	Water = 34	83.2	-	-	(Alakalhunmaa et al. 2016)
Starch + lignin containing-NFC	3% amylopectin, 3% lignin containing-NFC	Thermal treatment	Lyophilization (CF)	0.033	3,400 kPa	1.35	100−250 µm	Water = 12	-	-		(Ago et al. 2016)
NFC aerogel (hydrophobic modification with silanes)	2 wt.%	Physical	Lyophilization (CF)	0.014	-	11	20–30 µm	Hexadecane = 45, distributed on top of the water phase.	-	-		(Cervin et al. 2012)
Xylan–cellulose composite foams	5 wt.% xylan, 1.25 wt.% NFC	Heating	Lyophilization (UF)	0.025	285 kPa	-	20–50 µm	-	-	-	-	(Köhnke et al. 2012)

Glucuronoxy-lan citrate-chitosan foam	1% chitosan in 1% of derivative of glucuronoxylan citrate solution	Chemical	Lyophilization	0.0025	1.61 N/mm^2 Tensile strength	-	-	Water =78 NaCl (0.9%) = 98	-	-	-	(Salam et al. 2011)
Starch citrate-chitosan foam	1% chitosan in 1% of derivative of starch citrate solution	Chemical	Lyophilization	0.004	1.8 N/mm^2 Tensile strength	-	-	Water = 113 NaCl (0.9%) = 139	-	-		(Salam et al. 2011)
Low-methoxyl pectin aerogel	4 wt.%	Immersing in EtOH	sc-CO_2	-	-	510	19 nm	-	-	-	0.0213	(Horvat et al. 2017)
High-methoxyl pectin aerogel	4 wt.%	Immersing in EtOH	sc-CO_2	-	-	384	17 nm	-	-	-	0.0230	(Horvat et al. 2017)
Xanthan gum aerogel	4 wt.%	Immersing in EtOH	sc-CO_2	-	-	363	20 nm	-	-	-	0.0270	(Horvat et al. 2017)
Guar gum aerogel	4 wt.%	Immersing in EtOH	sc-CO_2	-	-	111	14 nm	-	-	-	0.0885	(Horvat et al. 2017)
Guar gum aerogel	1 wt.%	Enzymatic oxidation	Lyophilization (UF)	0.016	227 kPa	-	-	Water = 42	-	0	-	(Mikkonen et al. 2014)
Barley β-glucan aerogel	5 wt.%	Heating and cooling	sc-CO_2	0.2	-	166	2.7 nm	-	-	70	-	(Comin et al. 2012)
Tamarind seed xyloglucan aerogel	1 wt.%	Enzymatic oxidation	Lyophilization (UF)	0.012	359 kPa	-	< 100 μm	Water = 20	-	0	-	(Mikkonen et al. 2014)

*EtOH = ethanol, sc-CO_2 = supercritical CO_2, CF = conventional freezing, UF = unidirectional freezing, CMC = carboxy methyl cellulose, NFC = nanofibrillated cellulose, VS = volumetric shrinkage, TC = thermal conductivity.

3 AIMS OF THE STUDY

This thesis aimed to study the polysaccharides guar galactomannan (GM) and tamarind seed xyloglucan (XG) as aerogel-forming matrices using the environmentally friendly enzymatic-oxidation cross-linking technique and to investigate the effect of nanofibrillated cellulose (NFC) as a reinforcement material on the catalytic activity of the enzyme and on the properties of aerogels.

The specific objectives were to:

- Develop biocomposite polysaccharide-based aerogels via the environmentally friendly enzymatic-modification pathway (Study I, II, and III).
- Evaluate the effects of NFC as a reinforcing agent on the catalytic activity of the enzyme and the formation of composite hydrogels followed by lyophilization to aerogels, and to study the hydrogel's properties in relation to the aerogel's properties (Study I).
- Exploit synchrotron X-ray microtomography (XMT) as an advanced characterization technique to study the role of NFC addition in combination with ice-templating methods (conventional and unidirectional ice templating) on the quantitative and qualitative morphological features of the lyophilized aerogels in relation to their mechanical and shape recovery behavior (Study II).
- Study the supercritical CO_2 drying technique as a way to preserve the fine morphology of the aerogels for a high surface area and to systematically study the compatibility of various solvents with the hydrogel's structure in terms of volumetric shrinkage and its related properties using one-step and five-step solvent-exchange processes (Study III).
- Understand the effect of supercritical CO_2 drying on volumetric shrinkage and to characterize the aerogel's properties (Study III).

4 MATERIALS AND METHODS

This section briefly summarizes the materials and methods used in the thesis. More detailed descriptions can be found in the original publications (I-III).

4.1 Materials

Two galactose-containing polysaccharides, guar gum galactomannan (GM) (Study I, II, and III) and tamarind seed xyloglucan (XG) (Study I and II) were used as aerogel-forming matrices.

Galactose oxidase (GaO-I), donated by Dr. Sybe Hartmans (DSM Biotechnology Center, Netherlands), was used in Studies I and II. GaO-II, donated by Prof. Harry Brumer from the KTH Royal Institute of Technology and Wallenberg Wood Science Center (WWSC), as well as by Prof. Lisbeth Olson, from Chalmers and WWSC (Sweden), was used in Study III. Both GaO-I and GaO-II were produced by *Picihia pastoris*. The nanofibrillated cellulose (NFC-I) used in Study I was prepared from never-dried birch kraft pulp by mechanical disintegration through a high-pressure fluidizer for six passes. Prior to disintegration, the sorbed metal ions were removed, and the carboxyl groups present in the pulp were converted to their sodium form following the procedure described by Swerin (Swerin 1998). Further treatments, such as enzymatic or chemical treatments, were not applied. Natural NFC (NFC-II) and anionic NFC (NFC-III) were used in Study II and III, respectively, and were purchased from UPM, Finland. NFC-II was refined from birch pulp without chemical derivatization. The fiber of NFC-II was 10 nm to 50 nm wide and several micrometers long. NFC-III was obtained from bleached birch kraft pulp and was chemically modified with anionic groups and refined. The fiber width of NFC-III was 4–10 nm with a length of several micrometers. Sample compositions, samples codes, and processing conditions are presented in Table 3.

4.2 Enzymatic oxidation and hydrogel formation

GM and XG were stirred in Milli-Q water (10 mg/ml) at room temperature (RT). The samples were kept overnight at 4°C for complete hydration. NFC (1% dry content) was added to GM and XG solutions at different ratios (5%, 15%, and 25% of the weight of the polysaccharides) and mixed with an Ultra Turrax for five minutes at 9,500 rpm. Control samples were also prepared without the addition of NFC. Enzymes (GaO, catalase, HRP) were added, and the mixture was continuously stirred at 4°C for two days (Studies I and II) and for four days (Study III), depending on the GaO-I or GaO-II enzyme. The enzyme dosages (GaO: 1.8–4.5 U/mg [Studies I and II] and 0.165 U/mg [Study III] of galactosyl units, catalase: 115 U/mg, HRP: 1.5 U/mg) were used. After the enzymatic treatment, hydrogels were obtained, and the enzymes were inactivated by heating the samples in boiling water for five minutes. Air bubbles were removed by heating the hydrogels under vacuum for about 10–15 minutes.

Table 3: Sample codes, sample compositions, and processing conditions.

Sample codes*	Amount of NFC (wt.% of the GM/XG)	Types of NFC	Total concentration of biopolymers in aerogels	GaO enzyme	Lyophilization		Supercritical CO_2 drying		
					Ice-templating method*	Lyophilization	Solvent exchange steps	Supercritical CO_2 drying	
GM	0	NFC-I	1 wt.%	–	–	–	–	–	Study I
GM-25NFC	25			–	–	–	–	–	
XG	0			–	–	–	–	–	
XG-25NFC	25			–	–	–	–	–	
GMox	0			GaO-I	CF	x	–	–	
GMox-5NFC	5				CF	x	–	–	
GMox-15NFC	15				CF	x	–	–	
GMox-25NFC	25				CF	x	–	–	
XGox	0				CF	x	–	–	
XGox-5NFC	5				CF	x	–	–	
XGox-15NFC	15				CF	x	–	–	
XGox-25NFC	25				CF	x	–	–	
GMox-CF	0	NFC-II		GaO-I	CF	x	–	–	Study II
GMox-25NFC-CF	25				CF	x	–	–	
GMox-UF	0				UF	x	–	–	
GMox-25NFC-UF	25				UF	x	–	–	
XGox-CF	0				CF	x	–	–	
XGox-25NFC-CF	25				CF	x	–	–	
XGox-UF	0				UF	x	–	–	
XGox-25NFC-UF	25				UF	x	–	–	
GMox-CF-MC	0				CF	x	–	–	
GMox-25NFC-CF-MC	25				CF	x	–	–	
GMox-EtOH	0	NFC-III		GaO- II	–	–	5	x	Study III
GMox-DMSO	0				–	–	5	x	
GMox-25NFC-EtOH	25				–	–	5	x	
GMox-25NFC-DMSO	25				–	–	5	x	

*GM = guar galactomannan, XG = tamarind seed xyloglucan, ox = enzymatically oxidized, NFC = nanofibrillated cellulose and numbers 5, 15, and 25 indicate the concentration of NFC, GaO = galactose oxidase, CF = conventional freezing, UF = unidirectional freezing, MC = mechanically compressed, EtOH = ethanol, DMSO = dimethyl sulfoxide. Types of NFC and GaO are explained in section 4.1.

After the air was removed, the hydrogels were allowed to cool and then carefully molded into cubic petri dishes (Study I and II) and cylindrical petri dishes (48-well plate, Study III) for solvent exchange and supercritical CO_2 drying, avoiding the formation of new air bubbles. For study II, the hydrogels were filled into polyether-ether-ketone (PEEK) capillaries (wall thickness = 0.0175 mm and internal diameter = 0.8 mm) using a small syringe and were inserted into hydrogels molded in cubic petri dishes to keep them in a vertical position (Figure 8).

4.3 Analysis of degree of oxidation

The degree of oxidation of enzymatically treated GMox and XGox was determined using Parikka et al.'s method (Parikka et al. 2010) (Studies I, II, and III). Briefly, $NaBD_4$ (3 molar equivalents related to the maximum molar amount of galactosyl units in the sample) was added into the hydrogel (approximately 0.5 ml, 5 mg of polysaccharide), and the solution was stirred overnight. Polysaccharides were precipitated by adding EtOH, transferred to a pear-shaped flask and vacuum dried for 80–90 min at 40°C. Acid methanolysis was performed using Sundberg, Lillandt, and Holmbom's method (Sundberg et al. 1996). The samples were analyzed with GC-MS using a HP-5 column in an HP5890 gas chromatograph connected to an HP5972 Mass Selective Detector mass spectrometer. The degree of oxidation was determined by comparison of the ratio of the 361 m/z and 362 m/z ions of the silylated galactosyls, with 361 corresponding to the unoxidized galactosyls and 362 to the oxidized galactosyls (Parikka et al. 2010).

4.4 Characterization of hydrogels

4.4.1 Viscoelastic characterization of hydrogels

Rheological measurements of the hydrogels (Study I) were performed in analytical triplicate, using a controlled stress rheometer (Rheostress RS600, Thermo Haake, Germany) by following Sandolo, Matricardi, Alhaique, and Coviello's method (Sandolo et al. 2007). Hydrogels were shaped using a die of 36 mm in diameter and kept at RT for 24 hours before the measurements. Viscoelastic moduli (elastic modulus, G′, and the viscous modulus, G″) were determined as a function of the frequency, and the mechanical spectra were recorded in the frequency range of 0.001 to 10 Hz. The parallel plate-plate was 35 mm in diameter, and the gap between the two plates ranged from 0.5 to 3 mm, depending on the samples (native or oxidized). However, the stress and frequency sweep for a sample were conducted on the same gap between plates. All measurements were performed within the linear viscoelastic region, where the viscoelastic moduli were independent of the stress amplitude.

4.4.2 Texture profile of hydrogels

A Texture Analyser TA-XT2i (Stable Microsystems, Godalming, UK) was used to characterize the hydrogels using the Texture Profile Analysis compression test adopted from Deszczynski, Kasapis, and Mitchell (Deszczynski et al. 2003). The hydrogels were molded (diameter = 26 mm) and kept

at RT for 24 hours before the analyses, and during the measurements, the room was conditioned with a controlled relative humidity of 40–45%. Two consecutive cycle compressions of a cylindrical gel (removed from the dice) were performed using a cylinder probe, diameter of 20 mm. Analytical triplicate hydrogel samples were compressed to a distance of 2 mm at a rate of 2 mm/s for the test speed, and 2 mm/s for the post-test speed. The compressive modulus was measured from the stress-strain curve of the hydrogels. Various other key parameters were derived from the force–time plot: maximum compressive force, i.e. hardness, adhesiveness, cohesiveness, springiness, and resilience.

4.5 Aerogel formation

Aerogels were prepared using two drying techniques, lyophilization and supercritical CO_2.

4.5.1 Lyophilization

Hydrogels were frozen using conventional freezing at -70°C for 3–4 hours (Study I and II) and unidirectional freezing using liquid nitrogen for 15–20 min (Study II) to align the ice crystals along the freezing direction. Lyophilization of the pre-frozen hydrogels was performed at 1 mbar atmospheric pressure for about 48 hours. After drying, the aerogel specimens were stored in a dry desiccator before the analyses.

4.5.2 Supercritical CO_2 drying

Supercritical CO_2 (sc-CO_2) drying was carried out with a research visit to the Institute for Thermal Separation Process, Hamburg University of Technology (TUHH), Germany. In this study (Study III), only GM was selected as the aerogel-forming matrix due to its formation of stiff hydrogels, with NFC-III at a concentration of 25%, only, as a reinforcing agent.

The sc-CO_2 drying consisted of two steps, the solvent exchange and drying. During solvent exchange, the water of the hydrogels was replaced with a solvent that was compatible with the hydrogel's structure and that is miscible with sc-CO_2. Thirteen different solvents, ethanol, isopropyl alcohol (IPA), propylene carbonate, glycerol, acetone, butanone (also known as methyl ethyl ketone [MEK]), 1-butanol, dimethyl sulfoxide (DMSO), ethylene glycol (1,2-ethanediol), propylene glycol (1,2-propanediol), methanol, and N′N-Dimethyl formamide (DMF), were initially used to see the effect of the solvents on the shrinkage of hydrogels. One piece (approximately 1 g) of hydrogel was added into a 50 mL falcon tube with 30 g of a particular pure solvent (one step solvent exchange). The falcon tube was stirred at room temperature via shaking in an overhead shaker. The volume of the hydrogels was measured using a volumetric test tube before and after the solvent exchange (48 hours) to evaluate the volumetric shrinkage (Eqs. 1 and 2). The response of the hydrogels to the solvents could also be correlated through Hansen solubility parameters (Errede 1986). Hansen solubility parameters were developed as a way of predicting if one material will dissolve in another and form a solution (usually a solvent and a polymer) (Hansen 2007).

Hansen solubility parameters account for three types of interactions between molecules: dispersion forces (d), dipole-dipole bonding (p), and hydrogen bonding (h). The d, p, and h parameters for each solvent were taken from the Hansen solubility parameter hand book (Hansen 2007).

The stepwise solvent-exchange procedure consisted of the stepwise immersion of the initial hydrogels (taken out of the mold) in water/solvent solutions with increasing solvent concentrations (five steps: 20%, 40%, 60%, 80%, and 100%; six steps: 20%, 30%, 40%, 60%, 80%, and 100%). Water/solvent mixtures were used at a 30:1 ratio of solvent to hydrogel weight. The volume of the gels was measured before and after solvent exchange at each solvent-exchange step (24 hours per step). Volumetric shrinkage and volumetric yield were calculated with Eqs. 1 and 2. Three replicates were carried out for each solvent. The terms "alcogels" and "lyogels" are used for hydrogels after complete solvent exchange in ethanol and DMSO, respectively.

$$VS\ (\%) = \frac{VI - VSE}{VI}\ X\ 100\ \% \qquad (1)$$

$$VY\ (\%) = \frac{VSE}{VI}\ X\ 100\ \% \qquad (2)$$

VS = Volumetric shrinkage, VI = initial volume of the hydrogel, VSE = volume of the hydrogel after solvent exchange, and VY = volumetric yield.

sc-CO_2 drying was performed at 12 MPa and 40°C in a 250 mL autoclave using a continuous sc-CO_2 flow for four hours (ethanol) and seven hours (DMSO). The alcogels and lyogels were packed in filter paper, placed in the autoclave, and soaked in their respective solvents (ethanol/DMSO) to prevent shrinkage due to the evaporation of the solvent from the alcogel and lyogel networks before exposure to sc-CO_2.

4.6 Characterization of aerogels

4.6.1 BET-specific surface area

The Brunauer-Emmett-Teller (BET)-specific surface area was determined with N_2-physisorption using a Micromeritics TriStar II 3020 (Norcross, GA, USA) (Study I) and a Nova 4200e Surface Area Analyzer (Quantachrome GmbH & Co. KG, Odelzhausen, Germany) (Selmer et al. 2015) (Study III). The pore volume and mean pore diameter were estimated by using the Barrett-Joyner-Halendia (BJH) method (Selmer et al. 2015). Before the N_2-physisorption analysis, all of the samples were degassed under a vacuum at 150°C for 80–100 minutes and 40°C for 20 hours (Studies I and III, respectively).

4.6.2 Morphology of the aerogels

Scanning Electron Microscopy

Aerogel samples were coated with an Au/Pd thin film via the sputtering method. The surfaces of the specimens were viewed using focused ion beam scanning electron microscopy (FIB-SEM) in Study I, and the aerogels were milled open with 30 kV Ga+ ions using FIB-SEM (Quanta 3D 200i FIB-SEM). Marko Vehkamäki is acknowledged for the FIB-SEM analyses. SEMs of the sc-CO_2-dried aerogels were taken using a detector for secondary electrons with a Leo Gemini Zeiss 1530 SEM (Oberkochen, Germany) at 5 kV (working distance approximately 8 mm; Study III).

Synchrotron x-ray tomography (XMT) scanning

Aerogel samples in PEEK were glued onto carbon fiber rods (Figure 8). All of the samples were scanned at a height of 6 mm from the bottom to avoid any artifacts from the glue. In addition, small samples (≈ 1 x 1 x 17 mm in length, width, and height) from mechanically compressed cubical samples were carved with a razor blade and glued on the carbon rods. XMT scans were conducted on the oxidized GM and oxidized XG aerogels with and without NFC reinforcement (25%) at the beamline for Tomographic Microscopy and Coherent rAdiology experimenTs (TOMCAT) at the Paul Scherrer Institut (PSI) in Villigen, Switzerland. Details of the TOMCAT reconstruction pipeline are described in Hintermüller et al. (2010) and Marone and Stampanoni (2012). The VGStudioMax 2.1 software (Volume Graphics GmbH, Heidelberg, Germany) was used for 3D visualizations of the aerogel structures.

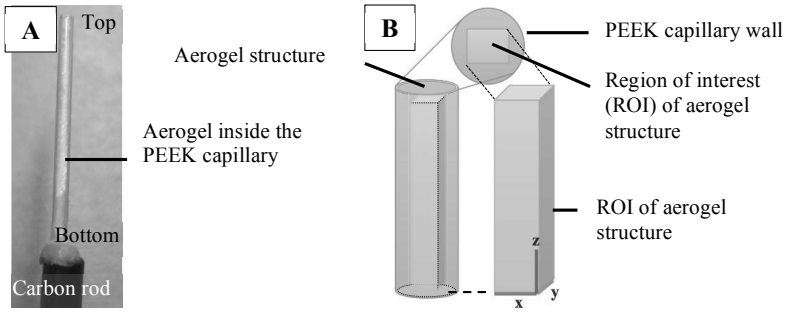

Figure 8: A) Formation of aerogels inside the polyether-ether-ketone (PEEK) capillary, B) graphical representation for the selected region of interest (ROI) of the aerogel structure to omit the PEEK capillary wall.

Quantitative data analyses, such as volume-weighted pore size distributions and volume-weighted wall-thickness distributions, were calculated using the local thickness plugin for the ImageJ software (Dougherty and Kunzelmann 2007). For quantitative analysis, first a bilateral filter was applied to reduce noise and smooth the images. The image was binarized (converted from grayscale to a black and white image) using a dual threshold (hysteresis) segmentation. After measuring the local thickness map of the pores and pore walls, the histograms of the two data sets were calculated

and presented as the volume-weighted pore size and wall-thickness distributions, respectively. All of the quantitative data analyses have been performed using the facilities from the Centre for Scientific Computing (CSC - IT Center for Science Ltd., Espoo, Finland).

4.6.3 Density and mechanical properties of aerogels

The density of the aerogels was determined from six analytical replicates by the displacement method using glass beads (0.2 mm diameter, 1.619 g/cm^3) as described by Mikkonen et al. (Mikkonen et al. 2014) (Studies I and III).

Aerogel samples were conditioned for 48 hours in desiccators containing $Mg(NO_3)_2$ to set the relative humidity between 50% and 55% (Studies I, II, and III). Cubical aerogel samples were compressed vertically for 6 mm at a rate of 1.3 mm/min using an Instron 33R4465 universal testing machine with a load cell of 100 N (Studies I and II). Unidirectional frozen cubical aerogel samples were compressed in the freezing direction. Compressive modulus and height recovery were determined. The data were obtained from ten replicates of each aerogel sample. Compressive moduli (Study I and II) and shape recovery (Study II) were determined. For study III, the Texture Analyser TA- XT2i (Stable Microsystems, Godalming, UK) was used for the mechanical testing of aerogels. A compression test was applied horizontally on the cylindrical aerogel (height = 5–10 mm and diameter = 4–6 mm), using a cylindrical probe with a diameter of 20 mm. Six samples were compressed to one-third of their original height at a rate of 2 mm/s test speed and 2 mm/s post-test speed. The maximum compressive force was measured from the resultant force-time plot.

4.6.4 Solvent residues in aerogels

The quantitative analyses of the ethanol residues in the sc-CO_2-dried aerogel were performed using the total ion chromatogram (TIC) according to VDA 278 (GCMS-QP2010 SE, Shimadzu). The values indicated were calculated as the toluene equivalent [ppmTE]. The weight of each sample was approximately 5 mg.

4.7 Principal components analysis

The data for the hydrogels and aerogels were analyzed with a multivariate statistical method using principal components analysis (PCA) to identify patterns in the data set. IBM SPSS 21 software (International Business Machines Corp. New York, US) was used for this purpose.

5 RESULTS

5.1 Hydrogel formation

Formation of the hydrogel is the first step towards obtaining aerogels. The hydrogels from GM and XG were obtained by enzymatic oxidation with GaO. GaO catalyzes the oxidation of the primary hydroxyl groups at C-6 of the terminal galactosyl units in GM and XG into aldehyde groups, which enables cross-linking to form hydrogels. NFC was added to GM and XG solutions prior to enzymatic oxidation and was entrapped into the matrix polysaccharide (GM and XG) hydrogels. The degree of oxidation (DO) was determined to see the enzymatic activity in the presence of the reinforcing agent and is presented in Table 4.

The DO was measured as percentage of galactosyl units oxidized, and the DO of oxidized GM (GMox) and oxidized XG (XGox) were 16% and 42%, respectively. When calculated for samples containing 5–25 % NFC, the DOs ranged from 22–26% and 41–63% galactosyl units oxidized for the NFC reinforced GMox and XGox, respectively (Table 4). The DO of the total carbohydrates (% of total GM and XG carbohydrates) was 6% and 7% for GMox and XGox, respectively. When calculated for samples containing 5–25% NFC, the DOs were 6.75–9.5% of the total carbohydrates (Study I). DO for NFC containing samples were calculated with assumptions that NFC did not take part in the oxidation.

According to the visual observations, the hydrogel formation of GMox seems to proceed faster than that of XGox. GM contains a higher amount of terminal galactosyl units (40%) that require less DO to form hydrogels as compared to XG, which contains only 16% terminal galactosyl units. Both GMox and XGox hydrogels exhibited an elastic gel structure, but the XGox hydrogels were more stretchy than the GMox hydrogels. Increment of the NFC additive from 5 to 25% resulted in an increase in the hydrogel's firmness and stiffness.

5.2 Hydrogel properties

5.2.1 Rheological properties

To study the effect of the addition of NFC on the properties of GMox and XGox hydrogels, rheological measurements were performed in order to determine the viscoelastic properties. A hydrogel is a gel in which the liquid component is water; it behaves like a solid-rubber material and has a characteristic rheological behavior in which the storage/elastic modulus value (G′) dominates over the loss/viscous modulus (G′′). The aqueous solution of native GM (1 wt.%) appeared to be a highly viscous solution when observed visually, and when analyzed for its rheological properties, the viscous modulus G′′ initially dominated the elastic modulus G′, and crossed over (the G′ outstripping the G′′) at a higher frequency. This indicated that the gel network was not formed (Figure 9A). Adding and physically mixing 25% NFC to the native GM (GM-25NFC) did not show any change in the viscoelastic (viscous and elastic) properties of the

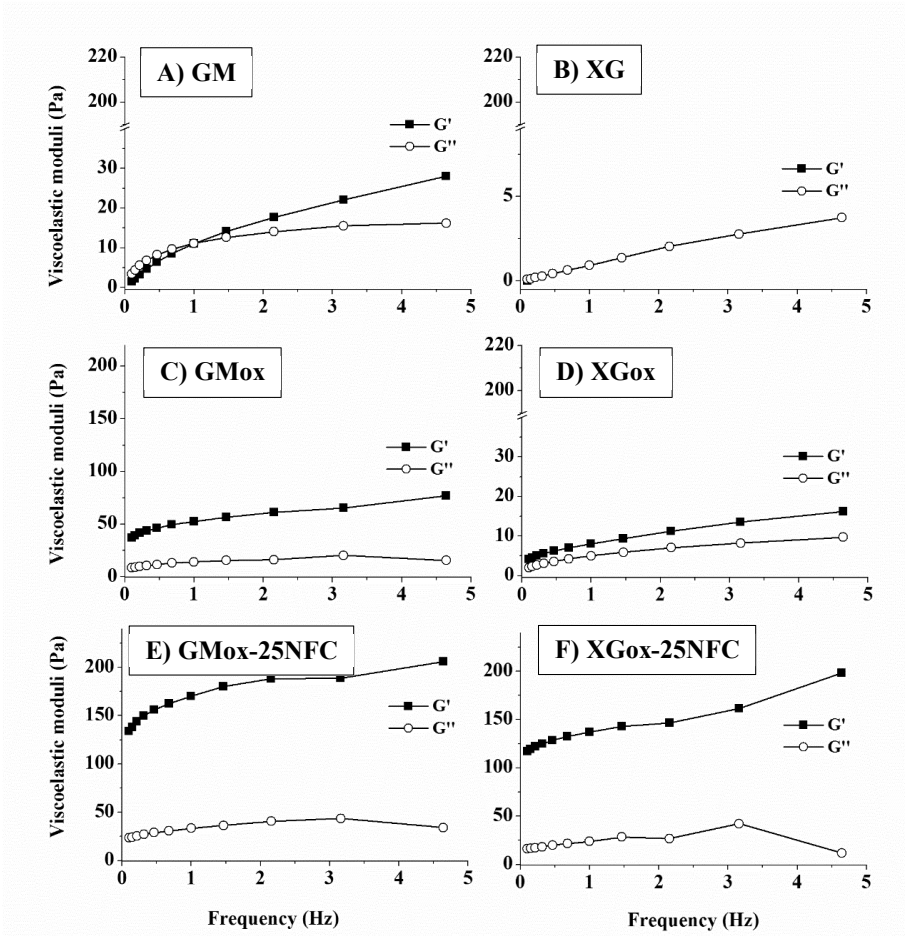

Figure 9: Elastic (G′) and viscous (G″) modulus of aqueous, native (A) guar galactomannan (GM) and (B) tamarind seed xyloglucan (XG). Elastic (G′) and viscous (G″) modulus of (C) oxidized guar galactomannan (GMox), (E) GMox with 25% NFC (GMox-25NFC), (D) oxidized tamarind xyloglucan (XGox), and (F) XGox with 25% NFC (XGox-25NFC). The results are averages from three replicates, and the error bars are omitted for clarity.

suspension. The native XG solution (1 wt.%) did not exhibit elastic properties, evidenced by the fact that the rheometer did not detect the G´ (Figure 9B), which only appeared at a low frequency with an added 25% NFC. Enzymatically oxidized GMox and XGox clearly showed gel formation based on visual observations, and this was confirmed with the rheometer by the dominance of elastic modulus G´ (Figure 9C and D). The values of the elastic modulus G´ at 1 Hz frequency were 52 and 12 Pa for GMox and XGox, respectively. The addition of NFC at concentrations of 5% and 15% progressively modified the viscoelastic properties of the GMox and XGox hydrogels

(Table 4). The GMox-5NFC hydrogel exhibited a higher elastic modulus G´ (76 Pa at 1 Hz) than the plain GMox hydrogel (52 Pa at 1 Hz). A further increase in the elastic modulus G´ to 81 Pa at 1 Hz was observed for the GMox-15NFC hydrogels (Study I). Interestingly, a large increase in the elastic modulus G´ (170 Pa at 1 Hz) was observed for GMox-25NFC (Figure 9E, Table 4). The viscoelastic properties of the XGox hydrogels responded in a similar fashion as the GMox ones upon the addition of 5–25% NFC, and the elastic modulus G´ increased from 36 Pa to 137 Pa at 1 Hz (Figure 9F, Table 4).

5.2.2 Textural properties

Hydrogels were further characterized for large deformations using the texture analyzer to evaluate the hydrogel properties and the effect of NFC reinforcement on the texture of the matrix polysaccharide (GMox or XGox). By visual observation, the plain GMox hydrogels maintained their cylindrical shape when the hydrogels were taken out of the dice. However, the cylindrical shape of the plain XGox hydrogels were deformed to some extent when they were removed from the dice as the hydrogels from the plain XGox were easily stretched without structural breakdown. The addition of NFC enhanced the shape retention of XGox and the firmness of the hydrogel's structure. All of the hydrogels showed an elastic nature, as none of them showed significant peak deviation from the main force-time plot, which means that the structure of the hydrogel did not break down during compression.

A large deformation at an initially low compressive force was observed in plain GMox hydrogels, though the addition of NFC (5%, 15%, and 25%) strengthened their texture, resulting in straight stress-strain curves with higher slopes. The same trend was also observed for the XGox hydrogels with 15% and 25% NFC. The stress of XGox and XGox-5NFC strongly increased after 10% strain. The compressive moduli (Young's moduli) of the hydrogels were calculated from the elastic region of the stress–strain curves at the initial slope of the curves and are presented in Figure 10. The compressive moduli of the GMox and GMox-5NFC hydrogels showed no significant difference (1.7 kPa and 1.8 kPa, respectively). However, a further increase in the NFC content to 15% and 25% gradually increased the compressive moduli of the GMox hydrogels (2.3–2.9 kPa; Figure 10). The compressive modulus of the plain XGox hydrogel (2.6 kPa) was higher than that of the plain GMox hydrogel (1.7 kPa; Figure 10). Compressive moduli of 2.9 and 3.5 kPa were observed for the XGox-5NFC and XGox-15NFC hydrogels, respectively. Interestingly, the XGox-25NFC hydrogels showed a significant difference from and double the compressive modulus (5.5 kPa) of the plain XGox hydrogels (2.6 kPa; Figure 10).

Various other key parameters were derived from the force–time plot: maximum compressive force, i.e. hardness (the peak force of the first compression cycle), adhesiveness, cohesiveness, springiness, and resilience (Table 4). Adhesiveness is the measure of the negative force between the two cycles. Cohesiveness indicates how the sample withstands a second deformation in relation to the sample's behavior under the first deformation. Springiness illustrates how a sample physically springs back after it has been deformed during the first compression, while resilience

shows how the sample regains its original shape. The GMox and XGox hydrogels showed a small decrease in hardness with increasing NFC content, and the plain XGox hydrogel showed an exceptionally high hardness of 9.98 N. The GMox hydrogels had less adhesiveness (0.01–0.02 N) than the XGox hydrogels (0.02–0.16 N), with and without the addition of 5–25% NFC. The GMox hydrogels with added NFC (5–25%) had a slightly higher cohesiveness, springiness, and resilience (0.44–0.59, 0.37–0.53, and, 0.28–0.45, respectively) than the corresponding XGox hydrogels (0.30–0.44, 0.23–0.36, and 0.16–0.30).

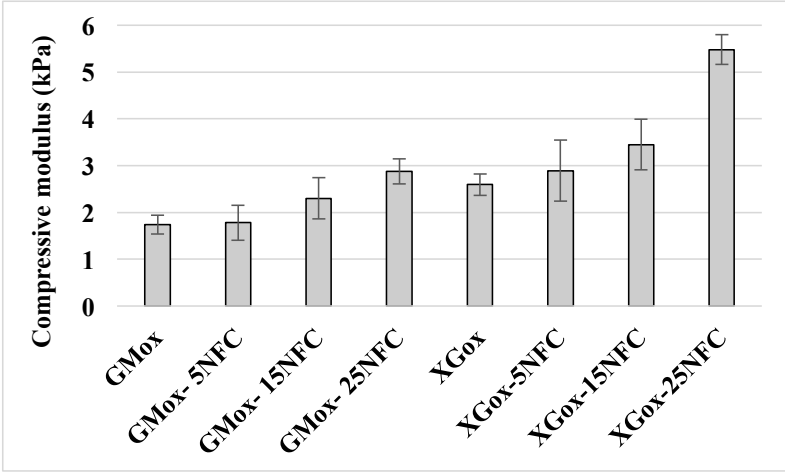

Figure 10: Compressive modulus of GMox and XGox hydrogels, with and without the addition of NFC (5%, 15%, and 25%) measured from the stress–strain curve of texture profile analyzer. The analyses were based on three analytical replicates.

Table 4: Degree of oxidation and properties of the hydrogels.

Sample	Degree of oxidation (% of galactose oxidized)	Degree of oxidation (% of total [GM and XG] carbohydrates)	Rheological measurements of hydrogels[a]		Textural properties of hydrogels[a]				
			G´´ (Pa)	G´ (Pa)	Maximum compressive force, i.e. hardness (N)	Adhesiveness (N)	Cohesiveness	Springiness	Resilience
*GM	-	-	-	-	-	-	-	-	-
*GM-25NFC	-	-	-	-	-	-	-	-	-
*XG	-	-	-	-	-	-	-	-	-
*XG-25NFC	-	-	-	-	-	-	-	-	-
GMox	16	6	14	52	0.68	0.01	0.59	0.53	0.45
GMox-5NFC	26	9.5	18	76	0.97	0.01	0.44	0.37	0.28
GMox-15NFC	20	6.8	16	81	0.43	0.01	0.57	0.46	0.43
GMox-25NFC	22	6.75	33	170	0.52	0.02	0.49	0.39	0.30
XGox	42	7	4	12	9.98	0.16	0.42	0.36	0.30
XGox-5NFC	63	9.5	7	36	2.08	0.03	0.36	0.27	0.24
XGox-15NFC	41	6.8	12	45	0.59	0.02	0.30	0.23	0.16
XGox-25NFC	58	6.75	24	137	0.51	0.03	0.44	0.34	0.24

*Unoxidized samples which did not form gels. GM = guar galactomannan, XG = xyloglucan, ox = enzymatically oxidized, NFC = nanofibrillated cellulose. The numbers 5, 15, and 25 indicate the percentage of NFC, G´´ = viscous modulus, G´ = Elastic modulus. [a]Average value at 1 Hz from three replicates. Cohesiveness, springiness, and resilience are unit-less and expressed as ratios.

Table 5: Density, volumetric shrinkage, and BET surface area of lyophilized and sc-CO_2-dried aerogels.

Sample	Density of aerogels (g/cm^3)			Volumetric shrinkage (%)					BET surface area (m^2/g)		
	Lyophilization	*sc-CO_2 drying		Lyophilization	sc-CO_2 drying				Lyophilization	*sc-CO_2 drying	
					Hydrogel→Lyogel/alcogel		Hydrogel→Aerogel				
		*EtOH	*DMSO	Hydrogel→Aerogel	DMSO	EtOH	DMSO	EtOH		EtOH	DMSO
*GMox	0.019	0.10	0.18	No shrinkage	70	88	93	90	2.3	219	182
GMox-25NFC	0.012	0.06	0.07	No shrinkage	29	45	83	82	3.8	322	333

*GM = guar galactomannan, ox = enzymatically oxidized, NFC = nanofibrillated cellulose and number 25 indicate the percentage of NFC, sc-CO_2 = supercritical CO_2 drying, EtOH = ethanol, DMSO = dimethyl sulfoxide. Lyogel = hydrogel after solvent exchange with DMSO, alcogel = hydrogel after solvent exchange with ethanol.

5.3 Hydrogel's structural response to solvents

5.3.1 Pure solvent – one-step solvent exchange

In supercritical CO_2 (sc-CO_2) drying, the liquid phase (water) of the hydrogels is replaced with a suitable solvent that is compatible with the hydrogel structure and miscible with the sc-CO_2. The compatibility of the solvent is considered very critical to avoid collapsing the 3D structure of the dried gel. In Study I, NFC was studied as a reinforcement at different concentrations (5%, 15%, and 25%). This study showed that the hydrogels and aerogels of both matrix polysaccharides (GMox and XGox) with added NFC at 25% exhibited significant differences in their properties compared to the other concentrations of NFC reinforcement (5% and 15%). So, in this study, the GM hydrogels (GMox) and NFC-reinforced (25 wt.%) GM hydrogels (GMox-25NFC) were considered for sc-CO_2 drying and tested for solvent compatibility using solvents of varying polarities.

One-step solvent exchange was performed with 13 different solvents: ethanol, isopropyl alcohol (IPA), propylene carbonate, glycerol, acetone, butanone (also known as methyl ethyl ketone [MEK]), 1-butanol, dimethyl sulfoxide (DMSO), ethylene glycol (1,2-ethanediol), propylene glycol (1,2-propanediol), methanol, and N′N-Dimethyl formamide (DMF), to observe the shrinkage of the GMox and GMox-25NFC hydrogels. Immersing the gel in the pure solvent caused considerable shrinkage in the hydrogel's structure. The volumetric shrinkage of the hydrogels is presented in Figure 11, arranged in increasing polarity for the solvent from 1-butanol to water. Less polar solvents, such as 1-butanol, IPA, and MEK, showed high volumetric shrinkage in both types of hydrogels, and there was less shrinkage with the increasing polarity of the solvents, except for propylene carbonate. The solvents 1-butanol, IPA, MEK, and propylene carbonate induced more than 80% volumetric shrinkage for both types of hydrogels (GMox and GMox-25NFC). GMox-25NFC hydrogels exhibited less shrinkage than did the plain GMox hydrogels, especially with acetone, methanol, ethanol, DMF, and DMSO. Interestingly, both GMox and GMox-25NFC hydrogels absorbed water and swelled when immersed in pure water, and the swelling volume of the GMox-25NFC hydrogels was higher than that of the GMox hydrogels. The swelling is shown as negative shrinkage in Figure 11. Solvents not only caused volumetric shrinkage, but also changed the other qualitative properties of hydrogels that could be observed visually, such as their shape, color, and transparency (Figure 12). All of the solvents affected these properties at different intensities, though the solvents 1-butanol, IPA, MEK, acetone, and propylene carbonate adversely affected the shape, color, and transparency of the hydrogels the most (Figure 12). The response of the hydrogels to the solvents could also be correlated through Hansen solubility parameters. Hansen solubility parameters account for three types of interactions between molecules: dispersion forces (d), dipole-dipole bonding (p) and hydrogen bonding (h). The volumetric yields of all of the hydrogels after one-step solvent exchange are presented as a function of the total solubility parameters, δt, for the respective solvents (Figure 13A). No clear trend was observed in the volumetric yields of the hydrogels with

respect to the solvent's total solubility parameters. However, the solvents with the total solubility parameters of 24.9, 26.7, and 29.6 (DMF, DMSO, and methanol, respectively) showed higher volumetric yields.

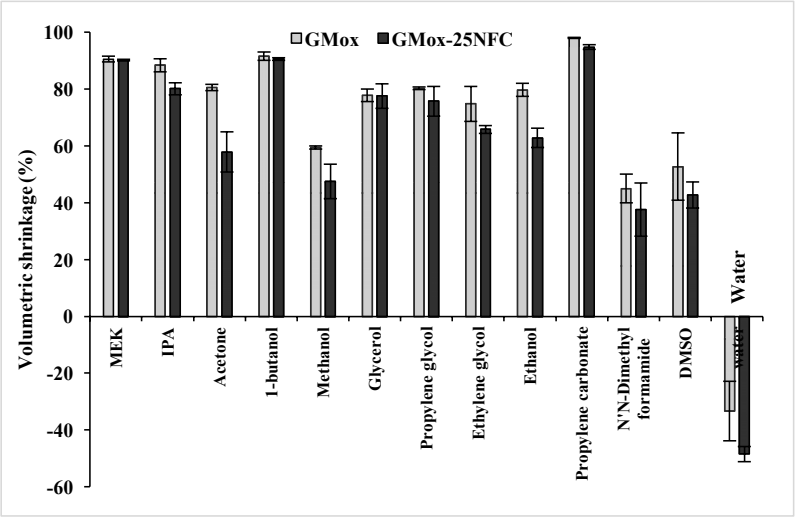

Figure 11: Volumetric shrinkage of the hydrogels in different solvents after one-step solvent exchange. Error bars represent standard deviation from three replicate samples.

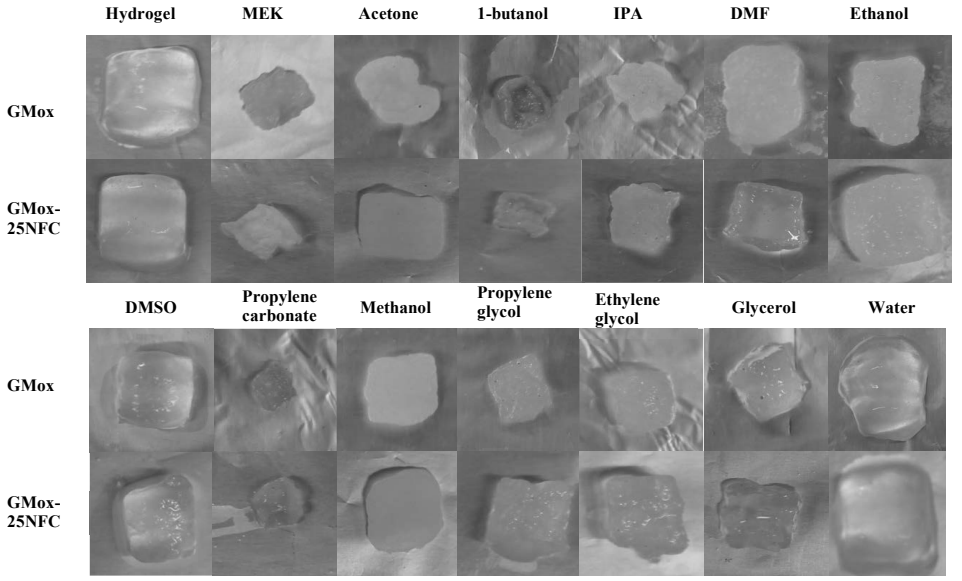

Figure 12: Photographs of the GMox and GMox-25NFC hydrogels after one-step solvent exchange in different solvents.

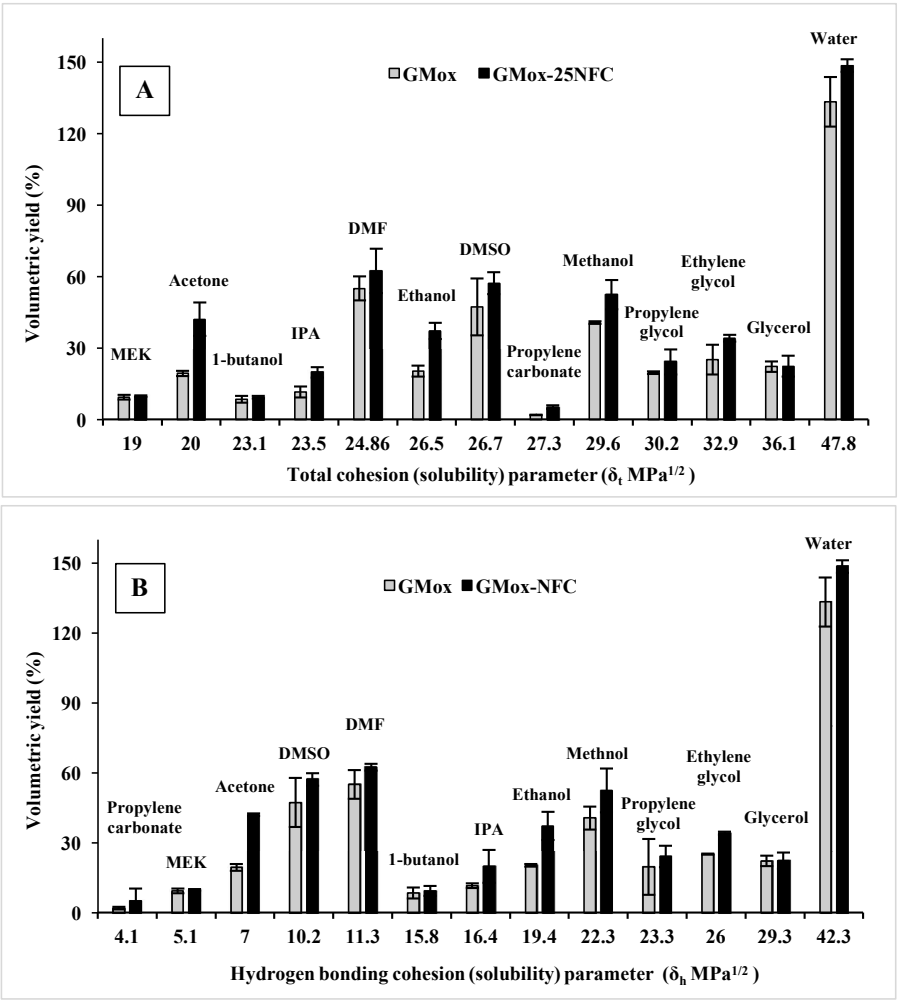

Figure 13: Relationship between the volumetric yields of the hydrogels and A) the Hansen total solubility parameters and the B) Hansen h component (hydrogen-bonding solubility parameter) of the respective solvent after one-step solvent exchange. The error bars represent standard deviations from three replicate specimens.

The volumetric yields of the hydrogels could also be influenced by a single dominant parameter rather than by the total solubility parameters, which comprise three individual components. When the volumetric yields of the hydrogels were presented as a function of the hydrogen-bonding Hansen solubility parameter (h), some trends could be observed in the data (Figure 13B). The volumetric yields followed a repeated increasing and decreasing pattern as a function of increasing h values. However, the other components of the total Hansen solubility parameter (d and p) did not follow these trends individually (data not shown).

5.3.2 Stepwise solvent exchange

The comparison of different solvents according to the Hansen solubility parameters provided direction for the choice of the solvents to be considered for further processing of the hydrogels to aerogels. The choice of solvent also depended on other factors, such as solvent compatibility with a supercritical fluid (CO_2) and the safety of the solvent. Ethanol and DMSO were used for further solvent concentration gradient studies and for sc-CO_2 drying due to their satisfactory performance.

Stepwise solvent exchange (five steps and six steps) was performed using ethanol and DMSO, and volumetric shrinkage was monitored at each step (Figure 14). GMox hydrogels preserved 80% of their volume after solvent exchange in a 20% ethanol solution (Figure 14A). Above a 40% ethanol solution, the GMox hydrogels showed large volumetric shrinkage and preserved only 20% of their original volume. An intermediate concentration of 30% ethanol was also used (six steps), and the overall volumetric yield had no difference as compared to the five-step solvent-exchange samples. A further increase in ethanol concentration led to only minor further decreases in the gel volume at 60% ethanol. No further volumetric shrinkage was observed at 80% and 100% ethanol. The GMox gels showed a different pattern of volumetric shrinkage with DMSO (Figure 14A). After solvent exchange in 20% DMSO, the GMox gels maintained 80% of their original volume. Interestingly, the GMox gels maintained more than 60% of their original volume after solvent exchange in 40% DMSO as compared to ethanol, where the largest volumetric shrinkage took place at this solvent concentration. However, after solvent exchange in 60% DMSO, the GMox gels showed a large volumetric shrinkage and preserved only 20% of their original volume. At 80% and 100% DMSO, no further volumetric shrinkage was observed for the GMox gels.

The GMox-25NFC gels showed a different shrinkage pattern (Figure 14B). GMox-25NFC showed swelling behavior after solvent exchange in a 20% solution for both ethanol and DMSO (Figure 14B). Both GMox and GMox-25NFC hydrogels displayed the swelling behavior in pure water (Figure 11), but surprisingly, only the GMox-25NFC hydrogels showed swelling during the stepwise solvent exchange. After solvent exchange in 40% and 60% ethanol, the GMox-25NFC hydrogels maintained 80% and 60% of their original volume, respectively, and did not show a further decrease in volume after solvent exchange in 80% and 100% ethanol. For DMSO, the GMox-25NFC hydrogels were able to preserve above 90%, 70%, and 60% of their original

volume after solvent exchange in 40%, 60% and 80% DMSO, respectively. Overall, the GMox-25NFC hydrogels maintained more than 50% of their original volume after the five-step solvent exchange with ethanol and DMSO.

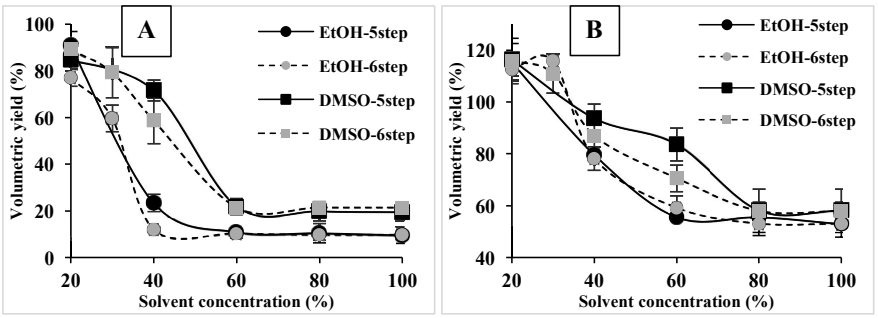

Figure 14: Volumetric yields of (A) GMox (B) and GMox-25NFC hydrogels at each step during the stepwise solvent exchange. Error bars represent standard deviations from three replicate specimens.

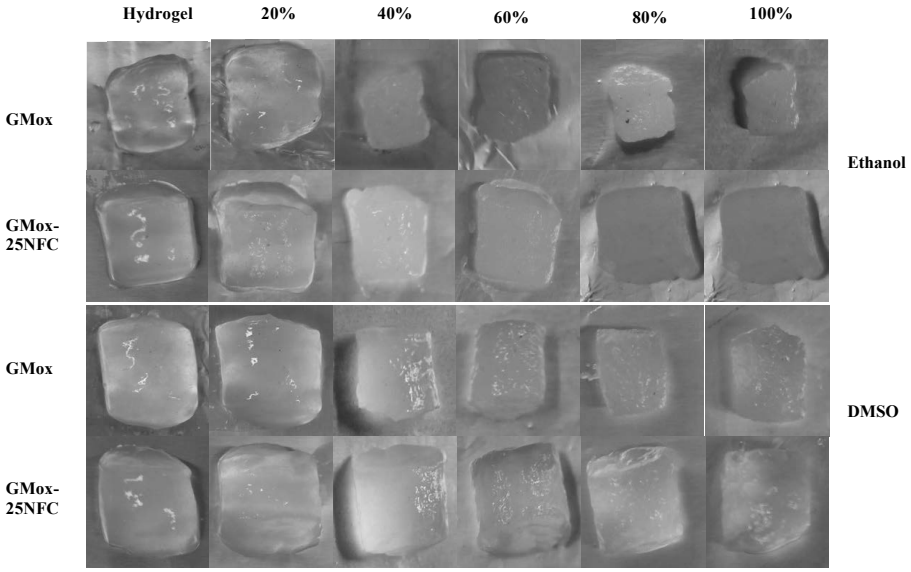

Figure 15: Visual observation of GMox and GMox-25NFC alcogels' and lyogels' shrinkage, shape, color, and transparency during the stepwise solvent exchange in ethanol and DMSO

Images of the alcogels (gel after solvent exchange in ethanol) and lyogels (gel after solvent exchange in DMSO) are presented in Figure 15 for visual observation of the shrinkage at every

step of the solvent exchange for ethanol and DMSO. The alcogels and lyogels of GMox-25NFC maintained a good appearance in terms of retained shape and smooth surface.

5.4 Aerogel formation

Aerogels were prepared using two different drying methods: lyophilization and supercritical CO_2.

5.4.1 Lyophilization

GMox and XGox aerogels with and without NFC were successfully prepared by lyophilization without structural collapse (Figure 16). Lyophilized aerogels did not show volumetric shrinkage in their outer dimensions, and the hydrogel's volume was fully replicated in the dry state (Study I and II). After lyophilization, in which the ice sublimated through the top surface of the specimens, the aerogels had a hard-upper crust, which was visually more noticeable in the top surface of the GMox than in the XGox aerogels.

5.4.2 Supercritical CO_2 drying

As a first step in supercritical CO_2 drying, the liquid phase (water) of the hydrogels was replaced with solvents, and their compatibility with the hydrogel's structure was tested with one-step solvent exchange. Based on this study, ethanol and DMSO were used to replace the liquid phase of the hydrogels in a stepwise solvent exchange. The alcogels and lyogels were dried using sc-CO_2 to prepare aerogels (Figure 16). During sc-CO_2 drying, shrinkage was observed in all types of aerogels (Table 5). Although DMSO effectively preserved the structure of the hydrogels during solvent exchange, large shrinkage occurred during the sc-CO_2 drying stage. Little shrinkage was observed in alcogels at the drying stage, as ethanol had already caused a higher volume shrinkage during the solvent exchange. Based on visual observations, the GMox-25NFC aerogels displayed a smooth and fine external surface with both solvents while wrinkles were observed on the GMox aerogel's surface. In addition, sc-CO_2 drying did not cause any cracks in the aerogel's surface.

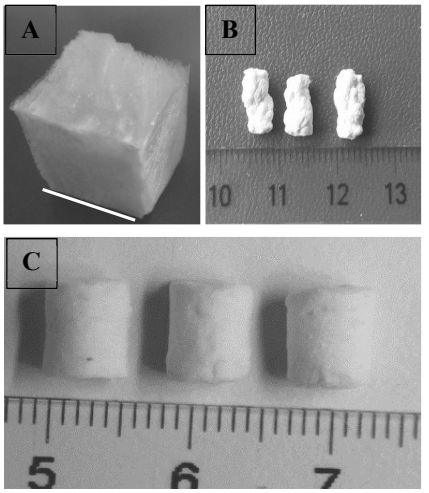

Figure 16: (A) Lyophilized GMox aerogel, (B) supercritical CO_2-dried GMox-EtOH, (C) and GMox-NFC-DMSO. The scale bar is 17 mm in (A).

5.5 Aerogel properties

Lyophilized and supercritical CO_2-dried aerogels showed different properties, which varied further with added NFC as a reinforcement.

5.5.1. Density of aerogels

Aerogels prepared by lyophilization were lightweight, and their density values were 0.019 ± 0.0009 and 0.012 ± 0.0009 g/cm^3 for the GMox and XGox aerogels, respectively. The density values of the NFC-reinforced aerogels were similar to those of the plain GMox and XGox aerogels. The GMox aerogels prepared by sc-CO_2 drying showed density values of 0.104 ± 0.03 g/cm^3 (GMox-EtOH) and 0.178 ± 0.02 g/cm^3 (GMox-DMSO), while the corresponding GMox-25NFC aerogels showed density values of 0.058 ± 0.01 g/cm^3 and 0.069 ± 0.01 g/cm^3, respectively (Table 5).

5.5.2 Morphology of aerogels

The morphology of the lyophilized aerogels, such as the shape and size of the pores, their distribution, the interconnection of pores, and the pore wall thickness, greatly depends on the growth of ice crystals during the freezing process. For sc-CO_2 drying, compatibility of the solvent with the hydrogel's structure and its miscibility with sc-CO_2 are the key parameters that determine the morphology of the aerogels. The behavior of the aerogel under mechanical stress, the shape recovery, and the specific surface area of the aerogels is highly dependent on the aerogel's morphology. The morphology of the aerogels was characterized using N_2-physisorption, and diploid microscopy probing techniques, such as SEM and a more sophisticated and high-resolution imaging technique like XMT, provided more insight into the inner structure of the aerogels.

BET-surface area

The surface area is an important characteristic of the aerogels from the perspective of possible applications, and this was measured with N_2-physisorption (Study I and III). The nitrogen sorption isotherms of GMox- and XGox-lyophilized aerogels reinforced with NFC were characterized as type II and IV according to the IUPAC classification system, reflecting the meso- and macroporous structures of the aerogels (Study I). Tested aerogels showed BET-specific surface areas between 2.3 and 4.8 m^2/g. The reinforcement by NFC at different levels did not affect the surface area (Table 5).

The BET surface areas of sc-CO_2-dried GMox aerogels were in the range of 182–219 m^2/g, depending on the solvent used for solvent exchange (Table 5). Remarkably, the sc-CO_2-dried GMox-25NFC aerogels showed an even higher BET surface area, up to 333 m^2/g. The BET surface area and pore radius (6.7–8.4 nm) indicated the presence of mesoporosity in the sc-CO_2-dried aerogels.

Scanning electron microscopy

The porous structure of the aerogels prepared by lyophilization (Study I) was characterized using focused ion beam–scanning electron microscopy (FIB-SEM).

The characteristic morphology and macrostructure differences among the GMox and XGox aerogels without NFC and with 25% NFC are presented in Figure 17. All lyophilized aerogels showed average macroporous structures, and pore sizes ranged from 125–250 μm, whether interconnected or individual. Figure 17A shows the FIB-milled surface of the GMox aerogel and the thin layer covering the top surface. Higher magnification of the FIB-milled area of the GMox-25NFC aerogel exposed the porous structures underneath (Figure 17B). The pores were interconnected, and the pore walls consisted of smooth films a few micrometers thick.

The porous structures of sc-CO_2-dried aerogels (Study III) were viewed using scanning electron microscopy (SEM) (Figure 17). The GMox and GMox-25NFC aerogels showed a mesoporous structure. GMox-25NFC aerogels showed a similar morphology to that observed for GMox aerogels, and differences were not observed between the morphology of aerogels prepared with ethanol and those prepared with DMSO. However, sc-CO_2 drying resulted in a completely different morphology of the obtained aerogels, with a high porosity and smaller pore-size distribution as compared to lyophilized aerogels (Figure 17).

Synchrotron X-ray microtomography (XMT)

SEM techniques are commonly used to visualize the porous structure of aerogels. However, these techniques are limited to surface characterization, and the internal structure was left to the imagination, providing an incomplete picture of the pore-size distribution within the aerogel matrix. In Study II, XMT was exploited to visualize the internal 3D structure of aerogels and to see the effects of ice templating and reinforcing by NFC on the pore size distribution of matrix polysaccharide (GMox and XGox) aerogels in relation to their mechanical behavior.

The resolution of XMT images depends on the dimensions of the aerogel samples. Cutting the polysaccharide aerogel samples into small sizes (e.g., < 1 mm width x length) for an XMT scan is difficult due to the elastic interconnected structure of the studied polysaccharide aerogels, which was noted in our earlier study (Mikkonen et al. 2014). Therefore, to avoid any structural damage at the sample-preparation stage, the samples presented here were prepared and characterized inside the small PEEK capillaries, unless otherwise mentioned. The PEEK capillary did not hinder the XMT signals. The results from the XMT were used to visualize the internal porous structure of the aerogels in 3D space. Furthermore, the results obtained from the quantitative analyses provided essential information for characterizing and examining the correlation of the aerogel's structure to the polysaccharide type, processing parameters, and mechanical performance.

Three-dimensional structure of aerogels

The XMT reconstruction can be viewed as a stack of two-dimensional grayscale images. These images clearly show bright areas corresponding to the solid polysaccharide structure and gray areas corresponding to the air voids. This contrast is produced due to the differences in the densities and the sample composition that directly reflect the change in the X-ray absorption in the sample. The shading (from white to gray) in the image corresponds to different X-ray absorptions due to the porosities of the aerogel. 3D renderings of the reconstructed volume are presented in Figures 18 to 22. The rendered volumes of all 3D images are 495.33 x 495.33 x 660.33 μm^3.

In lyophilization, the porous structure of the aerogels is the direct replica of the shape and size of the ice crystals formed during the ice-templating process; a pre-step of lyophilization. Two different ice-templating (freezing) conditions, conventional freezing (CF) and unidirectional freezing (UF), were applied to see the effect of freezing conditions on the porous structure and the pore size distributions within the aerogel matrix. GMox-CF aerogels exhibited anisotropic pore structures that could easily be seen when the sample was viewed along different axes (xy-axis, xz-axis, and yz-axis; Figure 18A). GMox-CF showed an intricate open cellular architecture of interconnected pores. The pore structure was irregularly arranged and showed porosities that reflected the random growth of ice crystals during conventional freezing. The pore wall, consisting of a thin film, was also observed around the pores. Reinforcing the GMox aerogel with 25% NFC remarkably changed the GMox aerogel structure (Figure 18B). The pores were also anisotropic, but smaller in size, and the porous structure was a highly-interconnected network of matrix polysaccharides.

When UF was used as an ice-templating method, the GMox-UF and GMox-25NFC-UF samples showed a structure that was oriented in the direction of freezing (Figures 19A and B). The oriented structure as a function of the direction of freezing was more prominent in the GMox-25NFC-UF sample (Figure 19B) compared to GMox-UF. Irrespective of the pore size, the pores were mostly connected to form nodular channels parallel to one another in the direction of freezing. The porous structures were anisotropic in the form of buttresses and exhibited smaller pore sizes as compared to those of GMox-UF (Figure 19A).

XGox-CF samples exhibited notably different morphologies as compared to those of the GMox-CF aerogels, in which the pore walls consisted of a well-defined thin film and the pores were heterogeneous in shape and size (Figure 20A). A thin film was also observed in the XGox-25NFC-CF samples. This thin film was not as smooth as in the XGox-CF sample, but was rather of a variable thickness (Figure 20B). A hexagonal, porous morphology was clearly observed in both the XGox-CF and the XGox-25NFC-CF samples, where the pores were well interconnected. UF resulted in a smaller pore size in XGox-UF (Figure 21A), where the porous structure was analogous to a honeycomb structure, and the pores were elongated in the direction of the freezing.

The XGox-UF aerogel reinforced with NFC showed a very similar geometry of the pores, and the UF resulted in the aligned structure of the pores (Figure 21B).

All the above-mentioned aerogel samples were prepared inside a capillary with an internal diameter of 0.8 mm, as explained in section 5.5.2.3. Next, a comparison of the aerogel's structures prepared in small dimensions was performed with samples prepared in large dimensions (Cubical aerogels: 17 x 17 x 17 mm^3). These cubical aerogel samples were compressed, as explained in section 4.6.3, before XMT scanning to observe any structural break down due to compression testing. Figure 23 represents the morphology of the bulk material (mechanically compressed [MC] cubical aerogel). The porous structure of the GMox-CF-MC was analogous to that of the GMox-CF (Figure 18A). The GMox-NFC-CF-MC aerogel showed a highly-interconnected structure (Figure 22B) compared to that of the respective GMox-CF-MC. The obtained aerogels exhibited a flexible structure that was squeezed when a compressive force was applied. Mechanical compression did not cause structural break down in the aerogel; instead, it bent the structure.

Quantitative morphology of aerogels

The digital nature of the XMT data enabled further quantitative analyses, such as the computation of the pore size and the pore wall thickness distributions.

Pore size distributions

The GMox-CF aerogels showed a random pore size distribution; although they had some large pores of over 300 μm, most of the pores were distributed in the range of 100 μm to 250 μm (Figure 23A). The addition of 25% NFC to the GMox-CF aerogels supports the effect of reinforcement on the pore size distribution (mostly in the range of 100 μm to 175 μm) of the polysaccharide aerogel (Figure 23B). The UF of the GMox-UF aerogels shifted most of the pore size distributions below 200 μm (Figure 23C). Considering both parameters, the NFC addition and UF, at the same time resulted in a pore size reduction of 50%, with most of the pores residing in the range of 25 μm to 85 μm (Figure 23D). The XGox-CF aerogel also exhibited pore size distributions between 50 μm to 200 μm, however, some pores over 400 μm were also observed (Figure 24A). The XGox-UF and XGox-25NFC-UF aerogels exhibited similar pore size distributions (Figures 24) as the GMox-UF and GMox-25NFC-UF aerogels (Figures 23). When comparing the pore size distributions of the MC cubical aerogel samples, most of the pores in the GMox-CF-MC aerogels were below the 200 μm mark, but some were larger than 400 μm (Figure 25A). The GMox-25NFC-CF-MC aerogels showed 50% of the pores were distributed below 100 μm and the remainder fell between 100 μm and 250 μm, with some pores as large as 300 μm (Figure 25B).

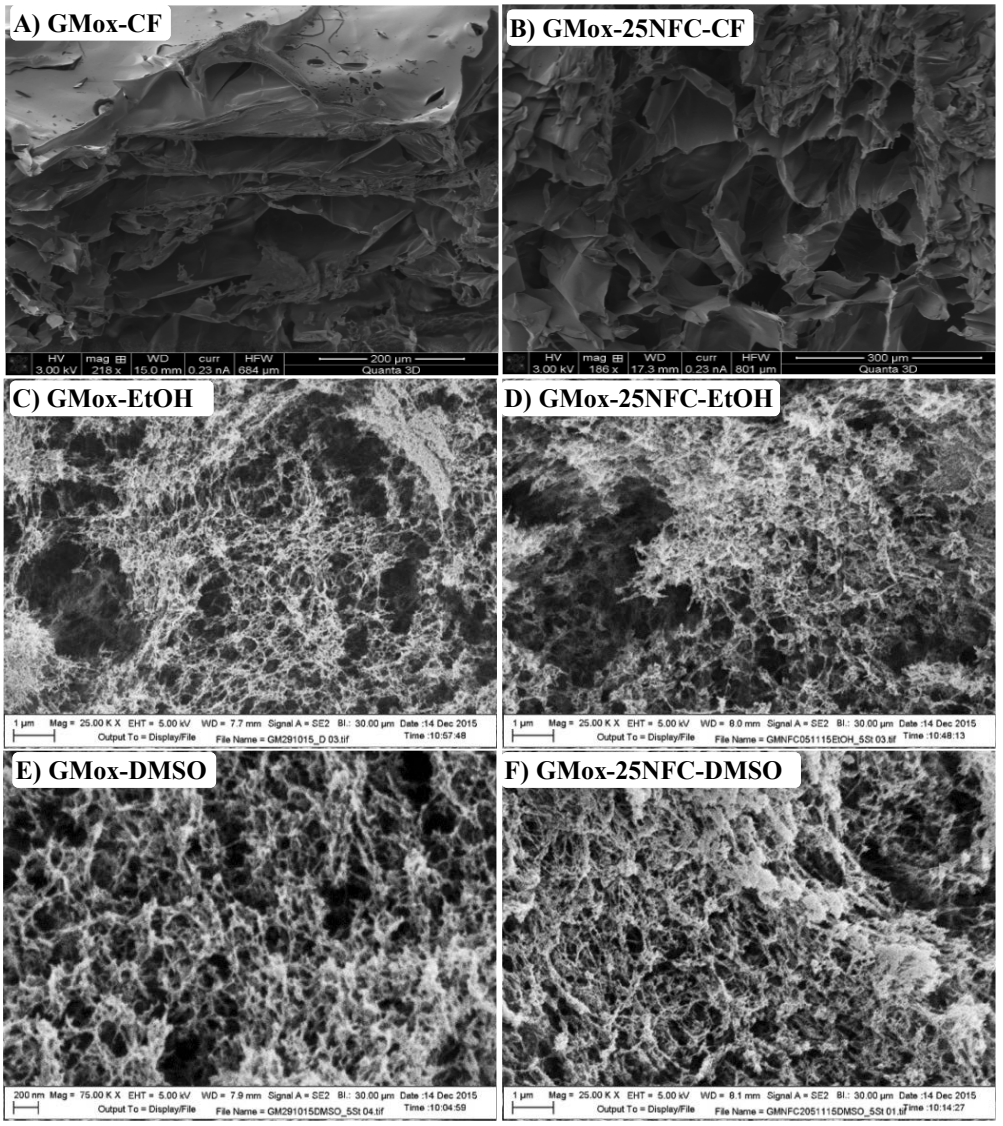

Figure 17: Focused ion beam scanning electron microscope (FIB-SEM) images of lyophilized aerogels. A) GMox-CF, and B) GMox-25NFC-CF. Scanning electron micrographs of sc-CO_2-dried GMox aerogels (C and E), and GMox-25NFC aerogels (D and F), using ethanol (EtOH) and dimethyl sulfoxide (DMSO) in a solvent exchange (five steps), respectively. CF = conventional freezing. The scale bars are 200 µm, 300 µm, and 200 nm for A, B, and E respectively, and 1 µm for C, D, and F.

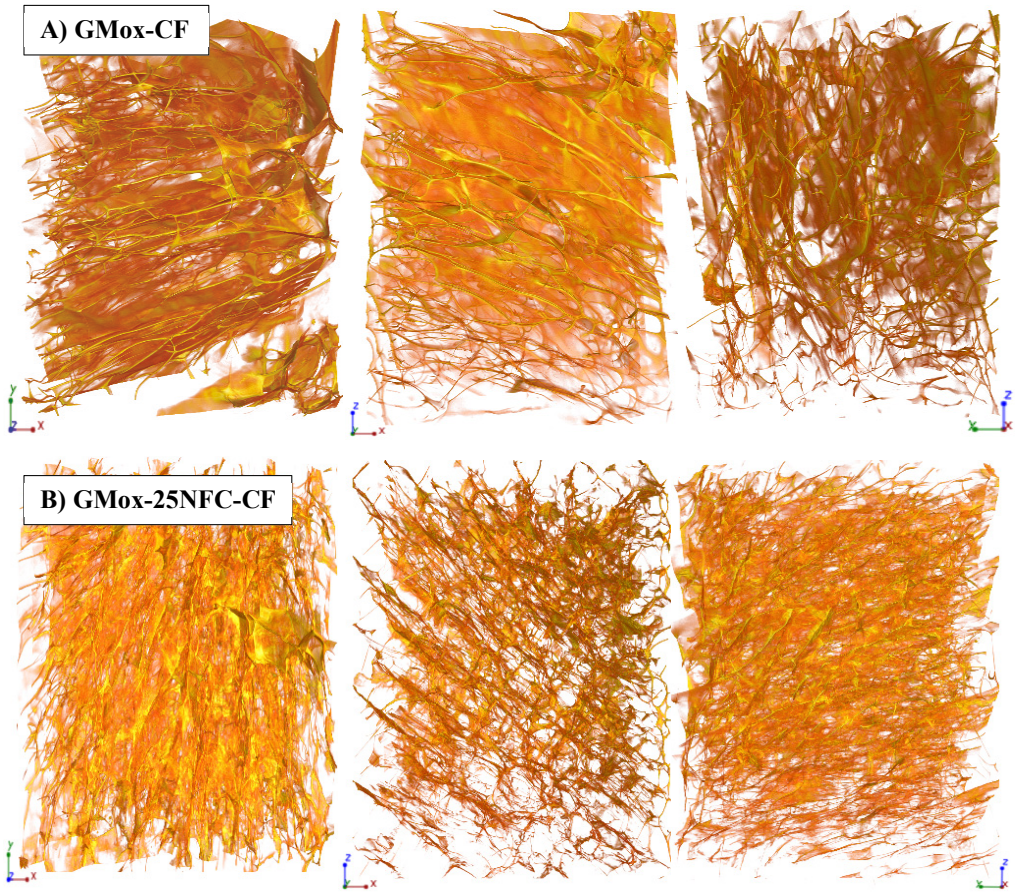

Figure 18: Three-dimensional reconstructed images from the synchrotron phase contrast microtomography of an A) oxidized GM (GMox) aerogel and B) an aerogel reinforced with 25% NFC (GMox-25NFC), prepared by conventional freezing (CF). The size is 495.33 x 495.33 x 660.33 μm^3 in the XYZ axis.

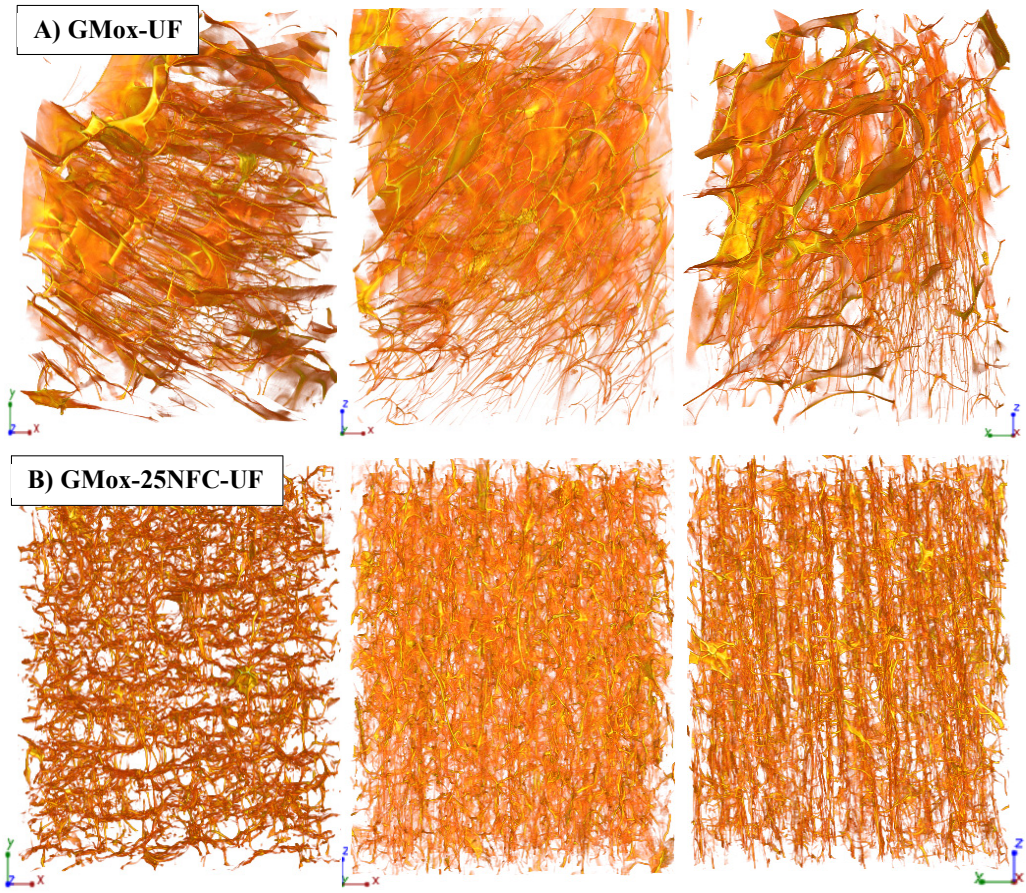

Figure 19: Three-dimensional reconstructed images from the synchrotron phase contrast microtomography of an A) oxidized GM (GMox) aerogel and B) an aerogel reinforced with 25% NFC (GMox-25NFC), prepared by unidirectional freezing (UF). The size is 495.33 x 495.33 x 660.33 μm^3 in the XYZ axis.

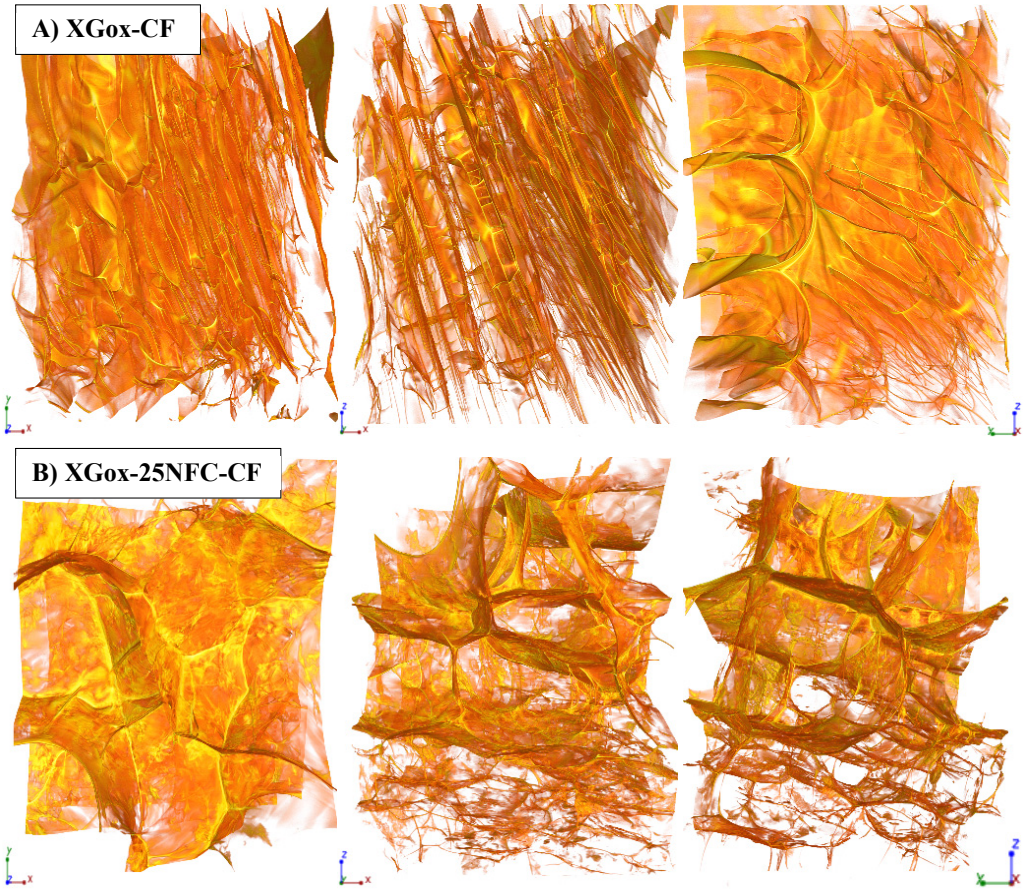

Figure 20: Three-dimensional reconstructed images from the synchrotron phase contrast microtomography of an A) oxidized XG (XGox) aerogel and B) an aerogel reinforced with 25% NFC (XGox-25NFC), prepared by conventional freezing (CF). The size is 495.33 x 495.33 x 660.33 μm^3 in the XYZ axis.

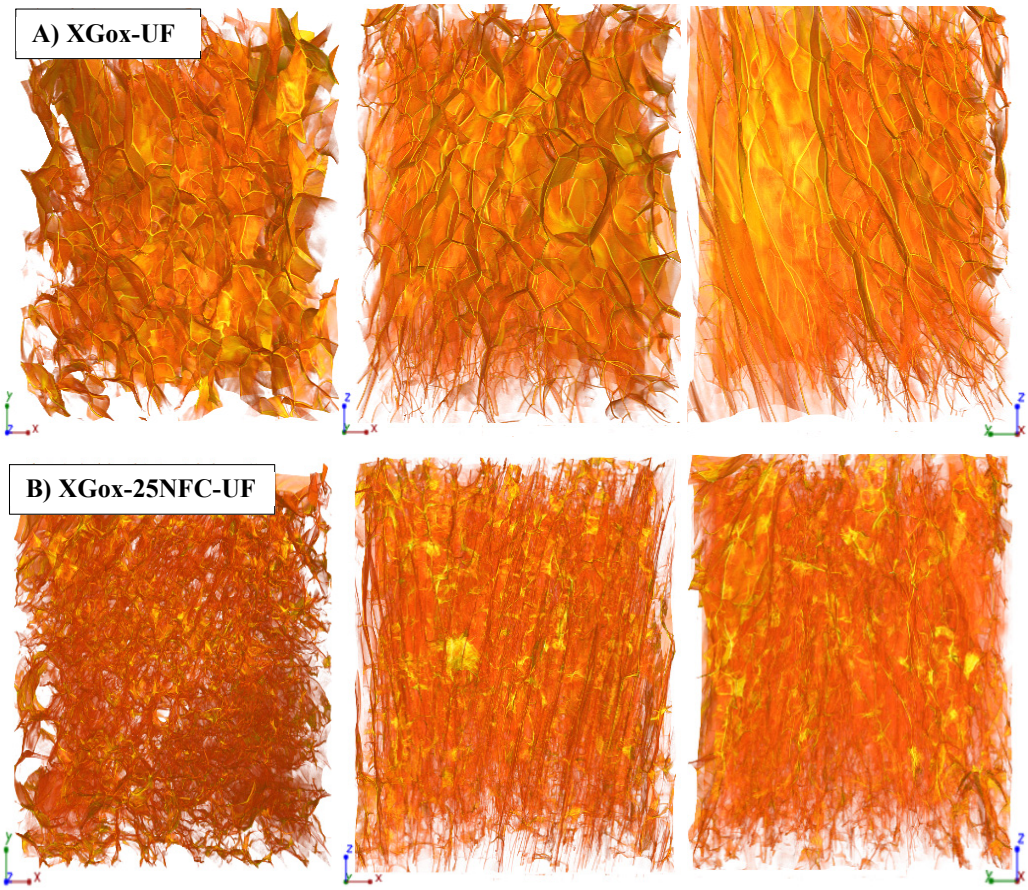

Figure 21: Three-dimensional reconstructed images from the synchrotron phase contrast microtomography of an A) oxidized XG (XGox) aerogel and B) an aerogel reinforced with 25% NFC (XGox-25NFC), prepared by unidirectional freezing (UF). The size is 495.33 x 495.33 x 660.33 μm^3 in the XYZ axis.

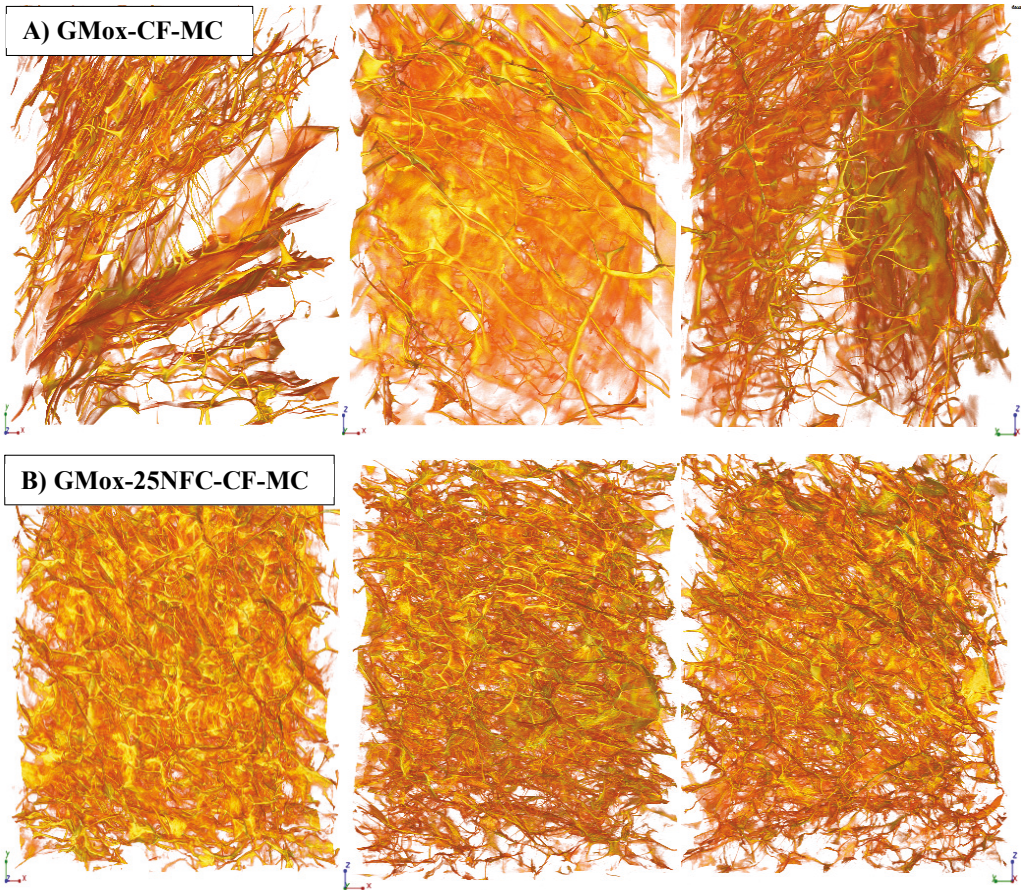

Figure 22: Three-dimensional reconstructed images from the synchrotron phase contrast microtomography of an A) oxidized GM (GMox) aerogel and B) an aerogel reinforced with 25% NFC (GMox-25NFC), prepared by conventional freezing (CF) from mechanically compressed (MC) aerogel. The size is 495.33 x 495.33 x 660.33 μm^3 in the XYZ axis.

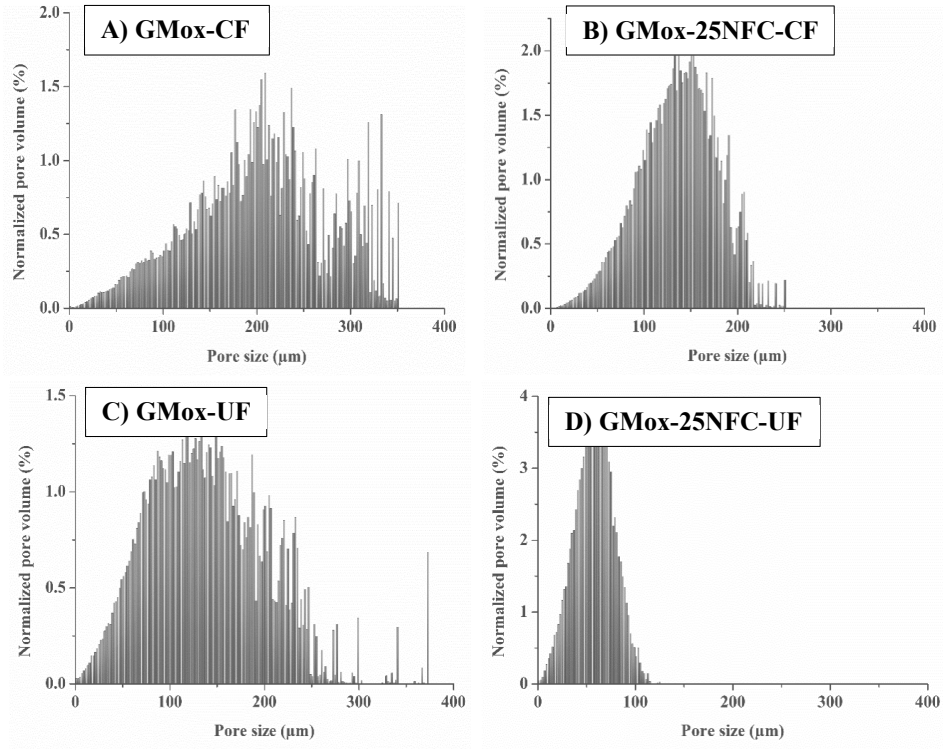

Figure 23: Pore size distributions of GMox (A and C) and GMox reinforced with 25% NFC (GMox-25NFC; B and D), prepared by conventional freezing (CF) and unidirectional freezing (UF).

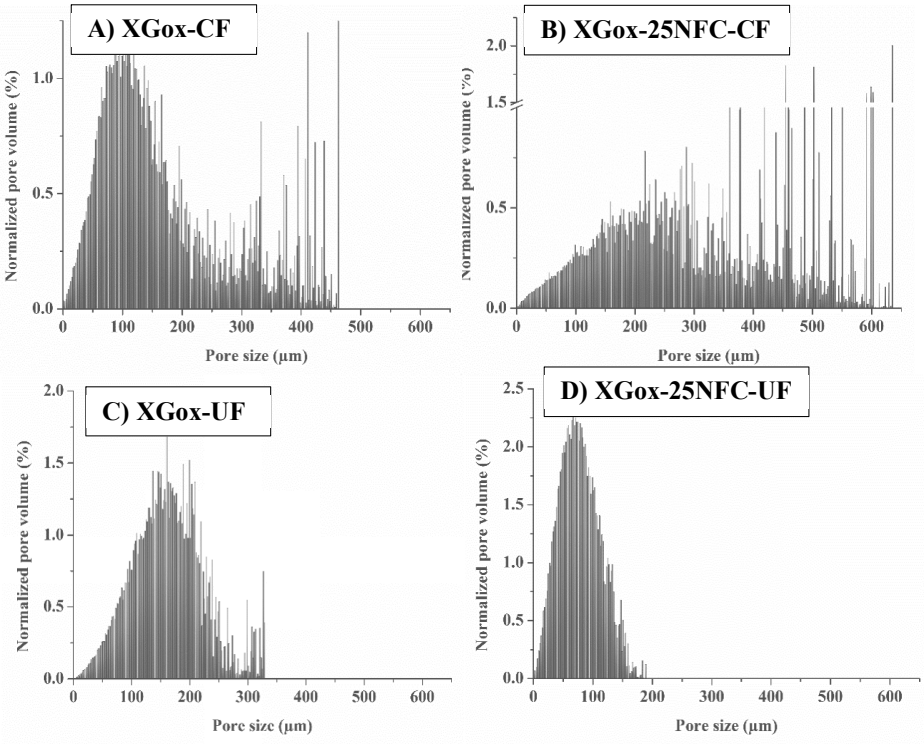

Figure 24: Pore size distributions of XGox (A and C) and XGox reinforced with 25% NFC (XGox-25NFC; B and D), prepared by conventional freezing (CF) and unidirectional freezing (UF).

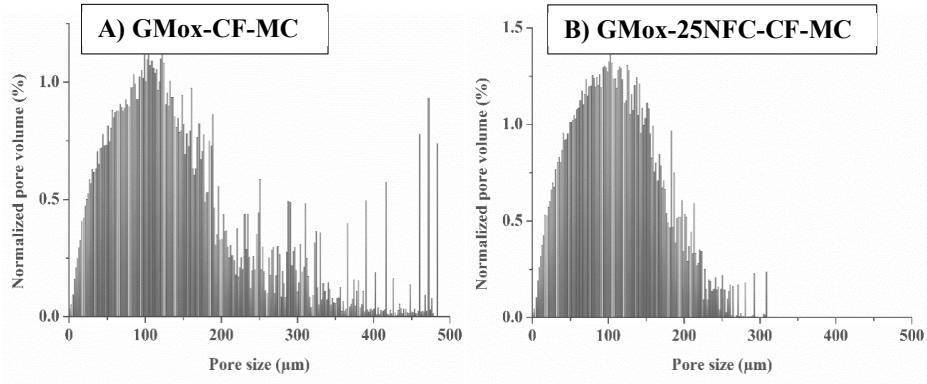

Figure 25: Pore size distributions of mechanically compressed (MC) aerogels of (A) GMox and (B) GMox reinforced with 25% NFC (GMox-25NFC), prepared by conventional freezing (CF).

Volume-weighted pore wall thickness distribution

The pore wall thickness of GMox and XGox aerogels with and without NFC was mostly in the range of 3 μm to 7 μm, regardless of the freezing method (Study II). Aerogel samples of GMox and GMox-25NFC from the MC cubical sample (Study II) also showed pore wall thicknesses comparable to those of the aerogel samples prepared inside the capillaries. The aerogels obtained did not show external volumetric shrinkage. However, the pore walls showed a bending/buckling structure that was observed in all of the aerogel samples (Study II and the supplementary data).

5.5.3 Mechanical properties

Mechanical behavior is a key characteristic of the aerogels that depends on the geometry of the pores (shape and size) in the 3D architecture of the material and the density. The drying method has a direct influence on the porous structure of the aerogels. Aerogels were prepared using two drying methods: lyophilization and supercritical CO_2. Both drying techniques resulted in completely different morphologies of the aerogels, so it is important to know the mechanical behavior of the lyophilized and supercritical CO_2-dried aerogels. The aerogels were compressed to one-third of their original height to characterize the mechanical behavior.

Lyophilized aerogels (Study I) showed ductile characteristics and were plastically deformed without fracture upon application of the compressive force, which was visually observed during the compression testing. During the mechanical compression testing, the structure of the GMox aerogels was more smoothly compressed than that of the XGox aerogels, where the structure bent inwards from one or two sides. In this study, NFC was added as a reinforcement at different concentrations (5%, 15%, and 25%) to observe the effect of reinforcement on the mechanical properties of the matrix polysaccharides (GMox and XGox). The GMox aerogels exhibited an increasing trend in compressive moduli with NFC reinforcement (Figure 26). The plain GMox aerogels had a compressive modulus of 74 kPa, and the GMox-5NFC aerogels had a compressive modulus of 104 kPa. At 15% (GMox-15NFC) and 25% (GMox-25NFC) NFC content, compressive moduli of 156 and 167 kPa were found, respectively. The plain XGox aerogels had a higher compressive modulus (106 kPa) than the corresponding plain GMox aerogel. However, only moderate increases in the compressive moduli were observed in the NFC-reinforced XGox aerogels. The compressive moduli were 115, 122, and 126 kPa for the XGox-5NFC, XGox-15NFC, and XGox-25NFC aerogels, respectively (Figure 26).

In Study II, aerogels were also prepared by lyophilization. The porous structure of the lyophilized aerogels is the direct replica of the ice crystals formed during the freezing process, which permits more control over the porosity of the aerogel. Therefore, two different ice-templating methods (CF and UF) were used in this study to affect the porous structure of the obtained aerogels and, hence, the mechanical and shape-recovery properties of the aerogels.

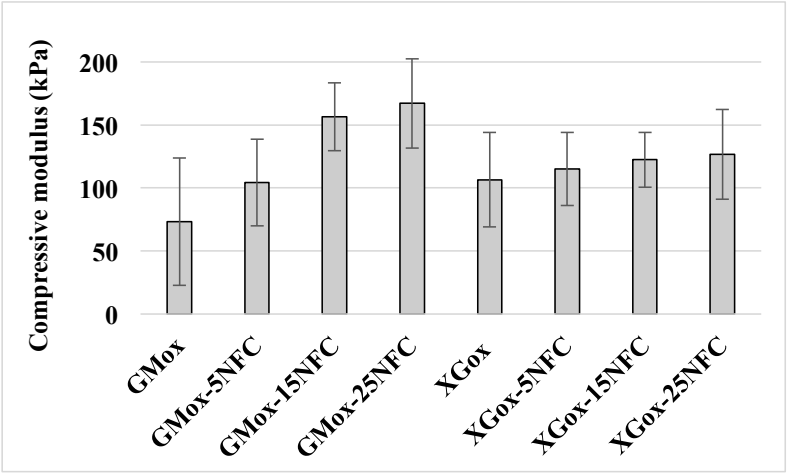

Figure 26: Compressive moduli of oxidized GMox and XGox aerogels with and without NFC reinforcement (5%, 15%, and 25%) prepared by lyophilization. The analyses were based on 10 analytical replicates. The error bars indicate standard deviation.

The compressive moduli of the aerogels were in the range of 16 kPa to 330 kPa, depending on the polysaccharide type, the addition of NFC, and the ice-templating method (Figure 27A). The GMox-UF aerogels showed a higher compressive modulus compared to the other aerogels. GMox-NFC-CF aerogels displayed a higher compressive modulus compared to GMox-CF. However, XGox-NFC-CF aerogels did not follow this trend, and the same was also true for both GMox-NFC-UF and XGox-NFC-UF aerogels. Reinforcement with NFC (25%) clearly exhibited significant effects on narrowing the pore size distributions. However, the effect of NFC on the mechanical properties was not clearly observed for XGox aerogels.

The shape recovery (height recovery after compression) of the aerogels is presented in Figure 27B. The GMox-UF and GMox-NFC-UF aerogels exhibited shape recovery, contrary to the corresponding aerogels prepared by conventional freezing. Shape recovery of the GMox and XGox aerogels was higher than that of the corresponding aerogels containing NFC as a reinforcement when the conventional freezing method was used. The shape recovery and compressive moduli of the XGox and XGox-NFC aerogels also followed the same trend within the freezing method (Figure 27B).

In Study III, another parameter was determined to calculate the stiffness of sc-CO_2-dried aerogels in response to added NFC. Due to volumetric shrinkage, the dimensions of the samples varied between GMox and GMox-25NFC, so the maximum force was calculated when the aerogels were compressed to one-third of their original height. GMox-EtOH and GMox-DMSO aerogels exhibited maximum forces of 20 N and 40 N, respectively (Figure 28). The suffix (EtOH and

DMSO) of each sample's name indicates the solvent used for solvent exchange. The higher maximum force for GMox-DMSO can be explained by the higher density of these aerogels. GMox-25NFC-EtOH and GMox-25NFC-DMSO aerogels showed maximum forces of 33 N and 45 N, respectively.

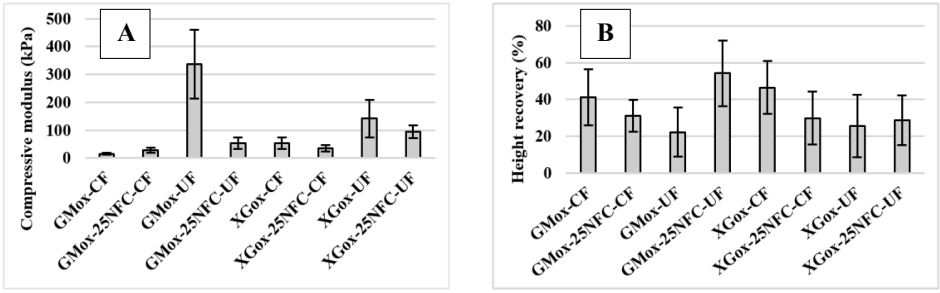

Figure 27: A) Compressive moduli and B) height recovery after the compression test of the aerogels. GM = guar galactomannan, XG = tamarind xyloglucan, ox = oxidized, NFC = nanofibrillated cellulose, CF = conventional freezing, UF = unidirectional freezing.

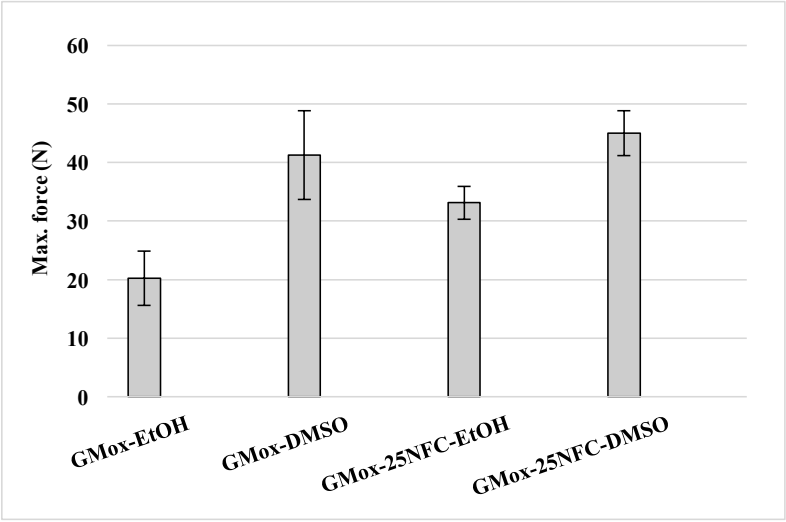

Figure 28: Maximum force during compression testing of sc-CO_2-dried aerogels. EtOH (ethanol) and DMSO indicate the solvent used for solvent exchange. Error bars represent standard deviation from six replicate measurements.

5.5.4 Correlations between the properties of the hydrogels and aerogels

Principal component analysis (PCA) was used as an explanatory tool for grouping the measured variables and envisioning the positions of different sample types in terms of their properties (Figure 29). The moduli of the hydrogels and aerogels, as well as the hydrogel adhesiveness, loaded positively on principal component 1 (PC1), whereas negative loadings for the cohesiveness, springiness, resilience, maximum compressive force (MCF) of hydrogels, and BET surface area of aerogels were obtained. Principal component 2 (PC2) separated the negatively loaded compressive modulus of the hydrogels, adhesiveness, MCF, and BET surface area from the other, positively loaded properties. The first two principal components (PC1 and PC2) explained 39.6% and 33.2% of the variance and resulted in a cumulative value of 72.8%. The factor scores (Figure 29B) distinguished the samples with positive scores on PC1 for GM-based and negative scores on PC1 for the XG-based hydrogels and aerogels, while PC2 separated the GM and XG hydrogels and aerogels according to the NFC content.

The variables with high PC1 loadings, that is, the viscoelastic properties of hydrogels and the stiffness of hydrogels and aerogels, were associated with high factor scores for the GMox samples. PC1 seemed to reflect the polysaccharide matrix composition and stiffness of the samples versus their textural properties (Figure 29A). The high PC2 loadings tended to follow the higher NFC content, regardless of the matrix biopolymer type (GM and XG). From the PCA

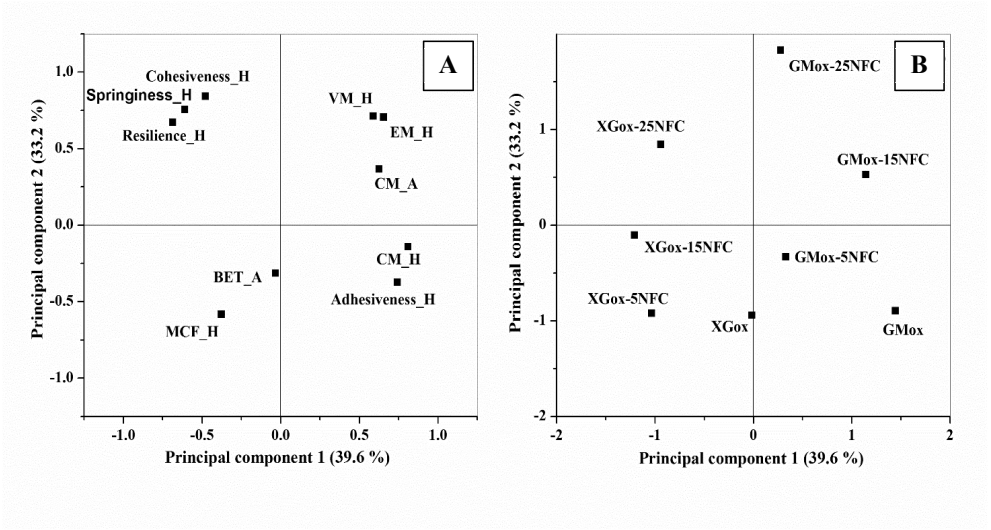

Figure 29: Principal component analysis (PCA) factor loadings for the various (A) hydrogel and aerogel properties and (B) factor scores for the sample types plotted against the first two principal components. H = hydrogels, A = aerogels, CM = compressive modulus, MCF = maximum compressive force, VM = viscous modulus, and EM = elastic modulus. The sample abbreviations and compositions are explained in Table 1.

results, we confirmed that the properties of GMox and XGox in hydrogel and aerogel form were determined by the NFC content and the interaction of the matrix biopolymer (GM and XG) with the NFC. The high G´ and G´´ of the NFC-reinforced GMox hydrogels, as determined with rheology, were associated with a high compressive modulus of the aerogels, indicating that highly elastic hydrogels may produce stiff aerogels.

6 DISCUSSION

Aerogel formation consists of two steps, the formation of the hydrogels followed by the removal of the liquid phase using techniques capable of leaving the hydrogel's 3D structure intact in dry form. GM and XG were used as aerogel-forming matrices and cross-linked using enzymatic oxidation to form hydrogels, a gel in which the solvent is water. NFC was used as a reinforcing agent to obtain composite GM- or XG-based aerogels.

6.1 Hydrogel properties

The native aqueous solutions of both matrix polysaccharides (GM and XG) are not able to form a gel, but rather display the properties of a viscous solution (Figure 9). These properties remained unchanged even with addition of 25% NFC. After enzymatic cross-linking, both GMox and XGox form hydrogels with added NFC. The degree of oxidation shows that the addition of NFC did not affect the enzymatic activity (Table 4).

6.1.1 Viscoelastic and textural properties of hydrogels

The viscoelastic properties of the hydrogels showed that the addition of NFC strengthened the structure of both GMox and XGox hydrogels, increasing with increasing quantities of NFC (5%, 15%, and 25%; Figure 9). However, the strengthening effect of the NFC depends on the type of matrix polysaccharide (GM or XG). The GMox hydrogels displayed three times higher elastic moduli (170 Pa) with the incorporation of 25% of NFC as compared to the plain GMox hydrogels. On the other hand, The XGox hydrogels showed an elastic modulus of 12 Pa, and the addition of 25% NFC increased the elastic modulus by eleven times (137 Pa; Table 4). When a large deformation was applied to the hydrogels (compression testing), the XGox ones exhibited a stronger structure as compared to the GMox hydrogels with added NFC (Figure 10), which supports the viscoelastic data. However, the GMox-based hydrogels reinforced with NFC (5–25%) displayed faster instant shape recovery as compared to the XGox-based hydrogels due to the higher cohesiveness and springiness values (Table 4).

GM tends to form different structural conformations in aqueous solutions, such as a flexible random coil, a star-like structural conformation (Wientjes et al. 2000), and a semi-helix and helix configuration were reported upon the removal of the D-galactosyl side group. These complex conformations and faster hydrogel formation, due to the higher oxidizable galactose content (40%), may affect the GM–GM and GM–NFC interactions and the formation of networks after the enzyme-induced gelation. Instead, XG tends to form flat, ribbon-like conformations, which are akin to cellulose (Umemura and Yuguchi 2005). A recent study reported that XG had rectilinear, slender and rod-like structures, which could aggregate as a cross-like shape, parallel-like shape assemblies, and probably rope-like shape structures (Kozioł et al. 2015). Furthermore, XG has a natural affinity to bind to cellulose surfaces (Zhao et al. 2014). Therefore, the enzyme-mediated gelation and adsorption of XG onto NFC surfaces may proceed simultaneously (slow

gel formation because of lower amount of oxidizable galactose units [16 %]), during the hydrogel formation that might explain the strong network development.

GM and XG are food-grade biopolymers (Mishra and Malhotra 2009; Wielinga 2009), and the GMox and XGox hydrogels are considered safe for food-related applications, such as low-calorie food applications, the formation of edible films for food packaging, and biomedical applications such as a topical therapy for skin and cell culture transportation (Chen et al. 2012; Li 2016), because these hydrogels are prepared using an environmentally friendly enzymatic technique without the addition of hazardous chemicals. The rheological and texture profile properties provide information about the hydrogels that is useful for their applicability and processability in industrial manufacturing, either as a hydrogel or during their conversion into dry aerogels.

6.1.2 Hydrogel's structural response to solvents

To proceed with the sc-CO_2 drying, a pre-step of replacing the water with a solvent compatible with the hydrogel's structure that was also miscible with sc-CO_2 was required. There is no study available on the sc-CO_2 drying of GMox-based hydrogels to aerogels. Therefore, GMox-based hydrogels were subjected to a one-step solvent exchange study with thirteen different solvents of varying polarities to see the structural shrinkage response to different solvents.

Immersing the GMox hydrogels directly into pure solvent showed a higher volumetric shrinkage of the hydrogels that was inversely proportional to the polarity of the tested solvents (Figure 11). However, GMox hydrogels with 25% NFC displayed low volumetric shrinkage. Furthermore, immersion of the hydrogels into pure solvent also caused other changes to their properties, such as changes in shape, color, and transparency (Figure 12). Hansen solubility parameters of the solvents were used to gain more understanding about the volumetric shrinkage response of the hydrogels.

When volumetric yields of the hydrogels were displayed as function of the solvent's total Hansen solubility parameters, δt, then no significant correlation was found in the data (Figure 13A). However, when the volumetric yields of the hydrogels were presented as a function of the hydrogen bonding component of the Hansen solubility parameter (h values), then the solvents were grouped based on functionality (Figure 13B). This showed that the volumetric yields of the enzymatically cross-linked GMox-based hydrogels seemed to be an increasing function of the hydrogen-bond component of the Hansen solubility parameter (h values) for the solvents that shared a chemical similarity. The Hansen solubility parameter provides a direction for solvent selection that is compatible with the hydrogels. However, the choice of solvent also depends on other factors, such as solvent miscibility with a supercritical fluid (CO_2) and the safety of the solvent. Based on these factors, ethanol and DMSO were selected for further solvent concentration gradient studies and for sc-CO_2 drying.

Immersion of the hydrogels stepwise in an increasing concentration of solvent showed low volumetric shrinkage and resulted in higher volumes of recovery. GMox and GMox-25NFC hydrogels exhibited different patterns of behavior as compared to each other within a solvent and with the different solvent types (ethanol or DMSO; Figure 14). Solvent concentrations of 40% and 60% for ethanol and DMSO, respectively, appeared to be critical concentrations for the studied hydrogels, as the maximum volumetric shrinkage was observed here. Severe structural changes occurred at this concentration range because the dehydration of hydrogel's structure and the hydrogel's body could not withstand the internal stress that lead to high volumetric shrinkage. This study showed that the compatibility of the solvent is very important to avoid higher volumetric shrinkage. These results also present the effective role of NFC in strengthening the structure of GMox hydrogels, as GMox-25NFC hydrogels showed good compatibility with both the ethanol and DMSO solvents. In earlier studies, the reported volumetric yields for polysaccharide-based hydrogels were in a similar range to the current study. For example, volumetric yields of 29% and 47% for calcium-alginate (1 wt.%) hydrogels after solvent exchange in ethanol and DMSO, respectively, were reported (Raman et al. 2015b). Calcium-alginate (2 wt.%) and potato starch (12.5 wt.%) hydrogels showed 36% and 23% volumetric yields, respectively, in ethanol (Mehling et al. 2009).

6.2 Effect of drying method on volumetric shrinkage

GMox- and XGox-based aerogels do not show any volumetric shrinkage during lyophilization and the aerogels retain almost all of the original volume of hydrogels (Figure 16). However, the GMox-based aerogels prepared by sc-CO_2 drying displayed significant volumetric shrinkage (Table 5). Studies showed that solvents such as DMSO have a good compatibility with hydrogel structures but exhibited higher volumetric shrinkage due to less miscibility with supercritical CO_2. In sc-CO_2 drying, the volumetric shrinkage can be minimized by using a mixture of solvents or using first DMSO followed by ethanol for solvent exchange before drying, which is a study that should be considered in the future. Volumetric shrinkage in the range of 60 to 85% was reported for sc-CO_2-dried polysaccharide-based aerogels, like from calcium-alginate, chitosan, and potato starch (Quignard et al. 2008; Mehling et al. 2009; Raman et al. 2015b). However, the volumetric shrinkage depends on the pre-history of the gels, such as the concentration, cross-linking technique, and solvent exchange procedure.

6.3 Effect of processing parameters on the aerogel's morphology

The properties of the aerogel are mainly based on the porous structure, which is more dependent on the type of drying method (Valentin et al. 2005; Quignard et al. 2008). In lyophilization, the porous structure is limited by the shape and size of the ice crystals formed during the freezing step, while the porous structure is least affected by sc-CO_2 drying if there is no volumetric shrinkage at the solvent exchange and drying steps.

Lyophilized GMox/XGox-based aerogels showed lower density values (Table 5) than those reported earlier for lyophilized polysaccharide-based aerogels (Table 2). However, sc-CO_2-dried GMox-based aerogels exhibited slightly higher density values due to volumetric shrinkage as compared to lyophilized aerogels (Table 5), but the values were still lower than those of many reported for sc-CO_2-dried polysaccharide aerogels (Table 2). The growth of ice crystals pushed the hydrogel's structure between the spaces of adjacent growing ice crystals, and when ice crystals were removed during lyophilization a well-defined pore wall was left behind (Figure 17) and larger pore sizes in the range of 125 to 250 μm were found (Figure 17). Therefore, the freezing step is very important, as it will determine the porous structure of the lyophilized aerogels. Larger pore sizes lead to a low BET-surface area (< 10 m^2/g) of these aerogels which is similar to earlier reported lyophilized NFC-xyloglucan (11.9 m^2/g) and NFC aerogel (11 m^2/g) (Table 5). Even lower BET-surface area was reported for starch and lignin composite aerogel (1.35 m^2/g) (Ago et al., 2016). On the other hand, the sc-CO_2-dried aerogels displayed a highly porous and highly interconnected network of aerogel matrix with a smaller pore size distribution (Figure 17). Due to the smaller pore size distribution, the sc-CO_2-dried GMox aerogels exhibited very high BET surface areas (ranging from 182 to 333 m^2/g) depending on the types of solvents used for the solvent exchange and types of aerogel (GMox or GMox-25NFC). Aerogel from GM (4 wt. % dry content) prepared by ethanol-induced gelation followed by sc-CO_2 drying showed lower BET-surface area (111 m^2/g) as compared to studied GM aerogels (1 wt. % dry content) (Table 5). However, literature showed that the BET-surface area of sc-CO_2 dried polysaccharide-based aerogels were up to 510 m^2/g for low methoxyl pectin aerogel (Horvat et al., 2017).

Morphological features, such as pore geometry, pore size distribution, and the visualization of the reinforcing agent and its distribution in the matrix, are very important in terms of applications and material properties. These features are not able to be measured with current probing techniques, such as electron microscopy or N_2-physisorption. Therefore, XMT was used to truly measure the morphology of the aerogels. The XMT technique displayed promising results, as the fine structure of the lyophilized aerogels was clearly observed in the 3D-rendered volume (Figures 18-22). The significant difference between the aerogels was observed in the geometry of the pores of both the GMox and the XGox samples and in their composite aerogels with added NFC within the same ice-templating method (Figure 18 and 20). The digital nature of the XMT data is another advantage, which allowed the processing of the data for quantitative measurements. For example, the pore sizes and pore wall distributions in the aerogels were calculated. Pore size distribution data depicted the significant effect of the NFC addition when these aerogels were prepared with CF (Figure 23 and 24). UF further narrowed the pore size distributions, which were more prominent in the aerogel samples containing NFC (25%; Figure 23 and 24). This showed that controlling the ice-templating conditions enabled the achievement of aerogels having an aligned structure and smaller pore size distributions without the addition of reinforcement. Considering both parameters (NFC addition and UF) at the same time resulted in aerogels with all pores below 100 μm. This was also true for XGox-based aerogels (Figure 24).

The hydrogel properties, such as stiffness and elasticity, are also considered key parameters in the ice-templating approach because they govern the critical freezing front velocity at which the biopolymer structure is trapped during solidification (Wegst et al. 2010). The structures of the XGox hydrogels are more stretchy as compared to the GMox hydrogels, which allowed their structure to quickly reposition between the growing ice crystals during conventional ice-templating (slow freezing), and the elasticity of the polysaccharide separated the ice crystals with a thin-film layer (Figure 20). The structure of the NFC-reinforced GMox and XGox hydrogels was stiff and constrained the size of the growing ice crystals.

The proper compatibility and interaction of the reinforcing agent with the matrix biopolymer are imperative for achieving a high-performance composite material. XMT was used to trace the NFC in the GMox and XGox matrices, though visualizing NFC in the 3D structure is difficult due to the similar attenuation of X-rays by NFC and the matrix polysaccharides. Therefore, in this study, the NFC was not distinguished from the matrix polysaccharides in their biocomposite aerogel structure. However, the XMT technique showed promising results in visualizing the detailed qualitative and quantitative morphological features of the lightweight bio-based materials. Quantitative morphological data from the XMT scans indicated that the pore size distribution of the aerogels could be tailored by the addition of NFC as a reinforcement, and fast freezing further assisted in the narrowing of the pore size distributions.

6.4 Mechanical properties

The mechanical behavior and shape recovery of the porous material depends on the geometry of the pores (shape and size) in the 3D architecture of the material (Sauter et al. 2013; Martoïa et al. 2016). The GMox- and XGox-based aerogels were ductile, and their structures were able to be squeezed into denser structures during compression testing instead of fracturing, as reported for calcium-alginate aerogels (Cheng et al. 2012). Both, GMox and XGox aerogels displayed stiff structures, with compressive moduli in the range of 75–100 kPa. However, the effect of the NFC reinforcement was much more prominent in the GMox aerogels (176 kPa) as compared to the XGox aerogels (126 kPa) (Figure 26).

Unidirectional ice-templating created a porous structure and larger pore walls that were perpendicular to the applied stress, which resulted in a higher resistance to compressive stress. Because of this, aerogels prepared by unidirectional ice-templating methods portrayed higher compressive moduli than those of the corresponding aerogels prepared by conventional ice-templating (Figure 27). However, the shape recovery behavior was contrary to the compressive moduli of the same aerogels (Figure 27B). Qualitative and quantitative data from the XMT, presented in Figure 18, were useful in explaining the reason behind this conflict. The larger pore walls buckled to their maximum capacity, and beyond that point, the compressive stress caused permanent deformations in the aerogel structure, which resulted in less shape recovery, as in the case of GMox-UF. These observations were not true for GMox-25NFC-UF aerogels (Figure

27B), because there was no permanent deformation that occurred due to the smaller pore size distributions. So, the composite aerogels exhibit higher shape recovery. The same observations were also true for XGox-UF and XGox-25NFC-UF.

Aerogels prepared by sc-CO_2 drying also significantly illustrated the strengthening effect of NFC (Figure 28). It is important to note that the choice of solvent and its compatibility with the structure had a direct link to their mechanical properties. GMox and GMox-25NFC aerogels prepared using DMSO in the solvent exchange displayed higher maximum force values (40 and 45 N, respectively) as compared to aerogels prepared using ethanol in the solvent exchange (20 and 31 N, respectively) (Figure 28). Most of the earlier studies on sc-CO_2 dried polysaccharide-based aerogels lack the information about mechanical testing (Table 2). The sc-CO_2 dried alginate-gelatin composite aerogels were mechanically tested in fully wet system (immersed in water for 20 h before testing) and showed the compressive modulus of 610 to 850 kPa (Baldino et al, 2016). Hybrid aerogels from alginate and starch exhibited compressive modulus of 60 to 560 kPa, which is also tested in wet system where aerogels were immersed in phosphate buffered-saline solution for 5-10 min before testing (Martins et al., 2015).

Correlation of the hydrogel's properties to the aerogel's properties was not straightforward, as it most likely depended on the drying method. There are some other factors, such as the stiffness of the hydrogel's structure, the amount of NFC reinforcement, the ice-templating method, the temperature of the ice-templating medium, the types of biopolymer, etc., that will also play a role.

6.5 Potential applications of studied polysaccharide-based aerogels

Polysaccharides are safe to use, biodegradable, and are derived from sustainable resources. The basic properties of polysaccharides remain intact after their selective modification using enzymatic oxidation, which has advantages over other inorganic methods for life-science applications. The polysaccharide-based aerogels presented here were prepared using two drying methods, lyophilization and sc-CO_2, via enzymatic oxidation, and they portrayed unique and different morphological features and related properties.

GMox- and XGox-based composite aerogels are safe for food and food-related applications because the cross-linking technique does not involve any toxic chemicals during the aerogel processing. Also, the aerogel-forming matrices (GM and XG) are food-grade additives that are already widely used as thickeners and stabilizers in the food industry (Wielinga 2009). Additionally, cellulose (NFC) is also used in food applications as a stabilizing agent, a functional food or drug for the treatment of intestinal disorders (using a formulation of 15 to 65% nanocellulose and 85 to 35% water-soluble saccharide), and in food packaging, as reviewed by Gómez et al. (Gómez H. et al. 2016).

GMox- and XGox-based composite aerogels displayed low density values, ductile structures, good mechanical stiffness, and shape recovery, which means they can be potentially utilized as

primary and secondary packaging materials to avoid mechanical abrasion to fruits and vegetables during transportation. Applications can be extended in the food sector by incorporating active ingredients prior to cross-linking or drying or after drying, such as antimicrobial agents, to develop active packaging materials (Lotfinia et al. 2013). Tirsodium citrate cross-linked starch aerogel prepared by lyophilization was loaded with volatile antifungal trans-2-hexenal. The sustained release of trans-2-hexenal resulted in slower lethality of *Aspergillus parasiticus* cells inoculated on pistachio nuts (Abhari et al., 2017). Due to the hydrophilic nature of polysaccharide-based aerogels (Mikkonen, Parikka et al. 2014), they have a potential application as absorbents. Lyophilized GMox- and XGox-based aerogels exhibited highly porous structures in which the pore size ranged from 125 to 250 μm, which is considered optimal for the growth of cells in soft-tissue regenerations as scaffold (Podlipec et al. 2014; Quraishi et al. 2015). The sc-CO_2-dried, GMox-based aerogels exhibited pore sizes in the nanometer range and resulted in a high surface area. Aerogels having such morphologies are beneficial for absorption and controlled release applications in the food industry, such as for flavor or nutraceutical ingredients or as carrier materials in the pharmaceutical industry (Comin et al. 2012; Yan et al. 2016).

Low thermal conductivity was reported for polysaccharide-based aerogels (Duong and Nguyen 2016; Horvat et al. 2017), suggesting thermal insulation applications, which could be accomplished with the further upgrade of flame retardant properties to the aerogel matrix (Fan et al. 2017). As mentioned earlier, GMox- and XGox-based composite aerogels are hydrophilic, which is considered a limiting factor for insulation applications. The aerogel structure can easily absorb and release moisture from and to the atmosphere, but structure of aerogels in term of shrinkage or breakdown remained stable at atmospheric humidity, according to the visual observation. However, surfaces can be easily modified to hydrophobic surfaces (Cheng et al. 2012). The enzyme-mediated gelation approach portrayed the incorporation of any ingredients or compounds into the gel matrix without compromising the cross-linking ability of enzymes, as demonstrated by the addition and entrapment of NFC. The advantage of using NFC as a reinforcement agent is that a new functionality on the NFC surface can be introduced using various surface-modification techniques (Missoum et al., 2013; Kalia et al., 2014), and that this functionality can be preserved in the aerogel matrix using enzymatic oxidation. The studied aerogels can be developed as conducting aerogels or magnetically responsive aerogels by the incorporation of carbon/graphene/nano-metallic particles. Moreover, the elastic behavior and textural profile properties of GMox- and XGox-based composite hydrogels showed potential for the pharmaceutical industry in toping applications containing active ingredients.

Both drying methods have their own merits and demerits. sc-CO_2 drying was successfully used to develop aerogels with meso- and macroporous structures, though the miscibility gap in the water/solvent/sc-CO_2 system has limitations. Lyophilized aerogels are limited to larger pore-sized structures, but can be used for loading active principles into the aerogel's matrices. This study showed that the careful selection of drying method, the control of processing conditions, and the addition of reinforcing agents will help to specifically tailor the properties of aerogels for certain

applications. In future, new drying techniques, such as microwave oven drying (Durães et al. 2013) will open new application opportunities for polysaccharide-based aerogels.

7 CONCLUSION

In this study, GaO was used to cross-link galactose-containing polysaccharides (GM and XG) in the presence of NFC as reinforcing agent to develop bio-based composite aerogels. The effect of NFC was studied on the formation of hydrogels and their properties, as well as on the properties of the corresponding aerogels. The role of NFC and the drying techniques (lyophilization and sc-CO_2) on the porous structure of the aerogels and their related properties were also investigated.

The results clearly portrayed that the cross-linking ability of GaO was not compromised with NFC reinforcement. This reinforcement improved the properties of GMox- and XGox-composite hydrogels, such as the shape retainability, stiffness, viscoelastic properties, and mechanical properties, as compared to the corresponding hydrogels made from plain GMox and XGox. However, the effect of NFC reinforcement depends on the type of matrix polysaccharide (GM or XG). The structures of all of the hydrogels were elastic and easy to mold into any desired shape. Textural profile analysis data showed that XGox-based hydrogels were more adhesive and stretchy as compared to GMox-based hydrogels. Solvent-exchange data revealed that volumetric shrinkage depends on the types of solvent, as the compatibility of solvent with hydrogel's structure is very important. Nevertheless, composite hydrogels exhibited significantly lower volumetric shrinkage as compared to plain polysaccharide hydrogels.

The characteristic morphology of lyophilized aerogels, such as pore size and shape, is directly based on the shape and size of the ice crystals formed during the ice-templating process. Because of this, the pore sizes of lyophilized aerogels were in the range of 125 to 250 μm, which results in a low specific surface area (< 10 m^2/g) for these aerogels. On the other hand, sc-CO_2 drying preserved the mesoporous structure of the aerogels, although this method caused significant volumetric shrinkage during the drying process. The porous structure of sc-CO_2-dried aerogels was notably different from the lyophilized aerogels. The size of the pores was a few nanometers to a few hundred nanometers, which resulted in specific surface areas up to 330 m^2/g. Mechanical testing data of aerogels showed that all of the obtained aerogels have a ductile structure and the structure was compressible when stress was applied. The lyophilized aerogels exhibited shape recovery behavior to some extent. Most importantly, GMox and XGox aerogels reinforced with NFC displayed a stiff and strong structure as compared to their corresponding plain aerogels.

In this thesis, XMT data revealed that it is a promising technique that can be utilized for the thorough characterization of the fine porous structure of bio-based aerogels in 3D space. Quantitative data from the XMT clearly demonstrated the effect of NFC reinforcement and ice-templating methods on the pore size distributions. Quantitative XMT data clearly depicted the effect of NFC in narrowing the pore size distribution and giving more homogeneous pores in the aerogel matrix. Interestingly, the pore size distribution can be narrowed to same range as observed with the addition of 25% NFC by just controlling the ice-templating method without NFC reinforcement. However, this pore size distribution was not homogeneous. Both the addition of

NFC and controlling the ice-templating method parameters worked together with a synergistic effect. The XMT data provided information about the shape recovery and mechanical behavior of the aerogels from their pore sizes and pore distribution within the aerogel matrix. Such information about the material's structure and function assists in the ability to design the porous structure of the aerogels in the future for desired applications by controlling the processing conditions. Such detailed information about the morphology is difficult to obtain with SEM techniques.

In short, this study showed that the properties of aerogels were dependent on many factors, such as the types of biopolymers (GM and XG) used, their interaction with NFC, and the morphology of the produced aerogel, including pore sizes and their distribution. This later characteristic was significantly dependent on the type of drying technique and pre-drying steps, which complicates the prediction of an aerogel's properties from a hydrogel's properties. Therefore, aerogels with desired characteristics can be obtained by the selection of starting material and drying technique with a careful control of processing parameters.

As shown here, enzyme-mediated gelation presented a promising technique to produce bio-based composite aerogels. This technique opens new possibilities for incorporating numerous reinforcing agents as well as biologically active ingredients into the aerogel matrix. The advantage of using NFC as a reinforcement agent is that a new functionality on the NFC surface can be introduced using various surface-modification techniques, and that this functionality can be preserved in the aerogel matrix using enzymatic oxidation. The obtained bio-based aerogels are hydrophilic in nature, however upon rehydration and ambient drying at room conditions will resulted in loss of structural integrity of the aerogels. But, these aerogels can withstand the atmospheric humidity conditions. The obtained bio-based composite aerogels can be labeled as "green materials," since the raw materials are isolated from renewable resources (plants) and there is no use of hazardous chemicals in the material preparation. These bio-based composite aerogels can also find various applications, such as for water absorbents, mechanical support for food packaging, biocompatible delivery systems, tissue-engineering scaffolds, and the encapsulation of active components, such as antioxidants.

8 REFERENCES

Abdul Khalil HPS, Davoudpour Y, Islam MN, Mustapha A, Sudesh K, Dungani R, Jawaid M. 2014. Production and modification of nanofibrillated cellulose using various mechanical processes: A review. Carbohydr.Polym. 99(0):649-65.

Abhari N, Madadlou A, Dini A. 2017. Structure of starch aerogel as affected by crosslinking and feasibility assessment of the aerogel for an anti-fungal volatile release. Food Chemistry 221:147-152.

Ago M, Ferrer A, Rojas OJ. 2016. Starch-based biofoams reinforced with lignocellulose nanofibrils from residual palm empty fruit bunches: Water sorption and mechanical strength. ACS Sustainable Chem.Eng. 4(10):5546-52.

Ahmed EM. 2015. Hydrogel: Preparation, characterization, and applications: A review. Journal of Advanced Research 6(2):105-21.

Alakalhunmaa S, Parikka K, Penttilä PA, Cuberes MT, Willför S, Salmén L, Mikkonen KS. 2016. Softwood-based sponge gels. Cellulose 23(5):3221-38.

Alemdar A, Sain M. 2008. Isolation and characterization of nanofibers from agricultural residues – Wheat straw and soy hulls. Bioresource Technology 99(6):1664-71.

Aminabhavi TM, Nadagouda MN, Joshi SD, More UA. 2014. Guar gum as platform for the oral controlled release of therapeutics. Expert Opinion on Drug Delivery 11(5):753-66.

Baldino L, Concilio S, Cardea S, Reverchon E. 2016. Interpenetration of natural polymer aerogel by supercritical drying. Polymers 8:106.

Barros A, Quraishi S, Martins M, Gurikov P, Subrahmanyam R, Smirnova I, Duarte ARC, Reis RL. 2016. Hybrid Alginate-based cryogels for life science applications. Chemie Ingenieur Technik 88(11):1770-8.

Błaszczyński T, Ślosarczyk A, Morawski M. 2013. Synthesis of silica aerogel by supercritical drying method. Procedia Engineering 57200-6.

Borges AC, Eyholzer C, Duc F, Bourban P, Tingaut P, Zimmermann T, Pioletti DP, Månson JE. 2011. Nanofibrillated cellulose composite hydrogel for the replacement of the nucleus pulposus. Acta Biomaterialia 7(9):3412-21.

Borisova A, De Bruyn M, Budarin VL, Shuttleworth PS, Dodson JR, Segatto ML, Clark JH. 2015. A sustainable freeze-drying route to porous polysaccharides with tailored hierarchical meso- and macroporosity. Macromolecular Rapid Communications 36(8):774-9.

Brun-Graeppi AKAS, Richard C, Bessodes M, Scherman D, Narita T, Ducouret G, Merten O. 2010. Study on the sol–gel transition of xyloglucan hydrogels. Carbohydr.Polym. 80(2):555-62.

Buchtová N, Budtova T. 2016. Cellulose aero-, cryo- and xerogels: towards understanding of morphology control. Cellulose 23(4):1-11.

Burruano BT, Schnaare RL, Malamud D. 2002. Synthetic cervical mucus formulation. Contraception 66(2):137-40.

Cai J, Liu S, Feng J, Kimura S, Wada M, Kuga S, Zhang L. 2012. Cellulose-silica nanocomposite aerogels by in situ formation of silica in cellulose gel. Angewandte Chemie International Edition 51(9):2076-9.

Cao Y, Ikeda I. 2009. Antioxidant activity and antitumor activity (in vitro) of xyloglucan selenious ester and sulfated [corrected] xyloglucan. Int. J. Biol. Macromol. 45(3):231-5.

Cerclier CV, Guyomard-Lack A, Cousin F, Jean B, Bonnin E, Cathala B, Moreau C. 2013. Xyloglucan–cellulose nanocrystal multilayered films: Effect of film architecture on enzymatic hydrolysis. Biomacromolecules 14(10):3599-609.

Cervin NT, Aulin C, Larsson PT, Wågberg L. 2012. Ultra porous nanocellulose aerogels as separation medium for mixtures of oil/water liquids. Cellulose 19(2):401-10.

Chen D, Guo P, Chen S, Cao Y, Ji W, Lei X, Liu L, Zhao P, Wang R, Qi C, Liu Y, He H. 2012. Properties of xyloglucan hydrogel as the biomedical sustained-release carriers. J.Mater.Sci.Mater.Med. 23(4):955-62.

Cheng HN, Gu Q. 2012. Enzyme-catalyzed modifications of polysaccharides and poly(ethylene glycol). Polymers 4(2):1311-30.

Cheng HN, Gu Q. 2002. Enzyme-catalyzed reactions of polysaccharides. In: RA Gross, H. N. Cheng, editors. Biocatalysis in polmer science. ACS Symposium Series, American Chemical Society. p 203-16.

Cheng Y, Lu L, Zhang W, Shi J, Cao Y. 2012. Reinforced low density alginate-based aerogels: Preparation, hydrophobic modification and characterization. Carbohydr.Polym. 88(3):1093-9.

Cheng Y, Brown KM, Prud'homme RK. 2002. Preparation and characterization of molecular weight fractions of guar galactomannans using acid and enzymatic hydrolysis. International Journal of Biological Macromolecules 31(1):29-35.

Chokboribal J, Tachaboonyakiat W, Sangvanich P, Ruangpornvisuti V, jettanacheawchanki S, Thunyakitpisal P. 2015. Deacetylation affects the physical properties and bioactivity of acemannan, an extracted polysaccharide from Aloe Vera. Carbohydrate Polymers 133:556-566.

Coma V. 2013. Polysaccharide-based biomaterials with antimicrobial and antioxidant properties. Polímeros 23287-97.

Comin LM, Temelli F, Saldaña MDA. 2012. Barley β-glucan aerogels as a carrier for flax oil via supercritical CO2. Journal of Food Engineering 111(4):625-31.

Coviello T, Matricardi P, Marianecci C, Alhaique F. 2007. Polysaccharide hydrogels for modified release formulations. J. Controlled Release 119(1):5-24.

Cuce E, Cuce PM, Wood CJ, Riffat SB. 2014. Toward aerogel based thermal superinsulation in buildings: A comprehensive review. Renewable and Sustainable Energy Reviews 34(0):273-99.

Cumpstey I. 2013. Chemical modification of polysaccharides. ISRN Organic Chemistry 2013(0):27.

Daas PJH, Schols HA, de Jongh HHJ. 2000. On the galactosyl distribution of commercial galactomannans. Carbohydrate Research 329(3):609-19.

Das D, Ara T, Dutta S, Mukherjee A. 2011. New water resistant biomaterial biocide film based on guar gum. Bioresource Technology 102(10):5878-83.

De France KJ, Hoare T, Cranston ED. 2017. Review of hydrogels and aerogels containing nanocellulose. Chem.Mater. 29(11):4609-31.

de Jong SJ, De Smedt SC, Demeester J, van Nostrum CF, Kettenes-van den Bosch JJ, Hennink WE. 2001. Biodegradable hydrogels based on stereocomplex formation between lactic acid oligomers grafted to dextran. Journal of Controlled Release 72(1):47-56.

de Souza Lima MM, Borsali R. 2004. Rodlike cellulose microcrystals: Structure, properties, and applications. Macromolecular Rapid Communications 25(7):771-87.

de Souza CF, Lucyszyn N, Woehl MA, Riegel-Vidotti IC, Borsali R, Sierakowski MR. 2013. Property evaluations of dry-cast reconstituted bacterial cellulose/tamarind xyloglucan biocomposites. Carbohydr.Polym. 93(1):144-53.

Dea ICM, Morrison A. 1975. Chemistry and interactions of seed galactomannans. Adv. Carbohydr. Chem. Biochem. 31(0):241-312.

Deszczynski M, Kasapis S, Mitchell JR. 2003. Rheological investigation of the structural properties and aging effects in the agarose/co-solute mixture. Carbohydr.Polym. 53(1):85-93.

Deutschmann R, Dekker RFH. 2012. From plant biomass to bio-based chemicals: Latest developments in xylan research. Biotechnology Advances 30(6):1627-40.

Deville S, Meille S, Seuba J. 2015. A meta-analysis of the mechanical properties of ice-templated ceramics and metals. Science and Technology of Advanced Materials 16(4):043501.

Deville S, Saiz E, Tomsia AP. 2007. Ice-templated porous alumina structures. Acta Materialia 55(6):1965-74.

Deville S, Saiz E, Tomsia AP. 2006. Freeze casting of hydroxyapatite scaffolds for bone tissue engineering. Biomaterials 27(32):5480-9.

Deze EG, Papageorgiou SK, Favvas EP, Katsaros FK. 2012. Porous alginate aerogel beads for effective and rapid heavy metal sorption from aqueous solutions: Effect of porosity in Cu2+ and Cd2+ ion sorption. Chemical Engineering Journal 209(Supplement C):537-46.

Dougherty R, Kunzelmann K. 2007. Computing local thickness of 3D structures with imageJ. Microscopy and Microanalysis 131678-9.

Du A, Zhou B, Zhang Z, Shen J. 2013. A special material or a new state of matter: A review and reconsideration of the aerogel. Materials 6(3):941-68.

Duong HM, Nguyen ST. 2016. Nanocellulose aerogels as thermal insulation materials. In: F. Pacheco Torgal, Cinzia Buratti, Siva Kalaiselvam, Claes-Göran Granqvist, Volodymyr Ivanov, editors. Nano and biotech based materials for energy building efficiency. Cham: Springer International Publishing. p 411-27.

Durães L, Matias T, Patrício R, Portugal A. 2013. Silica based aerogel-like materials obtained by quick microwave drying. Materialwissenschaft und Werkstofftechnik 44(5):380-5.

Eichhorn SJ, Dufresne A, Aranguren M, Marcovich NE, Capadona JR, Rowan SJ, Weder C, Thielemans W, Roman M, Renneckar S, Gindl W, Veigel S, Keckes J, Yano H, Abe K, Nogi M, Nakagaito AN, Mangalam A, Simonsen J, Benight AS, Bismarck A, Berglund LA, Peijs T. 2010. Review: current international research into cellulose nanofibres and nanocomposites. J.Mater.Sci. 45(1):1-33.

Errede LA. 1986. Polymer swelling. 5. Correlation of relative swelling of poly(styrene-co-divinylbenzene) with the Hildebrand solubility parameter of the swelling liquid. Macromolecules 19(6):1522-5.

Fan B, Chen S, Yao Q, Sun Q, Jin C. 2017. Fabrication of cellulose nanofiber/AlOOH aerogel for flame retardant and thermal insulation. Materials 10(3):E311.

Fischer F, Rigacci A, Pirard R, Berthon-Fabry S, Achard P. 2006. Cellulose-based aerogels. Polymer 47(22):7636-45.

Frollini E, Reed WF, Milas M, Rinaudo M. 1995. Polyelectrolytes from polysaccharides: Selective oxidation of guar gum — a revisited reaction. Carbohydrate Polymers 27(2):129-35.

Fujioka R, Tanaka Y, Yoshimura T. 2009. Synthesis and properties of superabsorbent hydrogels based on guar gum and succinic anhydride. J Appl Polym Sci 114(1):612-6.

García-González CA, Alnaief M, Smirnova I. 2011. Polysaccharide-based aerogels—Promising biodegradable carriers for drug delivery systems. Carbohydr.Polym. 86(4):1425-38.
García-González CA, Camino-Rey MC, Alnaief M, Zetzl C, Smirnova I. 2012. Supercritical drying of aerogels using CO_2: Effect of extraction time on the end material textural properties. The Journal of Supercritical Fluids 66297-306.
Gliko-Kabir I, Yagen B, Penhasi A, Rubinstein A. 1998. Low swelling, crosslinked guar and its potential use as colon-specific drug carrier. Pharm.Res. 15(7):1019-25.
Gliko-Kabir I, Yagen B, Baluom M, Rubinstein A. 2000. Phosphated crosslinked guar for colon-specific drug delivery. Journal of Controlled Release 63(1):129-34.
Gómez H. C, Serpa A, Velásquez-Cock J, Gañán P, Castro C, Vélez L, Zuluaga R. 2016. Vegetable nanocellulose in food science: A review. Food Hydrocoll. 57(0):178-86.
Gonçalves VSS, Gurikov P, Poejo J, Matias AA, Heinrich S, Duarte CMM, Smirnova I. 2016. Alginate-based hybrid aerogel microparticles for mucosal drug delivery. European Journal of Pharmaceutics and Biopharmaceutics 107160-70.
Gong H, Liu M, Zhang B, Cui D, Gao C, Ni B, Chen J. 2011. Synthesis of oxidized guar gum by dry method and its application in reactive dye printing. International Journal of Biological Macromolecules 49(5):1083-91.
Gong JP. 2010. Why are double network hydrogels so tough? Soft Matter 6(12):2583-90.
Gu Q, Cheng HN. 2005. Enzyme-catalyzed condensation reactions for polymer modifications. In: H. N. Cheng, R. A. Gross, editors. Polymer biocatalysis and biomaterials. American Chemical Society. p 427-36.
Gurav JL, Jung I, Park H, Kang ES, Nadargi DY. 2010. Silica aerogel: synthesis and applications. Journal of Nanomaterials 2010(0):11.
Gutiérrez MC, Ferrer ML, del Monte F. 2008. Ice-templated materials: Sophisticated structures exhibiting enhanced functionalities obtained after unidirectional freezing and ice-segregation-induced self-assembly. Chem.Mater. 20(3):634-48.
Habibi Y, Lucia LA, Rojas OJ. 2010. Cellulose nanocrystals: chemistry, self-assembly, and applications. Chem.Rev. 110(6):3479-500.
Hair LM, Pekala RW, Stone RE, Chen C, Buckley SR. 1988. Low-density resorcinol–formaldehyde aerogels for direct-drive laser inertial confinement fusion targets. Journal of Vacuum Science & Technology A: Vacuum, Surfaces, and Films 6(4):2559-63.
Han J, Zhou C, Wu Y, Liu F, Wu Q. 2013. Self-assembling behavior of cellulose nanoparticles during freeze-drying: Effect of suspension concentration, particle size, crystal structure, and surface charge. Biomacromolecules 14(5):1529-40.
Hansen CM. 2007. Hansen Solubility Parameters: A User's Handbook.
Henriksson M, Henriksson G, Berglund LA, Lindström T. 2007. An environmentally friendly method for enzyme-assisted preparation of microfibrillated cellulose (MFC) nanofibers. European Polymer Journal 43(8):3434-41.
Hintermüller C, Marone F, Isenegger A, Stampanoni M. 2010. Image processing pipeline for synchrotron-radiation-based tomographic microscopy. Journal of Synchrotron Radiation 17(4):550-559.
Hirschberg JHKK, Brunsveld L, Ramzi A, Vekemans JAJM, Sijbesma RP, Meijer EW. 2000. Helical self-assembled polymers from cooperative stacking of hydrogen-bonded pairs. Nature 407(6801):167-70.
Horvat G, Fajfar T, Perva Uzunalić A, Knez Ž, Novak Z. 2017. Thermal properties of polysaccharide aerogels. Journal of Thermal Analysis and Calorimetry 127(1):363-70.

Hrubesh LW, Pekala RW. 1994. Thermal properties of organic and inorganic aerogels. J.Mater.Res. 9(3):731-8.
Hüsing N, Schubert U. 1998. Aerogels—airy materials: Chemistry, structure, and properties. Angewandte Chemie International Edition 37(1-2):22-45.
Ikada Y. 2006. Challenges in tissue engineering. Journal of the Royal Society Interface 3(10):589-601.
Ikada Y, Jamshidi K, Tsuji H, Hyon SH. 1987. Stereocomplex formation between enantiomeric poly(lactides). Macromolecules 20(4):904-6.
Iqbal DN, Hussain EA. 2010. Physiochemical and pharmaceutical properties of guar gum derivatives. Asian Journal of Chemistry 22(9):7446-52.
Isogai A, Saito T, Fukuzumi H. 2011. TEMPO-oxidized cellulose nanofibers. Nanoscale 3:71-85.
Jayakumar R, Prabaharan M, Sudheesh Kumar PT, Nair SV, Tamura H. 2011. Biomaterials based on chitin and chitosan in wound dressing applications. Biotechnology Advances 29(3):322-37.
John MJ, Thomas S. 2008. Biofibres and biocomposites. Carbohydrate Polymers 71(3):343-64.
Kalia S, Boufi S, Celli A, Kango S. 2014. Nanofibrillated cellulose: surface modification and potential applications. Colloid and Polymer Science 292(1): 5-31.
Karaki N, Aljawish A, Humeau C, Muniglia L, Jasniewski J. 2016. Enzymatic modification of polysaccharides: Mechanisms, properties, and potential applications: A review. Enzyme and Microbial Technology 90(0):1-18.
Kato Y, Uchida J, Ito S, Mitsuishi Y. 2001. Structural analysis of the oligosaccharide units of xyloglucan and their effects on growth of COLO 201 human tumor cells. International Congress Series 1223(0):161-4.
Kistler SS. 1931. Coherent expanded-aerogels. J.Phys.Chem. 36(1):52-64.
Kobayashi Y, Saito T, Isogai A. 2014. Aerogels with 3D ordered nanofiber skeletons of liquid-crystalline nanocellulose derivatives as tough and transparent insulators. Angewandte Chemie International Edition 53(39):10394-7.
Kochumalayil J, Sehaqui H, Zhou Q, Berglund LA. 2010. Tamarind seed xyloglucan - a thermostable high-performance biopolymer from non-food feedstock. J.Mater.Chem. 20(21):4321-7.
Köhnke T, Elder T, Theliander H, Ragauskas AJ. 2014. Ice templated and cross-linked xylan/nanocrystalline cellulose hydrogels. Carbohydr.Polym. 100(0):24-30.
Köhnke T, Lin A, Elder T, Theliander H, Ragauskas AJ. 2012. Nanoreinforced xylan-cellulose composite foams by freeze-casting. Green Chem. 14(7):1864-9.
Korhonen JT, Kettunen M, Ras RHA, Ikkala O. 2011. Hydrophobic nanocellulose aerogels as floating, sustainable, reusable, and recyclable oil absorbents. Applied Materials and Interfaces 3:1813-1816.
Kozioł A, Cybulska J, Pieczywek PM, Zdunek A. 2015. Evaluation of structure and assembly of xyloglucan from tamarind seed (Tamarindus indica L.) with atomic force microscopy. Food Biophysics 10(4):396-402.
Lazaridou A, Biliaderis CG. 2007. Molecular aspects of cereal β-glucan functionality: Physical properties, technological applications and physiological effects. Journal of Cereal Science 46(2):101-18.
Lee J, Deng Y. 2011. The morphology and mechanical properties of layer structured cellulose microfibril foams from ice-templating methods. Soft Matter 7(13):6034-40.

Lee K, Aitomäki Y, Berglund LA, Oksman K, Bismarck A. 2014. On the use of nanocellulose as reinforcement in polymer matrix composites. Composites Sci.Technol. 105(0):15-27.
Leone G, Barbucci R. 2009. Polysaccharide based hydrogels for biomedical applications. In: Rolando Barbucci, editor. Hydrogels: Biological properties and applications. Springer Milan. p 25-41.
Li J. 2016. The functional and nutritional aspects of hydrocolloids in foods. Food Hydrocoll. 53(0):46-61.
Li Y, Zhang H, Fan M, Zhuang J, Chen L. 2016. A robust salt-tolerant superoleophobic aerogel inspired by seaweed for efficient oil-water separation in marine environments. Phys.Chem.Chem.Phys. 18(36):25394-400.
Li Z, Su Y, Xie B, Liu X, Gao X, Wang D. 2015. A novel biocompatible double network hydrogel consisting of konjac glucomannan with high mechanical strength and ability to be freely shaped. J. Mater. Chem. B 3(9):1769-78.
Liebner F, Potthast A, Rosenau T, Haimer E, Wendland M. 2008. Cellulose aerogels: Highly porous, ultra-lightweight materials. Holzforschung 62(0):129-135.
Limayem A, Ricke SC. 2012. Lignocellulosic biomass for bioethanol production: Current perspectives, potential issues and future prospects. Progress in Energy and Combustion Science 38(4):449-67.
Lin W, Lien C, Yeh H, Yu C, Hsu S. 2013. Bacterial cellulose and bacterial cellulose–chitosan membranes for wound dressing applications. Carbohydrate Polymers 94(1):603-11.
Liu LS, Kost J, Yan F, Spiro RC. 2012. Hydrogels from biopolymer hybrid for biomedical, food, and functional food applications. Polymers 4(2):997-1011.
Liu Z, Jiao Y, Wang Y, Zhou C, Zhang Z. 2008. Polysaccharides-based nanoparticles as drug delivery systems. Advanced Drug Delivery Reviews 60(15):1650-62.
Lotfinia S, Javanmard Dakheli M, Mohammadi Nafchi A. 2013. Application of starch foams containing plant essential oils to prevent mold growth and improve shelf life of packaged bread. Journal of Chemical Health Risks 3(4):9-18.
Lozinsky VI, Galaev IY, Plieva FM, Savina IN, Jungvid H, Mattiasson B. 2003. Polymeric cryogels as promising materials of biotechnological interest. Trends Biotechnol. 21(10):445-51.
Lu T, Li Q, Chen W, Yu H. 2014. Composite aerogels based on dialdehyde nanocellulose and collagen for potential applications as wound dressing and tissue engineering scaffold. Composites Science and Technology 94(0):132-8.
Mahajan HS, Deshmukh SR. 2015. Development and evaluation of gel-forming ocular films based on xyloglucan. Carbohydrate Polymers 122(Supplement C):243-7.
Marone F, Stampanoni M. 2012. Regridding reconstruction algorithm for real-time tomographic imaging. Journal of Synchrotron Radiation 19(6):1020-1037.
Martins M, Barros AA, Quraishi S, Gurikov P, Raman SP, Smirnova I, Duarte ARC, Reis RL. 2015. Preparation of macroporous alginate-based aerogels for biomedical applications. The Journal of Supercritical Fluids 106(0):152-9.
Martoïa F, Cochereau T, Dumont PJJ, Orgéas L, Terrien M, Belgacem MN. 2016. Cellulose nanofibril foams: Links between ice-templating conditions, microstructures and mechanical properties. Mater Des 104(0):376-91.
Mehling T, Smirnova I, Guenther U, Neubert RHH. 2009. Polysaccharide-based aerogels as drug carriers. J. Non Cryst.Solids 355(50–51):2472-9.

Mikkonen KS, Tenkanen M. 2012. Sustainable food-packaging materials based on future biorefinery products: Xylans and mannans. Trends in Food Science & Technology 28(2):90-102.
Mikkonen KS, Parikka K, Ghafar A, Tenkanen M. 2013. Prospects of polysaccharide aerogels as modern advanced food materials. Trends Food Sci.Technol. 34(2):124-36.
Mikkonen KS, Parikka K, Suuronen J, Ghafar A, Serimaa R, Tenkanen M. 2014. Enzymatic oxidation as a potential new route to produce polysaccharide aerogels. RSC Adv. 4(23):11884-92.
Mikkonen KS, Rita H, Helén H, Talja RA, Hyvönen L, Tenkanen M. 2007. Effect of polysaccharide structure on mechanical and thermal properties of galactomannan-based films. Biomacromolecules 8(10):3198-205.
Mishra A, Malhotra AV. 2009. Tamarind xyloglucan: a polysaccharide with versatile application potential. J.Mater.Chem. 19(45):8528-36.
Missoum K, Belgacem MN, Bras J. 2013. Nanofibrillated cellulose surface modification: A review. Materials 6(5):1745-66.
Moreira LRS, Filho EXF. 2008. An overview of mannan structure and mannan-degrading enzyme systems. Appl.Microbiol.Biotechnol. 79(2):165.
Moreno-Atanasio R, Williams RA, Jia X. 2010. Combining X-ray microtomography with computer simulation for analysis of granular and porous materials. Particuology 8(2):81-99.
Mudgil D, Barak S, Khatkar BS. 2014. Guar gum: processing, properties and food applications—A Review. Journal of Food Science and Technology 51(3):409-18.
Mudgil D, Barak S, Khatkar BS. 2011. Guar gum: processing, properties and food applications—A Review. J.Food Sci.Technol. 51(3):409-18.
Mukai SR, Nishihara H, Tamon H. 2004. Formation of monolithic silica gel microhoneycombs (SMHs) using pseudosteady state growth of microstructural ice crystals. Chem.Commun. (7):874-5.
Mulik S, Sotiriou-Leventis C. 2011. Resorcinol–formaldehyde aerogels. In: Michel A. Aegerter, Nicholas Leventis, Matthias M. Koebel, editors. Aerogels handbook. New York, NY: Springer New York. p 215-34.
Nakagaito AN, Yano H. 2004. The effect of morphological changes from pulp fiber towards nano-scale fibrillated cellulose on the mechanical properties of high-strength plant fiber based composites. Applied Physics A 78(4):547-52.
Nechyporchuk O, Belgacem MN, Pignon F. 2014. Rheological properties of micro-/nanofibrillated cellulose suspensions: Wall-slip and shear banding phenomena. Carbohydr.Polym. 112(0):432-9.
Nisbet DR, Crompton KE, Hamilton SD, Shirakawa S, Prankerd RJ, Finkelstein DI, Horne MK, Forsythe JS. 2006. Morphology and gelation of thermosensitive xyloglucan hydrogels. Biophys.Chem. 121(1):14-20.
Nishihara H, Mukai SR, Yamashita D, Tamon H. 2005. Ordered macroporous silica by ice templating. Chem.Mater. 17(3):683-9.
Nishinari K, Takemasa M, Zhang H, Takahashi R. 2007. Storage plant polysaccharides: Xyloglucans, galactomannans, glucomannans. In: J. P. Kamerling, editor. Comprehensive Glycoscience. Elsevier. p 613-52.
Nishino T, Takano K, Nakamae K. 1995. Elastic modulus of the crystalline regions of cellulose polymorphs. Journal of Polymer Science Part B: Polymer Physics 33(11):1647-51.

Nishiyama Y, Kim UJ, Kim DY, Katsumata KS, May RP, Langan P. 2003. Periodic disorder along ramie cellulose microfibrils. Biomacromolecules 4 (4): 1013-1017.
Olalekan AP, Dada AO, Adesina OA. 2014. Review: Silica Aerogel as a viable absorbent for oil spill remediation. Journal of Encapsulation and Adsorption Sciences 4(4):122-31.
O'Sullivan AC. 1997. Cellulose: the structure slowly unravels. Cellulose 4(3):173-207.
Pääkkö M, Ankerfors M, Kosonen H, Nykänen A, Ahola S, Österberg M, Ruokolainen J, Laine J, Larsson PT, Ikkala O, Lindström T. 2007. Enzymatic hydrolysis combined with mechanical shearing and high-pressure homogenization for nanoscale cellulose fibrils and strong gels. Biomacromolecules 8(6):1934-41.
Pääkkö M, Vapaavuori J, Silvennoinen R, Kosonen H, Ankerfors M, Lindstrom T, Berglund LA, Ikkala O. 2008. Long and entangled native cellulose I nanofibers allow flexible aerogels and hierarchically porous templates for functionalities. Soft Matter 4(12):2492-9.
Pal S, Mal D, Singh RP. 2007. Synthesis and characterization of cationic guar gum: A high performance flocculating agent. J Appl Polym Sci 105(6):3240-5.
Parija S, Misra M, Mohanty AK. 2001. Studies of natural gum adhesive extracts: An overview. Journal of Macromolecular Science, Part C 41(3):175-97.
Parikka K, Tenkanen M. 2009. Oxidation of methyl α-d-galactopyranoside by galactose oxidase: products formed and optimization of reaction conditions for production of aldehyde. Carbohydr.Res. 344(1):14-20.
Parikka K, Master E, Tenkanen M. 2015. Oxidation with galactose oxidase: Multifunctional enzymatic catalysis. J Molec Catal B 120(0):47-59.
Parikka K, Ansari F, Hietala S, Tenkanen M. 2012a. Thermally stable hydrogels from enzymatically oxidized polysaccharides. Food Hydrocoll. 26(1):212-20.
Parikka K, Leppänen A, Pitkänen L, Reunanen M, Willför S, Tenkanen M. 2010. Oxidation of polysaccharides by galactose oxidase. J. Agric.Food Chem. 58(1):262-71.
Parikka K, Leppänen A, Xu C, Pitkänen L, Eronen P, Österberg M, Brumer H, Willför S, Tenkanen M. 2012b. Functional and anionic cellulose-interacting polymers by selective chemo-enzymatic carboxylation of galactose-containing polysaccharides. Biomacromolecules 13(8):2418-28.
Pawar PMA, Koutaniemi S, Tenkanen M, Mellerowicz EJ. 2013. Acetylation of woody lignocellulose: significance and regulation. Frontiers in Plant Science 4:118.
Pawelec KM, Husmann A, Best SM, Cameron RE. 2014. A design protocol for tailoring ice-templated scaffold structure. J. R. Soc. Interface 11(92):20130958.
Peng X, Ren J, Zhong L, Sun R. 2011. Nanocomposite films based on xylan-rich hemicelluloses and cellulose nanofibers with enhanced mechanical properties. Biomacromolecules 12(9):3321-9.
Perez J, Munoz-Dorado J, de la Rubia T, Martinez J. 2002. Biodegradation and biological treatments of cellulose, hemicellulose and lignin: an overview. Int.Microbiol. 5(2):53-63.
Picout DR, Ross-Murphy SB, Errington N, Harding SE. 2003. Pressure cell assisted solubilization of xyloglucans: tamarind seed polysaccharide and detarium gum. Biomacromolecules 4(3):799-807.
Pierre AC, Pajonk G. 2002. Chemistry of aerogels and their applications. Chem.Rev. 102(11):4243-66.
Podlipec R, Gorgieva S, Jurašin D, Urbančič I, Kokol V, Štrancar J. 2014. Molecular mobility of scaffolds' biopolymers influences cell growth. ACS Appl. Mater. Interfaces 6(18):15980-90.

Pojanavaraphan T, Magaraphan R. 2008. Prevulcanized natural rubber latex/clay aerogel nanocomposites. European Polymer Journal 44(7):1968-77.
Pope EJA. 1995. Gel encapsulated microorganisms: Saccharomyces cerevisiae—Silica gel biocomposites. J. Sol Gel Sci.Technol. 4(3):225-9.
Pourhaghgouy M, Zamanian A. 2015. Physical and mechanical properties of the fully interconnected chitosan ice-templated scaffolds. J Appl Polym Sci 132(7):41476.
Prabaharan M. 2011. Prospective of guar gum and its derivatives as controlled drug delivery systems. International Journal of Biological Macromolecules 49(2):117-24.
Prajapati VD, Jani GK, Moradiya NG, Randeria NP, Nagar BJ, Naikwadi NN, Variya BC. 2013. Galactomannan: A versatile biodegradable seed polysaccharide. International Journal of Biological Macromolecules 60(Supplement C):83-92.
Qi X, Chen G, Gong X, Fu G, Niu Y, Bian J, Peng F, Sun R. 2016. Enhanced mechanical performance of biocompatible hemicelluloses-based hydrogel via chain extension. Scientific Reports 6(0):33603.
Quignard F, Valentin R, Di Renzo F. 2008. Aerogel materials from marine polysaccharides. New J.Chem. 32(8):1300-10.
Quraishi S, Martins M, Barros AA, Gurikov P, Raman SP, Smirnova I, Duarte ARC, Reis RL. 2015. Novel non-cytotoxic alginate–lignin hybrid aerogels as scaffolds for tissue engineering. The Journal of Supercritical Fluids 105(0):1-8.
Raman SP, Gurikov P, Smirnova I. 2015a. Hybrid alginate based aerogels by carbon dioxide induced gelation: Novel technique for multiple applications. The Journal of Supercritical Fluids 106(0):23-33.
Raman SP, Gurikov P, Dieringer P, Sun M, Smirnova I. 2015b. On the road to biopolymer aerogels—dealing with the solvent. Gels 1(2):291-313.
Ramanathan K, Kamalasanan MN, Malhotra BD, Pradhan DR, Chandra S. 1997. Immobilization and characterization of lactate dehydrogenase on TEOS derived sol-gel films. J. Sol Gel Sci. Technol. 10(3):309-16.
Reches M, Gazit E. 2003. Casting metal nanowires within discrete self-assembled peptide nanotubes. Science 300(5619):625-30.
Reddy N, Reddy R, Jiang Q. 2015. Crosslinking biopolymers for biomedical applications. Trends in Biotechnology 33(6):362-9.
Robitzer M, Tourrette A, Horga R, Valentin R, Boissière M, Devoisselle JM, Di Renzo F, Quignard F. 2011a. Nitrogen sorption as a tool for the characterisation of polysaccharide aerogels. Carbohydr.Polym. 85(1):44-53.
Robitzer M, Renzo FD, Quignard F. 2011b. Natural materials with high surface area. Physisorption methods for the characterization of the texture and surface of polysaccharide aerogels. Microporous and Mesoporous Materials 140(1):9-16.
Rouquerol J, Avnir D, Fairbridge CW, Everett DH, Haynes JH, Rnicone N, Pernicone N, Sing KSW, Unger KK. 1994. Recommendations for the characterization of porous solids. Pure and Applied Chemistry 6(8):1739-1758.
Rudaz C, Courson R, Bonnet L, Calas-Etienne S, Sallée H, Budtova T. 2014. Aeropectin: Fully biomass-based mechanically strong and thermal superinsulating aerogel. Biomacromolecules 15(6):2188-95.
Salam A, Venditti RA, Pawlak JJ, El-Tahlawy K. 2011. Crosslinked hemicellulose citrate–chitosan aerogel foams. Carbohydrate Polymers 84(4):1221-9.
Sandolo C, Matricardi P, Alhaique F, Coviello T. 2007. Dynamo-mechanical and rheological characterization of guar gum hydrogels. European Polymer Journal 43(8):3355-67.

Sauter T, Kratz K, Lendlein A. 2013. Pore-size distribution controls shape-memory properties on the macro- and microscale of polymeric foams. Macromolecular Chemistry and Physics 214(11):1184-8.
Scheller HV, Ulvskov P. 2010. Hemicelluloses. Annu. Rev. Plant Biol. 61(1):263-89.
Schoevaart R, Kieboom T. 2002. Galactose dialdehyde as potential protein cross-linker: proof of principle. Carbohydrate Research 337(10):899-904.
Schoevaart R, Kieboom T. 2004. Application of galactose oxidase in chemoenzymatic one-pot cascade reactions without intermediate recovery steps. Topics in Catalysis 27:1-4.
Sedighi Gilani M, Boone MN, Fife JL, Zhao S, Koebel MM, Zimmermann T, Tingaut P. 2016. Structure of cellulose -silica hybrid aerogel at sub-micron scale, studied by synchrotron X-ray tomographic microscopy. Composites Sci.Technol. 124(0):71-80.
Sehaqui H, Salajkova M, Zhou Q, Berglund LA. 2010. Mechanical performance tailoring of tough ultra-high porosity foams prepared from cellulose I nanofiber suspensions. Soft Matter 6(8):1824-32.
Sehaqui H, Salajkova M, Zhou Q, Berglund LA. 2009. Biomimetic aerogels from microfibrillated cellulose and xyloglucan. 17th International Conference on Composite Materials, ICCM-17, 27 July 2009 through 31 July 2009, Edinburgh, United Kingdom.
Selmer I, Kleemann C, Kulozik U, Heinrich S, Smirnova I. 2015. Development of egg white protein aerogels as new matrix material for microencapsulation in food. The Journal of Supercritical Fluids 106(0):42-9.
Shenoy MA, D'Melo DJ. 2010. Synthesis and characterization of acryloyloxy guar gum. J Appl Polym Sci 117(1):148-54.
Shirakawa M, Yamatoya K, Nishinari K. 1998. Tailoring of xyloglucan properties using an enzyme. Food Hydrocolloids 12(1):25-8.
Siebum A, van Wijk A, Schoevaart R, Kieboom T. 2006. Galactose oxidase and alcohol oxidase: Scope and limitations for the enzymatic synthesis of aldehydes. Journal of Molecular Catalysis B: Enzymatic 41(3):141-5.
Simi CK, Abraham TE. 2010. Biodegradable biocompatible xyloglucan films for various applications. Colloid Polym.Sci. 288(3):297-306.
Sing KSW, Everett DH, Haul RAW, Moscou L, Pierotti RA, Rouquerol J, Siemieniewska T. 2008. Reporting physisorption data for gas/solid systems. In: G. Ertl, H. Knözinger, F. Schüth, J. Weitkamp, editors. Handbook of Heterogeneous Catalysis. Wiley-VCH Verlag GmbH & Co. KGaA.
Singh B, Sharma S, Dhiman A. 2013. Design of antibiotic containing hydrogel wound dressings: Biomedical properties and histological study of wound healing. International Journal of Pharmaceutics 457(1):82-91.
Soderqvist Lindblad M, Albertsson AC, Ranucci E, Laus M, Giani E. 2005. Biodegradable polymers from renewable sources: rheological characterization of hemicellulose-based hydrogels. Biomacromolecules 6(2):684-90.
Soleimani Dorcheh A, Abbasi MH. 2008. Silica aerogel; synthesis, properties and characterization. J.Mater.Process.Technol. 199(1–3):10-26.
Stergar J, Maver U. 2016. Review of aerogel-based materials in biomedical applications. J. Sol Gel Sci. Technol. 77(3):738-52.
Sundberg A, Sundberg K, Lillandt C, Holmbom B. 1996. Determination of hemicelluloses and pectins in wood and pulp fibres by acid methanolysis and gas chromatography. Nordic Pulp and Paper Research Journal 11(4):216-9.

Swerin A. 1998. Rheological properties of cellulosic fibre suspensions flocculated by cationic polyacrylamides. Colloids Surf. Physicochem. Eng. Aspects 133(3):279-94.
Tako M. 2015. The Principle of Polysaccharide Gels. Advances in Bioscience and Biotechnology 6(1):15.
Thombare N, Jha U, Mishra S, Siddiqui MZ. 2016. Guar gum as a promising starting material for diverse applications: A review. Int. J. Biol. Macromol. 88(0):361-72.
Tiwari A, Prabaharan M. 2010. An amphiphilic nanocarrier based on guar gum-graft-poly(ε-caprolactone) for potential drug-delivery applications. Journal of Biomaterials Science, Polymer Edition 21(6-7):937-49.
Tripathy S, Das MK. 2013. Guar gum: Present status and applicatios. J. Pharm. Sci. Innovat 2(4):24-28.
Turbak AF, Snyder FW, Sandberg KR. 1983. Microfibrillated cellulose, a new cellulose product: properties, uses, and commercial potential.
Umemura M, Yuguchi Y. 2005. Conformational folding of xyloglucan side chains in aqueous solution from molecular dynamics simulation. Carbohydr.Res. 340(16):2520-32.
Valentin R, Molvinger K, Viton C, Domard A, Quignard F. 2005. From hydrocolloids to high specific surface area porous supports for catalysis. Biomacromolecules 6(5):2785-92.
Van Vlierberghe S, Dubruel P, Schacht E. 2011. Biopolymer-based hydrogels as scaffolds for tissue engineering applications: A review. Biomacromolecules 12(5):1387-408.
Voragen AGJ, Coenen G, Verhoef RP, Schols HA. 2009. Pectin, a versatile polysaccharide present in plant cell walls. Structural Chemistry 20(2):263.
Wahab IF, Razak SIA. 2016. Polysaccharides as Composite Biomaterials. In: Matheus Poletto, editor. Composites from renewable and sustainable materials. Rijeka: InTech. p Ch. 04.
Wang J, Zhou Q, Song D, Qi B, Zhang Y, Shao Y, Shao Z. 2015. Chitosan–silica composite aerogels: preparation, characterization and Congo red adsorption. J. Sol Gel Sci.Technol. 76(3):501-9.
Wang M, Anoshkin IV, Nasibulin AG, Ras RHA, Nonappa, Laine J, Kauppinen EI, Ikkala O. 2016. Electric behavior of native cellulose nanofibril/carbon nanotube hybrid aerogels under cyclic compression. RSC Advances 6(92):89051-89056.
Wang M, Anoshkin IV, Nasibulin AG, Korhonen JT, Seitsonen J, Pere J, Kauppinen EI, Ras RHA, Ikkala O. 2013. Modifying native nanocellulose aerogels with carbon nanotubes for mechanoresponsive conductivity and pressure sensing. Advanced materials 25(17):2428-2432.
Wegst UGK, Schecter M, Donius AE, Hunger PM. 2010. Biomaterials by freeze casting. Philos Transact A Math Phys Eng Sci 368(1917):2099-121.
Whittaker JW. 2003. Free radical catalysis by galactose oxidase. Chem.Rev. 103(6):2347-64.
Wielinga WC. 2009. Galactomannans. In: G. O. Phillips, P. A. Williams, editors. Handbook of Hydrocolloids. 2nd ed. Woodhead Publishing: Cambridge, UK. p 228-51.
Wientjes RHW, Duits MHG, Jongschaap RJJ, Mellema J. 2000. Linear rheology of guar gum solutions. Macromolecules 33(26):9594-605.
Xiong R, Lu C, Wang Y, Zhou Z, Zhang X. 2013. Nanofibrillated cellulose as the support and reductant for the facile synthesis of Fe3O4/Ag nanocomposites with catalytic and antibacterial activity. J. Mater. Chem. A 1(47):14910-8.
Yalpani M, Hall LD. 1982. Some chemical and analytical aspects of polysaccharide modifications. II. A high-yielding, specific method for the chemical derivatization of galactose-containing polysaccharides: oxidation with galactose oxidase followed by

reductive amination. Journal of Polymer Science: Polymer Chemistry Edition 20:3399–3420.
Yan C, Given PS, Huvard G, Mallepally RR, McHugh MA, inventors; Anonymous 2016 Aug 26, 2014. Method of loading flavor into an aerogel and flavor impregnated aerogel based on food grade materials. U.S. patent US 20160058045 A1.
Yang J, Li S, Luo Y, Yan L, Wang F. 2011. Compressive properties and fracture behavior of ceramic fiber-reinforced carbon aerogel under quasi-static and dynamic loading. Carbon 49(5):1542-9.
Yang X, Bakaic E, Hoare T, Cranston ED. 2013. Injectable polysaccharide hydrogels reinforced with cellulose nanocrystals: Morphology, rheology, degradation, and cytotoxicity. Biomacromolecules 14(12):4447-55.
York WS, Harvey LK, Guillen R, Alberhseim P, Darvill AG. 1993. Structural analysis of tamarind seed xyloglucan oligosaccharides using β-galactosidase digestion and spectroscopic methods. Carbohydrate Research 248(Supplement C):285-301.
Yuan J, Wen D, Gaponik N, Eychmüller A. 2013. Enzyme-encapsulating quantum dot hydrogels and xerogels as biosensors: Multifunctional platforms for both biocatalysis and fluorescent probing. Angewandte Chemie International Edition 52(3):976-9.
Yuguchi Y, Kumagai T, Wu M, Hirotsu T, Hosokawa J. 2004. Gelation of xyloglucan ID water/alcohol systems. Cellulose 11(2):203-8.
Zabed H, Sahu JN, Boyce AN, Faruq G. 2016. Fuel ethanol production from lignocellulosic biomass: An overview on feedstocks and technological approaches. Renewable and Sustainable Energy Reviews 66(0):751-74.
Zha J, Roggendorf H. 1991. Sol–gel science, the physics and chemistry of sol–gel processing. Adv Mater 3(10):522-7.
Zhang L, Zhou J, Hui PS. 2005. A comparative study on viscosity behavior of water-soluble chemically modified guar gum derivatives with different functional lateral groups. J.Sci.Food Agric. 85(15):2638-44.
Zhao Z, Crespi V, Kubicki J, Cosgrove D, Zhong L. 2014. Molecular dynamics simulation study of xyloglucan adsorption on cellulose surfaces: effects of surface hydrophobicity and side-chain variation. Cellulose 21(2):1025-39.
Zimmermann T, Bordeanu N, Strub E. 2010. Properties of nanofibrillated cellulose from different raw materials and its reinforcement potential. Carbohydr.Polym. 79(4):1086-93.